MATHEMATICAL MODELING OF EIF5B-MEDIATED NON-CANONICAL TRANSLATION INITIATION AS A CHEMOTHERAPEUTIC TARGET

ELIZABETH A. M. TROFIMENKOFF
Bachelor of Science, University of Lethbridge, 2020

A thesis submitted
in partial fulfilment of the requirements for the degree of

MASTER OF SCIENCE

in

CHEMISTRY

Department of Chemistry and Biochemistry
University of Lethbridge
LETHBRIDGE, ALBERTA, CANADA

MATHEMATICAL MODELING OF EIF5B-MEDIATED NON-CANONICAL TRANSLATION INITIATION AS A CHEMOTHERAPEUTIC TARGET

ELIZABETH A. M. TROFIMENKOFF

Date of Defence: July 29, 2022

Dr. M. Roussel	Professor	Ph.D.
Dr. N. Thakor	Associate Professor	Ph.D.
Thesis Co-Supervisors		
Dr. S. Wetmore	Professor	Ph.D.
Thesis Examination Committee Member		
Dr. I. Kovalchuk	Professor	Ph.D.
Thesis Examination Committee Member		
Dr. J. Hamel	Assistant Professor	Ph.D.
Chair, Thesis Examination Committee		

Dedication

This thesis is dedicated to the memory of

Mr. Dave Armstrong (Mo)

one of the best story tellers this world has ever seen, and will ever see.

Abstract

Glioblastoma is an extremely aggressive brain cancer that has a median survival time of 15 months, and a 95% mortality rate within 5 years. Standard-of-care therapy has not changed in over 15 years, and has unfortunately been limited in success. Glioblastomas tend to grow rapidly, creating hypoxic conditions within their cells. Under these conditions, the alpha subunit of eIF2 is phosphorylated, resulting in its inability to deliver the initiator tRNA to the ribosome during canonical translation initiation. In healthy cells, if the stress persists and is not alleviated, this may trigger a form of programmed cell death known as apoptosis. However, cancer cells exploit a non-canonical translation initiation pathway that replaces eIF2 with eIF5B to deliver the $tRNA_i$ to the pre-initiation complex. Some anti-apoptotic proteins are translated using this pathway, such as X-linked inhibitor of apoptosis (XIAP). The *XIAP* mRNA contains an IRES element which allows it to be translated using this non-canonical pathway. XIAP is up-regulated in glioblastoma cells, and therefore the eIF5B-mediated non-canonical translation initiation pathway is a promising therapeutic target for those suffering from this deadly disease. In this thesis, ordinary differential equation (ODE) and delay-differential equation (DDE) models are assembled to analyze the canonical and non-canonical translation initiation pathways. Four inhibitor classes are proposed and examined for both pathways. Results are presented in the forms of sensitivity analyses, 3D surface plots and contour plots which allow us to determine several potentially therapeutically effective combinations of inhibitor concentrations and K_D values for each mode of inhibition. The results indicate that a direct eIF5B inhibitor or non-canonical ternary complex inhibitor are the most promising therapeutic targets.

Acknowledgments

It is a rare occurrence to meet someone as passionate, motivated, fun and inspiring as you, Marc. I still remember the day I walked into your office to discuss my first independent study. You were so excited to discuss bifurcation diagrams with me, and I have to admit that it was contagious. Thank you for introducing me to a world full of math, science and wonder. It has completely changed my life and the way I view the world. As I sit here writing this acknowledgment, I can't believe how much I have grown and learned under your supervision. From my early baby-researcher days taking my first steps in the world of deterministic modeling, to my first publication on the importance of delays in mathematical modelling, to my honour's thesis on establishing an algorithm to validate the steady-state approximation, to this Master's thesis. Thank you from the bottom of my heart for being such an inspiration and for always being so understanding and compassionate. Thank you for your guidance. Thank you for your patience. Thank you for appreciating my silly jokes and science puns. But most of all, thank you for your faith in me. It goes without saying that I would not be here without you.

To the Roussel research group, you are all rock stars. It has been an absolute pleasure getting to know all of you over the years. Catharine, you are a super woman. Thank you for everything you do to keep our lab running smoothly, and for always being so kind and welcoming. Talmon and Mohammad, it has been so enlightening being a part of and watching your research journeys. I know you both will go on to do great things. Liv, I knew we were kindred spirits the day we met in the old lab. You are one of the smartest, kindest, wisest people I know, and it has been an honour to work with you the last few years. Thank you for always being up for a casual conversation about systems biology and how it

relates to the macroscopic world. Thank you for appreciating my humour and sharing the best memes. Thank you for your trust in discussing so many things over the years. Your friendship is invaluable, and I thank you for sharing this part of your life with me. I know that no matter where you may end up, they will be lucky to have you.

Over the years, I have been blessed to have so much encouragement and support, particularly from you, Stacey. Thank you for being on my Honour's thesis committee and asking such great questions. I have learned so much from you over the years, and I am so thankful you agreed to be a part of my Master's committee. Thank you for all of the time you have devoted to me throughout my academic career. Thank you for always being up for a quick visit in the hallways and for your faith in me. Most of all, thank you for being such a positive inspiration to me, and to all of the women and girls setting their sights on the world of STEM. You're a rock star.

Nehal, thank you for sharing your passion for eIF5B with me. This project has been so illuminating, and I cannot thank you enough for sharing your knowledge and wisdom with me over the years. Your time and encouragement have been invaluable. Igor, thank you so much for agreeing to be on my Master's committee. Thank you for your time in our meetings over the years, and for your dedication. JD, thank you for agreeing to chair my defence. It has been a delight getting to know you through ACID:BASE and I am looking forward to working with you in the future.

To my entire Master's committee, thank you from the bottom of my heart for all of your time. I know that you all have busy schedules on top of supervising students. Please know that your efforts, time, and dedication do not go unnoticed. I am immeasurably thankful for you.

Over the course of my program, I have had the opportunity to work with some incredible instructors. Ying, thank you for taking me on my very first semester as a grad student, and giving me the flexibility to allow me to grow into the TA I am today. Thank you for your guidance and your encouragement, and for believing in me. John, even though it was a

turbulent semester to say the least, I am so thankful we got to work together. Thank you for all of your support. Thank you for allowing me to design our worksheets and some of our exam questions. Being a part of the course delivery was such an illuminating experience, and I appreciate the time you took out of your busy schedule to aid me in it. It has been a delight working under your supervision, and I am looking forward to doing so again in the future.

I would also like to acknowledge an appreciate all of the time and effort that Susan Findlay and Susan Hill do within the department. Thank you both for everything you do for the grad student body and for all of your administrative work. You are super women.

To my mom and dad, there are no words that could properly express the appreciation I have for you two, but I will try my best. Thank you for always being there for me when I need it. It hasn't been the easiest few years, but I know that we are stronger together, and together we can get through anything: the three musketeers! All for one, and one for all. Thank you for always being so supportive and encouraging. You are my biggest cheerleaders, and are always in my corner. Simply put: you're the best, and thank you for being the best.

Grandma and Grandpa, thank you for always cheering me on, even though I may not make sense half the time. You are always so engaged and supportive, and having you and your love by my side throughout my whole life has been such a blessing. Thank you for our Friday dice games and piano sessions, and for always supplying pancakes and waffles on demand. You've taught me that life isn't always about rolling 1's and 5's, sometimes the most unexpected results come from simply trusting the process, having faith, and rolling the dice.

Nana and Papa, I know you'll never be able to read this, but thank you for a lifetime of love and memories. Papa, I can still hear your voice like it's yesterday, telling me to do my best, and being so proud of me knowing that I did, regardless of the outcome. Nana, as I sit here writing this, it seems impossible that I can't go visit and tell you about it in person.

Thank you for always listening to my ”fun” science facts and for your undying love and support. Your passion for life and all it has to offer will stay with me forever. Thank you for sharing with me one love, one lifetime. To all my grandparents, I love you. It is such an honour to be your granddaughter.

To my incredible found-family Harper-Hugo, Will, Tamika, Josh, Taylor, Liv, Gaston and River, and so many more, you have been there for me through thick and thin, and I am so thankful for you all. Thank you for printing off posters I have made and posting them on your walls, for all of the postcards, cards, stickers, movie nights, surprise visits and so much more. It has made the last two years feel as normal as possible given the circumstances. Thank you for all of the words of encouragement, for always cheering me on and celebrating the little things with me.

Travis, thank you for all of the love and support you have given me over the years. You have always been there to listen, offer advice (or a cat – although, what is the difference really), and go on a spontaneous adventure. Thank you for reminding me that it is okay to enjoy the small things in life and to take things one step at a time. I am so thankful for you in every way. I would also like to acknowledge and thank our cats Kali, Pippin, Simon and Omen who have always been there for me throughout this degree. Even at 4:30 a.m.

Thank you to the University of Lethbridge and the Alberta RNA Research and Training Institute for giving me the opportunity to pursue my academic dreams, and for granting me my numerous scholarships over the years. The support has made a world of difference to me. Finally, thank you to the New Frontiers in Research Fund, which funded the work in this thesis.

Contents

List of Tables

List of Figures

List of Abbreviations

Abbreviation	Term
Apaf-1	apoptotic peptidase activating factor 1
BIR	baculovirus IAP repeat
BTIC	brain tumour initiating cell
cIAP1	cellular inhibitor of apoptosis protein 1
CITE	cap-independent translation enhancers
COL1A1	type-1 collagen
CrPV	cricket paralysis virus
DDE	delay-differential equation
EGFR	epidermal growth factor receptor
eIF	eukaryotic initiation factor
FGF	fibroblast growth factor
FTC	fundamental theorem of calculus
GEF	guanine nucleotide exchange factor
HCV	hepatitis-C virus
HER2	human epidermal growth factor receptor 2
IAP	inhibitor of apoptosis
ICD	interdigital cell death
IHC	immunohistochemistry
IRES	internal ribosome entry site
MGMT	O6-methylguanine-DNA methyltransferase
ODE	ordinary differential equation
PABP	poly-A binding protein
PCD	programmed cell death
PIC	canonical pre-initiation complex
PIC_{nc}	non-canonical pre-initiation complex
RBS	ribosome binding site
RIB	80S ribosome
RIB5B	eIF5B-bound 80S ribosome
RNAP	RNA polymerase

Abbreviation	Term
TC	canonical ternary complex
TC_{nc}	non-canonical ternary complex
TMZ	temolozomide
TNF	tumour necrosis factor
uORF	upstream open reading frame
UTR	untranslated region
XIAP	X-linked inhibitor of apoptosis

Chapter 1

Introduction

1.1 Motivation and Objectives

Glioblastoma is an extremely aggressive brain cancer that affects approximately 4 per every 100,000 Canadians each year [1], with a median survival of 15 months [2], and a 95% mortality rate within 5 years [3]. Glioblastoma accounts for approximately 54% of all gliomas, and 16% of brain tumors [4]. At present, there is no cure for patients suffering from glioblastoma. However, some treatment options aimed at reducing patient suffering are currently available, including surgery, radiation and chemotherapy, all of which have numerous associated complications. Traditional chemotherapies involve DNA-damaging agents such as temozolomide (TMZ), and have unfortunately been limited in success.

Glioblastomas tend to grow quickly, which results in hypoxic conditions within their cells [5]. Under these conditions, the alpha subunit of eIF2 is phosphorylated, resulting in its inability to deliver the initiator tRNA to the pre-initiation complex during canonical translation initiation [6]. However, glioblastoma cells can exploit a non-canonical translation initiation pathway that replaces eIF2 with eIF5B to deliver the initiator tRNA to the pre-initiation complex. This non-canonical pathways can be used to translate pro-survival mRNAs. Therefore, it is important to determine new targets within the eIF5B-mediated non-canonical translation initiation pathway involved in the survival of glioblastoma cells so that new treatment options may be derived for patients suffering from the disease. This pathway is discussed in detail in section 1.6.

1.2 Glioblastoma

Programmed cell death (PCD) is an important part of cell regulation, growth and development in organisms throughout their lifetime. Perhaps one of the most widely studied and well-known examples of programmed cell death is interdigital cell death (ICD), which results in defined, non-webbed digits [7]. Apoptosis is a form of programmed cell death, which is involved in numerous processes including ICD [8, 9, 7]. Misregulation of PCD has been linked to many diseases including cancer and Alzheimers, among others [10, 11].

The most commonly described pathways of apoptosis are the extrinsic and intrinsic pathways. In the extrinsic pathway, apoptosis is signalled by the binding of a death ligand to a tumour necrosis factor (TNF) death receptor [9, 10]. An adapter protein is then recruited to create a death-inducing signalling complex (DISC). Upon DISC formation, caspase-8 is activated, which then activates an executioner caspase, caspase-3, thereby initiating apoptosis [12].

Intrinsic apoptosis is induced upon changes in the mitochondrial permeability. This occurs when irreparable damage has been done to the DNA, or if the cell is under stress conditions such as hypoxia, among others [9, 10]. Under these conditions, pro-apoptotic proteins such as cytochrome-c are released into the cytoplasm. Upon release, an apoptosome complex is assembled, comprised of cytochrome-c, apoptotic peptidase activating factor 1 (Apaf-1) and caspase-9. This complex then activates caspase-3, thereby initiating apoptosis.

Inhibitors of apoptosis (IAPs) interact with and inhibit caspases by either promoting their degradation or by preventing them from interacting with their substrates [13, 14]. X-linked inhibitor of apoptosis (XIAP) is a protein involved in the regulation of cell death or apoptosis [15]. XIAP is a well characterized endogenous inhibitor of caspases with three baculovirus IAP repeat (BIR) domains, all three of which have a high affinity for caspases [14]. XIAP inhibits caspase-3 and -7 through the binding of its BIR2 domain and the region between BIR1 and BIR2 [14]. Additionally, XIAP's BIR2 domain blocks caspase-

3's substrate-binding pocket, thereby inhibiting caspase-3 [14, 16, 17]. Furthermore, XIAP promotes the degradation of caspase-3, which further enhances its anti-apoptotic effect [17].

Cancer cells avoid apoptosis through a number of pathways which can include the utilization of anti-apoptotic proteins such as XIAP [18]. XIAP is present in glioblastoma cells, and its high expression has been linked to glioblastoma cell survival [19]. *XIAP* mRNA is translated through a non-canonical pathway which utilizes eukaryotic initiation factor 5B (eIF5B) to deliver the initiator tRNA, a role normally played by eIF2 in the canonical pathway [18]. Recent evidence suggest that eIF5B is not essential for the survival of the cell [18, 20, 21]. Furthermore, eIF5B is over-expressed in many malignancies and it drives non-canonical translation of several proto-oncogenes [22, 23, 24]. Therefore, eIF5B may be a useful target for chemotherapy, as it plays a role in tumour growth and survival. Understanding the non-canonical translation initiation pathway may provide us with important information to aid in the development of new, innovative approaches to combat this mortal disease.

One such innovative approach includes the development and analysis of a mathematical model of non-canonical translation initiation to better understand the mechanistic role of eIF5B in glioblastoma cell survival, and determine whether it or other complexes are promising therapeutic drug targets. This thesis describes and analyzes a series of models: the non-canonical translation initiation mechanism involved in XIAP synthesis, four inhibition mechanisms that target the non-canonical pathway, either via eIF5B or other targets in the non-canonical pathway, and the canonical mechanism of protein synthesis focused on analyzing the effects of the inhibition mechanisms on the synthesis of important proteins such as type-1 collagen (COL1A1) and β-actin. Important questions I consider and attempt to answer in this thesis are: What concentration of eIF5B is required to inhibit the synthesis of anti-apoptotic proteins such as XIAP sufficiently to be an effective chemotherapy? To what extent can we target eIF5B without having too strong an effect on mRNA translation via the canonical pathway in non-tumour cells? Are there other possible therapeutic tar-

gets in the non-canonical translation initiation pathway? And to what extent can we direct a therapy towards these alternative targets without having too strong an effect on mRNA translation via the canonical pathway in non-tumour cells?

Several therapies are currently in clinical trial stages. These are discussed in section 1.3. Section 1.4 outlines and describes the canonical pathway. Section 1.5 discusses some cap-independent translation initiation mechanisms, as well as elements within the mRNAs that facilitate these mechanisms. The non-canonical eIF5B-mediated translation initiation pathway is described in section 1.6, which highlights eIF5B's mechanistic role in delivering the initiator tRNA to the 40S ribosome. Section 1.7 presents the mathematical methods used to derive the models analyzed and discussed in this thesis, and section 1.7.1 briefly discusses the software used in this thesis. The research questions and overview of the results are presented in section 1.8. This chapter concludes with an outline of this thesis in section 1.9.

1.3 Glioblastoma therapies

As noted above, temolozomide (TMZ) is the most common drug administered to patients with glioblastoma. Standard-of-care includes TMZ chemotherapy treatments in addition to radiotherapy. TMZ is a DNA alkylating agent that induces cell cycle arrest at the G2/M phase, which eventually leads to apoptosis [25]. About 50% of patients do not respond to the treatment [26]. In part, this is due to O6-methylguanine-DNA methyltransferase (MGMT), a DNA repair enzyme [26, 27].

Other drugs involved in glioblastoma treatment are currently being studied. These include: Depatux-M (ABT-414), which selectively kills tumor cells that over-express wild-type or mutant forms of epidermal growth factor receptor (EGFR) [28]; dendritic cell vaccine (DCVAX-L), which is a vaccine derived from patient dendrite cells used to aid the patient's immune system in targeting brain cancer cells [29]; enzastaurin, which is a protein kinase C inhibitor [30]; and LWW31, which is an eIF5B inhibitor [31]; among others. Some of these are already in clinical trials [28, 29, 30], while other therapies are still being

developed [31].

ABT-414 has reached phase II in clinical trials after promising phase I results [28]. However, the phase II results indicated that there was no significant effect on patient survival even in combination therapy with TMZ compared to standard-of-care. Unfortunately, the ABT-414 monotherapy group reported a clinically significant decrease in the global health of this group compared to the baseline, and visual disorders were also self-reported by patients in this group.

Interestingly, the DCVAX-L phase III trial showed promising results, with an increased mean survival of around 23.1 months, compared to 15 months typically observed with standard-of-care [29]. Additionally, only 2.1% of patients experienced serious adverse events related to the treatment, which included cerebral edema, seizures, nausea and lymph gland infection.

In a 2013 phase II trial, patients treated with enzastaurin had similar life expectancy rates as those receiving standard-of-care therapy [32]. The median overall survival was 15.0 months, and only 53.6% of patients were progression free at 6 months and alive after 12 months after treatment. About 66.7% of patients reported treatment-emergent adverse events related to enzastaurin, which included vertigo, nausea, vomiting, fatigue, pneumonia, brain edema, and pulmonary embolisms, among others.

To date, there is no therapy or combination of therapies that have been effective in completely curing the patient from glioblastoma. By far, the most promising therapy explored in this section is DCVAX-L, which showed a much longer median survival compared to standard-of-care. Additionally, across all reports, patients who underwent tumour resection, and combination therapy had the longest survival. Although several therapies are being studied and pursued, to my knowledge, only LWW31 focuses on the non-canonical translation initiation pathway involved in the synthesis of XIAP. Therefore, the information provided in this thesis will be instrumental in developing a novel medication for patients suffering from glioblastoma.

1.4 Cap-dependent canonical eukaryotic translation initiation

There are four primary steps in canonical eukaryotic translation initiation: the formation of the 43S pre-initiation complex (PIC), recruitment of the mRNA to the 43S PIC, scanning of the mRNA to find the AUG[1] start codon, and finally the assembly of the full 80S ribosome through the recruitment of the 60S subunit.

There are many eukaryotic initiation factors (eIFs) involved in the formation of the 43S PIC [34, 35]. In this step, eIF3 and eIF5 block the E site of the 40S ribosomal subunit, and eIF1 blocks the A site so that the initiator aminoacyl tRNA, Met-tRNA$_i$, can be introduced to the P site. This is illustrated in step (A) in figure 1.1. This Met-tRNA$_i$ is recruited by eIF2, and with the addition of GTP, creates a ternary complex (TC). The TC is placed in the P site, and eIF2 then works with eIF1 to continue blocking the A site of the 40S ribosomal subunit. This is step (B) in figure 1.1.

In order to recruit the mRNA to the 40S subunit, eIF4E, 4G, and poly-A binding protein (PABP) bind to the 5' m^{7}G cap (henceforth referred to as the 5' cap) at the 5' end of the mRNA. The poly-A tail folds back to bind to PABP and eIF4G to form a loop-like structure [35]. eIF4G then recruits eIF3 on the PIC. These are illustrated in steps (C) and (D) in figure 1.1.

At the start of the scanning process, the 43S PIC is already assembled, however the Met-tRNA$_i$ is not in the typical binding orientation, despite its location in the P site. Only when the PIC reaches the AUG start codon does it have the proper base pairing on the mRNA to be positioned in the typical tRNA binding orientation. At this occurrence, eIF5 induces the GTPase activity of eIF2, which hydrolyzes the GTP, resulting in the dissociation of GDP and eIF2 from the complex [35, 36]. This step is illustrated in step (E) in figure 1.1.

After the start codon is reached, eIF5B binds to the 48S PIC and recruits the 60S riboso-

[1]Translation can initiate at other codons rather than AUG, but at a much lower efficiency, and non-canonical start codons often only differ from AUG by one nucleotide [33]. There are more non-canonical than canonical start codons in an mRNA, however, since the AUG start codon has the highest efficiency, it is typically selected in translation initiation. Upstream and downstream elements enhance this difference in efficiency.

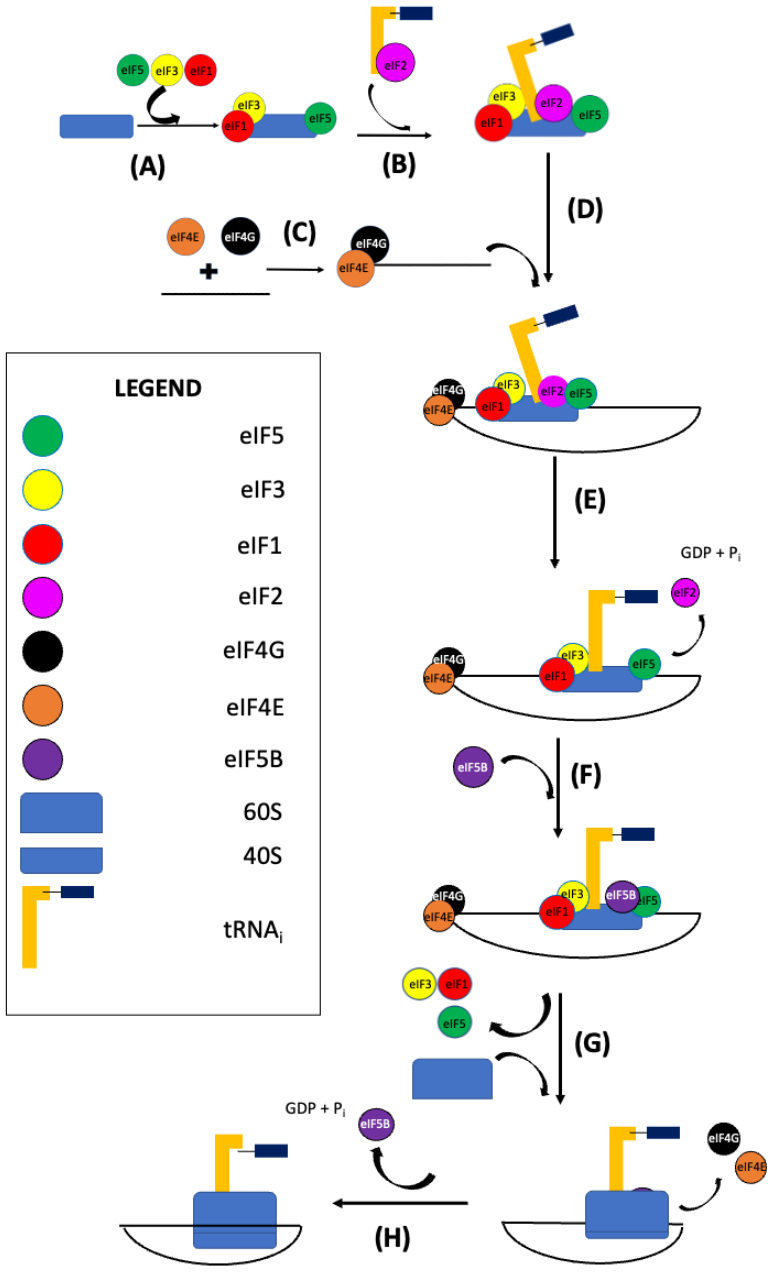

Figure 1.1: The canonical translation initiation mechanism. Steps (A)–(D) show the synthesis of the 48S PIC and eIFs 4G and 4E binding to the 5' cap of the mRNA. Steps (E) and (F) show ribosome scanning for the AUG start codon, and GTP hydrolysis and dissociation of eIF2, followed by eIF5B recruitment to the pre-initiation complex. Step (G) shows the dissociation of eIFs 1, 3 and 5, and the recruitment of the 60S ribosomal subunit to the pre-initiation complex. Finally, the GTP on eIF5B is hydrolyzed in step (H) and eIF5B dissociates from the complex, resulting in the fully assembled 80S ribosome.

mal subunit [37, 38]. In addition to this role, recent cryoEM studies have highlighted eIF5B contacts with the Met-tRNA$_i$ [39]. These contacts stabilize the initiator tRNA at the P-site through domains III and IV of eIF5B [40]. When the initiator tRNA is in the proper position, initiation factors 1, 3, and 5 dissociate from the complex, which is followed by 60S binding resulting in the formation of the assembled 80S ribosome [41, 42, 43]. Upon this assembly, initiation factors 4E and 4G leave the initiation complex [35]. The GTP on eIF5B is then hydrolyzed, and the ribosome transitions into the elongation phase of translation. These final steps are illustrated in steps (F)–(H) in figure 1.1.

It should be noted that previous research has indicated that eIF5B does not have a guanine nucleotide exchange factor (GEF), as its affinities for GTP and GDP are less than an order of magnitude in difference, and they both dissociate quickly [44]. The consequences of this with respect to this thesis are explained further in chapter 4.

1.5 Cap-independent translation initiation

There are a variety of elements within an mRNA that impact its translation. Perhaps the most commonly known element is the AUG start codon, however, as was already mentioned earlier, there are other possible start codon sequences.

As noted earlier, the pre-initiation complex that assembles at the 5' cap facilitates translation initiation. However, some cellular mRNAs have sequences within their 5' untranslated regions (UTRs) that can facilitate translation initiation without the need for the cap structure. These are known as internal ribosome entry sites (IRESs) [45]. IRES elements were originally discovered in viral RNAs [46]. These IRES sequences result in specific secondary and tertiary structures that can recruit the small ribosomal subunit without the need for an mRNA cap structure [18, 21, 47]. The mechanism of initiation also varies, as the initiation factors required are different, and scanning is not a requisite to find the AUG start codon for some IRESs. Some IRES structures resemble that of a tRNA, which facilitates the binding of the small ribosomal subunit, and sometimes the IRES-containing mRNA

binds in such a way that scanning for the AUG codon is not needed [48]. Additionally, some IRESs have a similar function to the Shine-Dalgarno sequence in bacteria to facilitate the proper placement of the mRNA on the 43S PIC [49]. Interestingly, approximately 10% of mRNAs in humans contain a functional IRES sequence [50]. The non-canonical mechanism using an IRES element is further elaborated upon in the next subsection.

Cancer cells use and exploit non-canonical translation mechanisms to facilitate their growth and survival when the canonical mechanism is not available to them due to consequences of stress conditions. The mechanism of interest for this thesis is the eIF5B-mediated translation initiation on the IRES-containing mRNA mechanism which is described in the next subsection.

Although they are not used in this study, it is important to recognize that there are a number of other cap-independent mechanisms used in protein translation. Indeed, even within the IRES classification, there is great diversity as there are four groups of viral IRESs, and two types of cellular IRESs [48]. In addition to IRES elements, some eukaryotic mRNAs include cap-independent translation enhancers (CITEs) [51], which recruit initiation factors and assemble the ribosome. It is clear that there are a number of ways for translation initiation to occur, and although this thesis primarily focuses on two pathways (non-canonical cap-independent eIF5B-mediated translation initiation, and canonical cap-dependent translation initiation), it is important to acknowledge and appreciate the diversity within translation initiation mechanisms.

1.6 Non-canonical eIF5B-mediated translation initiation

A different mechanism of translation initiation can occur when the cell is under stress conditions. One such common stress condition is hypoxia, which occurs when the cell has a low oxygen concentration. Hypoxia is common in tumours, as the cancerous cells grow and replicate at elevated rates. The challenges in providing the core of a rapidly growing tumour with both nutrients and oxygen results in what is known as the necrotic core, the

inner part of the tumour that is comprised of dead cancer cells [52, 53, 54]. Under hypoxic conditions, the α subunit on the majority of the cellular eIF2 is phosphorylated, and thus its ability to bring the Met-tRNA$_i$ to the 43S PIC is reduced [6]. In this case, eIF5B can replace eIF2, and recruit the Met-tRNA$_i$ to the complex, which is comparable to the translation process in bacteria [6]. In fact, eIF5B is an analog to IF2 [34], which is the bacterial translation factor that creates a ternary complex with the initiator tRNA. Additionally, the eIF5B-mediated non-canonical pathway is not cap-dependent, and therefore the eIFs needed for non-canonical translation initiation are slightly different. In fact, the PIC can interact with the AUG codon on the mRNA without the involvement of eIFs 4F, 4A, 4B, 1, and 1A [21]. In some cases, eIF3 and eIF5B are the only initiation factors required for translation initiation of an mRNA containing an IRES [21, 6].

As noted above, this non-canonical pathway is bacterial-like. The non-canonical pathway can therefore be broken down into four distinct steps: the formation of the pre-initiation complex comprised of eIF3 and the 40S ribosomal subunit (illustrated in step (A) in figure 1.2), recruitment of the mRNA to the PIC (illustrated in step (B) of figure 1.2), recruitment of the non-canonical ternary complex (TC$_{nc}$) comprised of eIF5B, Met-tRNA$_i$ and a GTP molecule (illustrated in step (C) of figure 1.2), and the final assembly of the 80S ribosome (illustrated in steps (D) and (E) in figure 1.2). Note that, unlike in the canonical pathway, the mRNA is recruited to the 43S PIC *before* the TC$_{nc}$ is bound.

The non-canonical translation pathway promotes cell survival, despite being under stress conditions that could, if prolonged, trigger apoptosis. The IRES-mediated mechanism described here is used in the translation of anti-apoptotic proteins such as XIAP [18], and has been linked to the survival of glioblastoma cells as well [20]. This thesis will use *XIAP* as an example IRES-containing mRNA to understand the role of eIF5B in non-canonical translation initiation.

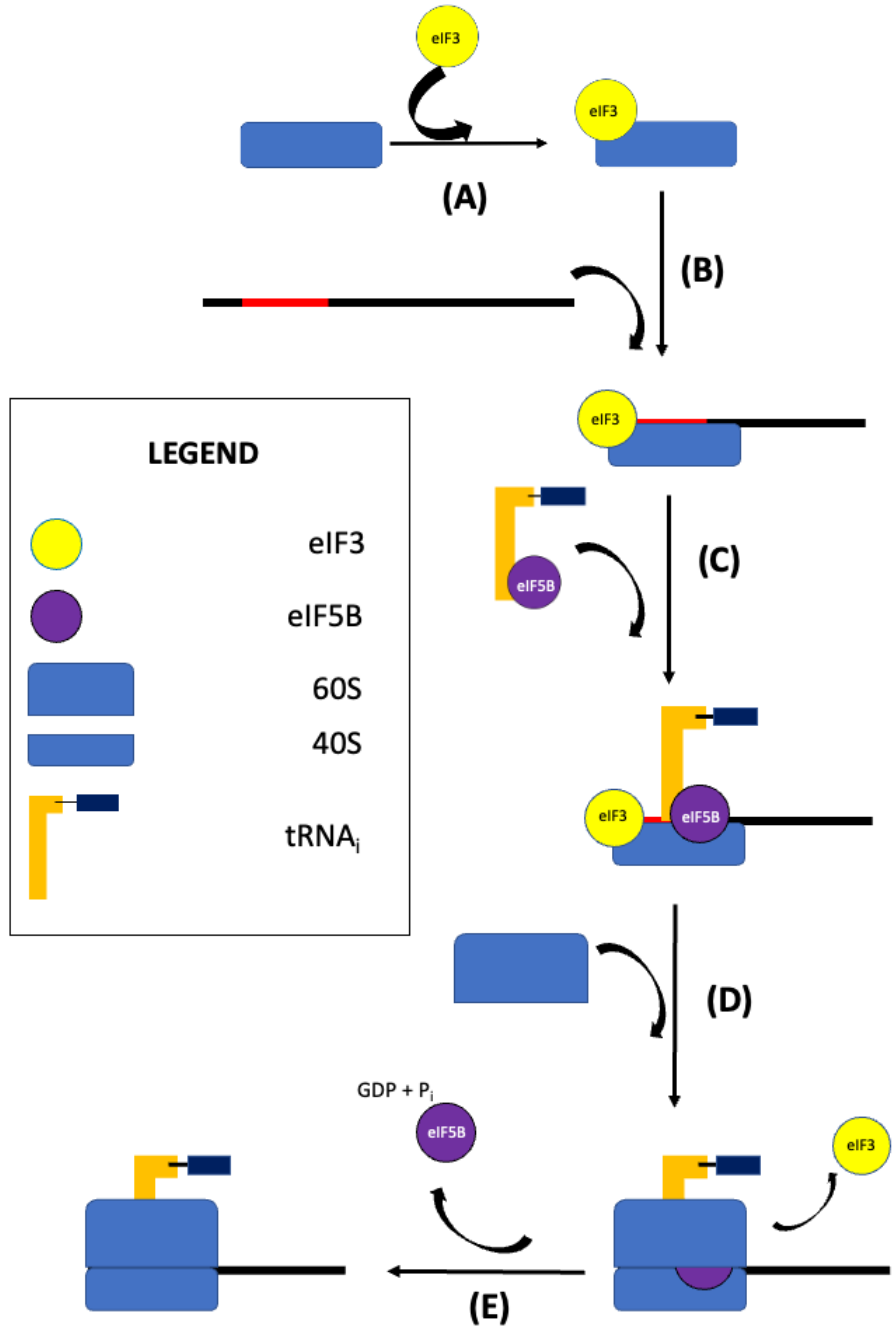

Figure 1.2: The eIF5B-mediated translation initiation mechanism. Step (A) shows eIF3 binding to the 40S ribosome. Step (B) shows the IRES-containing mRNA recruitment to the pre-initiation complex. The eIF5B-TC is recruited to the pre-initiation complex in step (C). The 60S subunit binds to the pre-initiation complex in step (D), which triggers the dissociation of eIF3. Finally, the GTP on the eIF5B is hydrolyzed, and eIF5B dissociates from the pre-initiation complex, resulting in a translation-competent ribosome.

Although eIF5B is involved in both pathways, the literature suggests it plays a critical role in the facilitation of the non-canonical pathway that favours glioblastoma cell survival [42].

1.7 Mathematical modeling

Chemical and biochemical systems can be represented by a series of chemical equations, which can, in turn, be transformed into a series of ordinary differential equations (ODEs) using the law of mass action. Deterministic differential-equation modeling methods were used throughout the entirety of this study. There are approximately 10^6 free ribosomes and 15×10^6 molecules of initiator tRNA in the cell [55, 56]. Without ribosomes and initiator tRNA molecules, translation and, particularly, translation initiation cannot occur. As these two critical components of translation initiation are abundant in the cell, we can consider their concentrations to be constant throughout the calculations, as the fluctuations in their concentrations will be inconsequential compared to their initial concentrations. Although the concentration of mRNA is not present at the same scale, we can still use deterministic modeling methods as a predictive tool. Deterministic models, such as ODE models, look at averages in homogenous systems [57], which will be described later in this section. Deterministic differential-equation models provide fast and efficient simulations. Therefore, these models are useful in preliminary analysis of biochemical systems, and particularly in the systems described above. Predicting the properties (such as the necessary concentration and K_D for 50% reduction in translation competent ribosomes) of potential inhibitors to be used in a chemotherapy is an important first step in deciding whether the inhibitor is promising, which is a critical discussion point of this thesis. Although ODE models are useful, pure mass-action models may turn out to be excessively detailed. Therefore, other modeling techniques need to be used so that the focus remains on the essential interactions rather than assembling a large model that provides little insight.

One technique is to apply delays to the model which results in delay-differential equa-

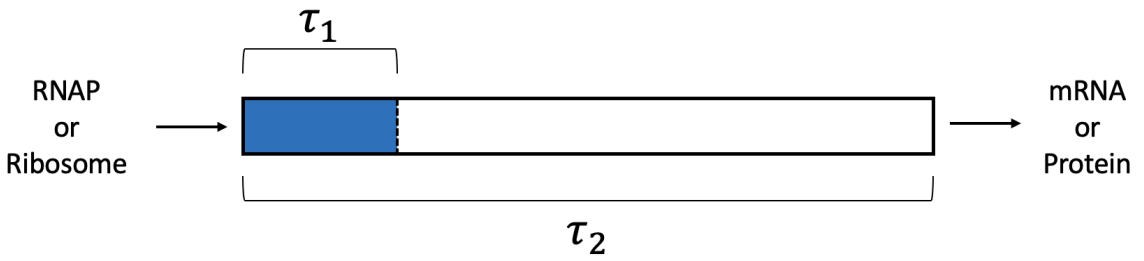

Figure 1.3: Delays in eukaryotic canonical gene expression. The RNA polymerase (RNAP) binds to the promoter region on the DNA, and it takes some time, τ_1, for the promoter to become available again. Similarly, the ribosome binds to the ribosome binding site (RBS) on the mRNA, and it takes some time, τ_1, for that to become available again. In this figure, therefore, τ_1, represents the clearance delays in either transcription or translation. It takes some time, τ_2, for either the mRNA to be transcribed or the protein to be translated, and therefore τ_2 represents the synthesis delays in gene expression. The highlighted blue box represents the promoter region of the DNA or the RBS on the mRNA.

tions (DDEs). Although some reactions can occur quickly, biochemical systems in particular do not operate on instantaneous time scales. That is, it takes time for cells to perform specific functions such as metabolize sugars, or transcribe and translate mRNAs. In gene expression, there are two forms of delays that need to be considered within their respective mathematical models: clearance delays, which describe the time required to clear the promoter region on the DNA during transcription, or the ribosome binding site (RBS) during translation; and synthesis delays, which account for the time required to transcribe the mRNA or translate a protein. These delays are illustrated in figure 1.3.

Delays are necessary to consider when constructing a mathematical model. Even small clearance delays should not be dismissed. During a previous study, we analyzed two models that represented the same biochemical system, one of which contained clearance delays, and the other not [58]. Unless *ad hoc* adjustments to a binding constant were made, which is generally regarded as poor practice [59], the two models produced different qualitative and quantitative results. A similar observation is made in this thesis as well in chapter 3.

One of the difficulties that comes with mathematical modeling is the absence of quantitative data. Some rate constants and binding constants are difficult to measure experimentally, and some simply have not been measured. Furthermore, biological concentrations

of species are not always consistent. Depending on the conditions within and surrounding the cell, and the stage of the cell cycle, some proteins are either up-regulated or down-regulated, which help to maintain homeostasis within the cell, or signal cell death, among others. Additionally, some concentrations of biological molecules have been measured, but not in the organism or tissue of interest. Therefore, it is sometimes necessary to infer or approximate values. The concern is that results are dependent on the parameters of the model, and if the parameters are unknown or imprecisely known, this may impact the data accumulated from a mathematical study. However, there are ways to understand the effects of the approximated parameters on the results. There are some mathematical analyses that can suggest which parameters would be most important to measure, and which might be less important. One way that is utilized in this thesis is sensitivity analysis. There are two forms of sensitivity analyses: global sensitivity analysis, where the behaviour of the system is addressed over a wide range of operating conditions; and local sensitivity analysis, in which a particular set of parameter values is focused on [60]. This thesis utilizes local sensitivity analysis methods to evaluate the effect of the unknown or approximated parameters on the system.

There are two kinds of outputs of local sensitivity analyses: absolute sensitivities and relative sensitivities. Local absolute sensitivities represent a variable's sensitivity to a parameter at a specific value, or $\frac{\partial x}{\partial k}$, where x is the steady-state concentration of a variable of the system, and k is a parameter. Relative sensitivities are dimensionless, that is they have no units. Similarly to absolute sensitivities, they represent the dependence of a variable on a parameter, however, they provide relative changes. These calculations are further discussed in section 3.2.

There are a number of other mathematical modeling methods available to study chemical and biochemical systems. Earlier it was mentioned that the metabolism of sugars does not occur on an instantaneous time scale. In addition, metabolism models can be quite complex mechanistically. Moreover, parameterization of the models can be difficult, as

Michaelis constants are typically reported in the literature, rather than binding constants or dissociation constants. Therefore, considering other modeling frameworks can be useful.

Stochastic models have some advantages compared to deterministic models depending on the system. In particular, stochastic models include randomness, whereas deterministic models such as ODE models look at averages in homogenous systems [57]. Mathematical biological studies often use stochastic modeling as fluctuations in concentrations become more important in small populations [61]. In large populations, these fluctuations are often lost as we average the results together. The result of averaging a stochastic process describing a linear chemical system is a set of ODE equations [57]. ODE models, such as those explored in this thesis, consider homogenous, that is, well mixed, systems. This, of course, is difficult to achieve when concentrations of species are very small. However, deterministic methods are simpler, and more easily applied, analyzed and understood. They also provide specific outputs and valuable insight to the dynamics of the system of interest, which we will observe and discuss in chapters 3 and 4 of this thesis. Stochastic modelling methods produce a range of possible outcomes, and therefore are useful when considering small populations and/or distributions.

1.7.1 Mathematical modeling tools

There are a number of different programs available to perform analyses on mathematical models. The software packages used in this thesis were Copasi (v. 4.29), Matlab 2021 and Maple 2021. Each was chosen for its specific strengths. Copasi is a user-friendly, versatile tool that can perform numerous analyses on models such as steady-state analyses, time courses, sensitivity analyses, metabolic control analyses, and much more. However, it cannot perform analysis on models with delays. Matlab is well-known for its differential-equation integrator capabilities, and can perform analyses on models with delays such as time course and bifurcation analyses, among others. Maple is a symbolic algebra program that can integrate equations and perform a number of other analyses on equations with

delays including time course analysis, sensitivity analyses and bifurcation analyses, and much more. Although all three were used in this thesis, the majority of the calculations and analyses were performed using Maple (2021).

1.8 Research questions and results overview

Before any new therapies can be developed, it is important to ask the following questions: To what extent should the concentration of eIF5B be reduced to effectively inhibit the non-canonical mechanism outlined above? What kind(s) of inhibitor(s) are required to inhibit this pathway to attain that concentration? What parts of the mechanism are suitable for inhibition such that it does not severely impact canonical translation initiation? At what concentration of eIF5B is the canonical mechanism impacted? How dependent are the two mechanisms on eIF5B? What properties (e.g. concentrations and disassociation constants) of the inhibitor(s) are necessary for the most efficient inhibition with minimal negative effects on the patient?

There are a number of different inhibition target possibilities, as are discussed in detail in section 3.3. Obviously, the greater the binding constant, or smaller the dissociation constant, and the higher the concentration of the inhibitor, the greater the level of inhibition is. However, high concentrations of chemotherapy can be generally toxic to the patient, as well as dangerous to other biological mechanisms, namely the canonical translation initiation mechanism in this case. Therefore, there is a trade-off that must be considered when designing a new therapy to inhibit the eIF5B-mediated non-canonical translation initiation mechanism. Fortunately, the canonical mechanism is not locally sensitive to fluctuations in the concentration of eIF5B, as found in chapter 4, which leads to the best inhibitors being those that target eIF5B directly, or the eIF5B-TC involved in delivering Met-tRNA$_i$ to the pre-initiation complex. The effects of introducing these inhibitors to the canonical mechanism are explored using two example proteins, type-1 collagen and β-actin in chapter 4.

1.9 Thesis outline

The next few chapters explore a number of mathematical models relating to the mechanisms described above. Chapter 2 constructs and analyzes the IRES and eIF5B-mediated non-canonical translation initiation mechanism without the inclusion of a clearance delay. Chapter 3 outlines and analyzes the non-canonical model with a clearance delay, as well as four inhibition mechanisms, providing the local sensitivity analysis results of each. Chapter 4 describes and analyzes the canonical model, the effects of the inhibition mechanisms at both hypoxic and unstressed conditions, and provides the results of local relative sensitivity analyses. A discussion of the results obtained throughout the thesis is provided in chapter 5. Finally, chapter 6 includes some concluding remarks and offers some potential future initiatives.

Chapter 2

eIF5B-mediated translation initiation without a clearance delay

2.1 Non-canonical model - no delay

We will start by analyzing the following model for non-canonical translation initiation formalized from figure 1.2, where the subscript *nc* identifies non-canonical complexes, PICm_{nc} is a pre-initiation complex, TC$_{nc}$ represents the ternary complex formed by eIF5B, the initiator tRNA, and a GTP molecule (not shown),[2] RIB5B is the assembled ribosomal complex containing bound eIF5B, and RIB is the completely assembled ribosomal initiation complex ready to enter into the elongation phase of translation:

$$40S + \text{eIF3} \underset{k_{-1}}{\overset{k_1}{\rightleftharpoons}} \text{PIC1}_{nc} \tag{2.1a}$$

$$\text{PIC1}_{nc} + \text{mRNA} \underset{k_{-2}}{\overset{k_2}{\rightleftharpoons}} \text{PIC2}_{nc} \tag{2.1b}$$

$$\text{eIF5B} \; + \; \text{tRNA}_\text{i} \underset{k_{-3}}{\overset{k_3}{\rightleftharpoons}} \text{TC}_{nc} \tag{2.1c}$$

$$\text{PIC2}_{nc} + \text{TC}_{nc} \underset{k_{-4}}{\overset{k_4}{\rightleftharpoons}} \text{PIC3}_{nc} \tag{2.1d}$$

$$\text{PIC3}_{nc} + 60S \underset{k_{-5}}{\overset{k_5}{\rightleftharpoons}} \text{PIC4}_{nc} \tag{2.1e}$$

$$\text{PIC4}_{nc} \xrightarrow{k_6} \text{RIB5B} + \text{eIF3} \tag{2.1f}$$

$$\text{RIB5B} \xrightarrow{k_7} \text{RIB} + \text{eIF5B} + \text{mRNA} \tag{2.1g}$$

[2]The GTP molecule is not shown in the mechanism, as this model operates under the assumption that eIF5B binding to the initiator tRNA is the rate limiting step in this process.

Table 2.1: Abbreviations for the biochemical complexes present in the eIF5B-mediated translation initiation model without a clearance delay.

Biological Complex	Abbreviation
40S· eIF3	$PIC1_{nc}$
40S· eIF3· mRNA	$PIC2_{nc}$
40S· eIF3· mRNA· TC_{nc}	$PIC3_{nc}$
RIB5B· eIF3	$PIC4_{nc}$
80S · eIF5B	RIB5B
80S	RIB

A table of the biochemical complex abbreviations is found in table 2.1.

It is important to note that equations (2.1f) and (2.1g) are not reversible, as we assume it is more thermodynamically favourable for the process to proceed and create the completed initiation complex than it is to reassemble either of the reactant complexes. There is evidence to support this, as when eIF5B binds to the PIC, it displaces eIF3 (and other eIFs in the canonical pathway), suggesting that the binding of eIF5B induces a conformational change of the 40S ribosomal subunit, thus lessening its binding affinity for the other eIFs [62]. However, the 60S subunit binds quickly (i.e. less than 4 seconds) after eIF5B has bound in the canonical pathway [37], and is assumed to bind quickly in the non-canonical pathway as well. Therefore, as no data was available to the best of my knowledge regarding the precise step when eIF3 dissociates in the non-canonical pathway, eIF3 was assumed to dissociate after the 60S binding step. Finally, (2.1g) is not reversible due to the hydrolysis of GTP, resulting in the dissociation of eIF5B as shown in step (E) of figure 1.2.

2.2 Parameters

As mentioned previously, *XIAP* is an example of a mRNA that, under hypoxic conditions, is translated using a non-canonical mechanism. Throughout the eIF5B-mediated translation initiation chapters of this thesis, *XIAP* is used as an mRNA to analyze the mechanistic role of eIF5B.

XIAP (Uniprot ID: P98170) is a protein comprised of 497 residues [17, 63]. *XIAP*

mRNA is translated through an eIF5B-mediated translation initiation pathway described above [18], and, as previously mentioned, XIAP is an anti-apoptotic protein involved in glioblastoma [19, 20].

As mentioned previously, some binding constants and other relevant data have not been measured in the species or tissue of interest. Such is the case for many binding constants required for the construction and analysis of this model. Therefore, some of the dissociation constants used in this model were borrowed from interactions within different species (primarily yeast), or from interactions with the HCV IRES, as the translation initiation mechanism for the HCV virus is similar to that of the eIF5B-mediated translation initiation pathway described above [6].

The K_D of eIF3 interacting with the 40S subunit in humans is 6 nM [64]. The K_D of eIF5B binding to Met-tRNA$_i$ is 2.7 μM [65]. The IRES binds to the 40S subunit in two steps: a fast and a slow step [66]. The fast step is the initial binding to the small subunit,

$$40\text{S} + \text{mRNA} \underset{k_{-a}}{\overset{k_a}{\rightleftharpoons}} 40\text{S}\cdot\text{mRNA}$$

where $k_a = 0.017\,\text{nM}^{-1}\text{s}^{-1}$, and $k_{-a} = 0.07\,\text{s}^{-1}$, which results in a K_D value of approximately 4.2 nM [66]. The next step is a slow step isomerization step. The K_{RI} (reverse isomerization equilibrium constant) is 0.055. Taken together, this results in an overall K_D of 0.23 nM. However, these rate constants were measured for the cricket paralysis virus (CrPV) 40S–IRES complex in the absence of any other factors including eIF3. Additionally, the time it takes for the isomerization step may vary depending on the species. Moreover, *CrPV* contains a viral IRES whose translation does not require any other factors, whereas *XIAP* contains a cellular IRES whose translation depends on both eIF3 and eIF5B. Therefore, as this study examines the *XIAP* IRES in the presence of eIF3 and eIF5B in humans, the K_D for the IRES binding to the 40S subunit was approximated to be 1 nM, which is approximately one order of magnitude greater than the calculated value above.

After the 80S ribosome has been assembled in the canonical pathway, eIF5B takes approximately 29.1 s to hydrolyze GTP and dissociate from the complex [37]. For a first-order reaction, the average time is $\frac{1}{k}$. Therefore,

$$k_7 = \frac{1}{29.1\,\mathrm{s}} = 0.035\,\mathrm{s}^{-1}.$$

As there is no difference between the non-canonical and canonical RIB5B complexes, the same rate constant for eIF5B dissociation was used.

2.2.1 Value approximations

A model of canonical translation was published previously [56], which included a Copasi input file. Using this model, several calculations were performed which are outlined below to establish conditions that were true to the cellular environment. Some modifications were made to this model to simulate stress conditions which are explained below.

Recall that this non-canonical pathway is chosen under hypoxic stress conditions that result in the phosphorylation of eIF2α. When this subunit is phosphorylated, it inhibits its guanine nucleotide exchange factor eIF2B when the two bind together [67], and therefore, its GDP is unable to be exchanged for GTP. Moreover, eIF2 binds to eIF2B in a 2:1 ratio, and eIF2B and $\mathrm{tRNA_i}$ compete for the same active site on eIF2α [67].

To simulate the effect of the previously mentioned phosphorylation of eIF2α, the model by Firczuk *et al.* (2013) [56] was consulted, and the concentration of eIF2-GDP was decreased 10-fold, while the concentration of eIF2B was decreased 5-fold, as per the previously mentioned 2:1 ratio. No data was available on the level of phosphorylation to the best of my knowledge, however, as was noted in section 1.6, it is known that the majority of eIF2 is phosphorylated [6], so a 10-fold estimate was considered. A steady-state calculation was performed, and these values were used for the total concentrations of eIF3, eIF5B, $\mathrm{tRNA_i}$, 40S, and 60S, as these concentrations represented the *free* species available to perform non-canonical translation initiation. After the steady-state calculation, this yielded the

total concentrations of 40S, 60S, eIF3, eIF5B and $tRNA_i$, which can be found in table 2.3.

At any given time in the cell cycle, there are some $PIC1_{nc}$ complexes available. This value does not and should not start at zero when analyzing the transient behaviour of the system, as will be explored further in the next chapter. Therefore, the steady-state concentration of $PIC1_{nc}$ should be solved for. We begin by using an ICE chart for step (2.1a) to solve for $PIC1_{nc}$ using the expression for K_D:

$$K_{D_{PIC1}} = \frac{[40S]_T(x)}{[eIF3]_T - x},$$

where x is the concentration of eIF3 in μM at the steady-state, $[eIF3]_T - x$ is the concentration of $PIC1_{nc}$, and $K_{D_{PIC1}} = 6\,nM$ [64]. This resulted in a linear expression, where [eIF3] = $2.3\times10^{-4}\mu$M and [$PIC1_{nc}$] = 0.2098μM. The concentrations calculated in this analysis are found in table 2.2.

As mentioned earlier, the cellular concentration for eIF5B in the cell fluctuates, therefore, the free steady-state concentration of eIF5B·GTP calculated using the model by Firczuk *et al.* [56] was used. After running the above steady-state calculation considering the phosphorylation of eIF2, the concentration of eIF5B·GTP was $0.20\,\mu$M.

A similar procedure was performed to solve for [TC_{nc}]:

$$K_{D_{TC}} = \frac{[tRNA_i]_T(y)}{[eIF5B]_T - y}.$$

where y is steady-state concentration of eIF5B, $[eIF5B]_T - y$ is the concentration of TC_{nc}, and $K_{D_{TC}} = 2.7\,\mu$M [65]. This results in a linear expression where $[eIF5B] = 0.019\,\mu$M, and $TC_{nc} = 0.18\mu$M. The resulting concentrations are found in table 2.2.

No quantitative data was available for the rate constant describing the rate of dissociation of eIF3 from the 80S complex, therefore this value was assumed to be the same as eIF3 dissociation from the 40S subunit, which was previously reported by Fraser *et al.* (2007) [64]. To the best of my knowledge, values were not available for k_4, k_{-4}

Table 2.2: Approximated values in the non-canonical model without a clearance delay. [c] is a calculated value. Concentrations of translation initiation factors (μM) were calculated using the model provided by Firczuk *et al.* (2013) [56] via the procedure outlined in section 2.2.

Parameter	**Concentration (μM)**	**Source**
$[\text{eIF3}]_\text{T}$	0.21	[c][56]
[eIF3]	2.3×10^{-4}	[c]
$[\text{40S}]_\text{T}$	5.3	[c][56]
$[\text{PIC1}_{nc}]$	0.2098	[c]
$[\text{eIF5B}]_\text{T}$	0.20	[c][56]
[eIF5B]	0.019	[c]
$[\text{tRNA}_\text{i}]_\text{T}$	26	[c][56]
$[\text{TC}_{nc}]$	0.18	[c]

and k_{-5}. Concentration values and transcript numbers for *XIAP* mRNA were not available. An average number of transcripts from Schwannhausser (2011) [68] was approximately 40 transcript copies per average cell for those whose levels were able to be measured. This was assumed to be the basal level of expression for *XIAP* mRNA. However, the expression of XIAP is up-regulated in glioblastoma cells nearly 30-fold [19]. Therefore, a copy number of 1,200 transcripts per cell was used, generating a concentration of approximately $2.0 \times 10^{-3}\,\mu$M, assuming the volume of a eukaryotic cell is 10^{-12} L [69, 70]. A list of parameter values is found in table 2.3 with calculated values ([c]) from the data provided above, references if the direct data was available, or assumed values ([a]) if data was not available.

The rate constants provided in table 2.3 were calculated from the dissociation constants reported in the literature. These rate constants were calculated with the assumption of an efficient initiation process, that is one in which the process proceeds forward with little dissociation and re-association of species impacting the rate of translation initiation. For example, in step (2.1a), we assume that after eIF3 binds to the 40S, it tends to stay bound rather than dissociate. Unless the forward and/or reverse rate constants were known, they were calculated or assumed with this forward-biased initiation pathway in mind. For example, let's consider step (2.1c). The K_D for this step is $2.7\,\mu$M [65]. Therefore, via this forward-

biased approach, the forward rate constant was preliminarily chosen to be $1\,\mu\mathrm{M}^{-1}\mathrm{s}^{-1}$, and the reverse rate constant to be $2.7\,\mathrm{s}^{-1}$. However, the forward rate constant for TC synthesis in canonical translation is $0.11\,\mu\mathrm{M}^{-1}\mathrm{s}^{-1}$. As the eIF2-TC is the prominent TC in canonical translation initiation, the forward rate constant in the non-canonical pathway should be smaller than that in the canonical pathway. Therefore, the forward and reverse rate constants for TC_{nc} synthesis were decreased 100-fold to $0.01\,\mu\mathrm{M}^{-1}\mathrm{s}^{-1}$ and $0.027\,\mathrm{s}^{-1}$, respectively, to account for the cell choosing the eIF2-TC under unstressed conditions.

The reason for the forward-biased assumption is perhaps more apparent in the next chapter, however, it is beneficial to highlight here as well. If the process of initiation is assumed to be as efficient as possible, then the inhibitors proposed to inhibit this eIF5B-mediated non-canonical mechanism will also be optimized to be the most efficient. In other words, when we examine the properties of possible inhibitors, as we do in the next chapter, the effective concentrations will be at the uppermost limit, and the effective dissociation constants will be at the lowermost limit, thus providing future researchers with parameter limits in their following experiments.

2.3 Constructing the eIF5B-dependent non-canonical translation initiation model without a clearance delay

Now that we have derived expressions for $\mathrm{PIC1}_{nc}$ and TC_{nc} in terms of eIF3 and eIF5B, respectively, we can construct the rest of the model. Before the law of mass action is applied to the model in section 2.1, we must consider the mass conservation relations, primarily those of eIF3, mRNA, and eIF5B. These are as follows:

$$[\mathrm{eIF3}]_\mathrm{T} = [\mathrm{eIF3}] + [\mathrm{PIC1}_{nc}] + [\mathrm{PIC2}_{nc}] + [\mathrm{PIC3}_{nc}] + [\mathrm{PIC4}_{nc}], \tag{2.2a}$$

$$[\mathrm{mRNA}]_\mathrm{T} = [\mathrm{mRNA}] + [\mathrm{PIC2}_{nc}] + [\mathrm{PIC3}_{nc}] + [\mathrm{PIC4}_{nc}] + [\mathrm{RIB5B}], \tag{2.2b}$$

$$[\mathrm{eIF5B}]_\mathrm{T} = [\mathrm{eIF5B}] + [\mathrm{TC}_{nc}] + [\mathrm{PIC3}_{nc}] + [\mathrm{PIC4}_{nc}] + [\mathrm{RIB5B}], \tag{2.2c}$$

Table 2.3: Table of parameters in the non-canonical model without a clearance delay. [a] is approximated value. [c] is calculated value. Concentrations of parameters (μM) were calculated using the model provided by Firczuk *et al.* (2013) [56] via the procedure outlined in section 2.2.

Parameter	**Value**	**Source**
k_1	$1000\,\mu\mathrm{M}^{-1}\mathrm{s}^{-1}$	[c][64]
k_{-1}	$6\,\mathrm{s}^{-1}$	[c][64]
k_2	$1000\,\mu\mathrm{M}^{-1}\mathrm{s}^{-1}$	[c][71]
k_{-2}	$2\,\mathrm{s}^{-1}$	[c][71]
k_3	$0.01\,\mu\mathrm{M}^{-1}\mathrm{s}^{-1}$	[c][65]
k_{-3}	$0.027\,\mathrm{s}^{-1}$	[c][65]
k_4	$1000\,\mu\mathrm{M}^{-1}\mathrm{s}^{-1}$	[a]
k_{-4}	$1\,\mathrm{s}^{-1}$	[a]
k_5	$0.81\,\mu\mathrm{M}^{-1}\mathrm{s}^{-1}$	[72]
k_{-5}	$1\,\mathrm{s}^{-1}$	[a]
k_6	$6\,\mathrm{s}^{-1}$	[a]
k_7	$0.035\,\mathrm{s}^{-1}$	[37]
$[\mathrm{eIF3}]_\mathrm{T}$	$0.21\,\mu\mathrm{M}$	[c][56]
$[\mathrm{eIF5B}]_\mathrm{T}$	$0.20\,\mu\mathrm{M}$	[c][56]
$[\mathrm{mRNA}]_\mathrm{T}$	$2.0\times10^{-3}\,\mu\mathrm{M}$	[a][19, 68]
$[\mathrm{tRNA_i}]$	$26\,\mu\mathrm{M}$	[c][56]
[40S]	$5.3\,\mu\mathrm{M}$	[c][56]
[60S]	$7.6\,\mu\mathrm{M}$	[c][56]

where the subscript T denotes the total concentration of the species. Additionally, as there are approximately 6×10^6 ribosomes per cell [73], and 10^6 free ribosomes in mammalian cells [55], we can assume that the concentrations of the 40S and 60S ribosomal subunits are constant. Therefore, there will be no rate equations for 40S and 60S, which makes these species parameters of the model. Furthermore, eIF3 and eIF5B have mass conservation equations, and therefore we do not need to consider their rate equations. The total concentrations of eIF3 and eIF5B are parameters in the calculation of the PIC1_{nc} and TC_{nc} concentrations, respectively, and therefore they are parameters of the model. The concentration of tRNA_i is held constant due to its high concentration of $26\,\mu$M [56]. The total concentration of mRNA is held constant in this model as we assume the synthesis and degradation of mRNA are balanced over the time scale of the calculations. At any given time in the translation process, some of the mRNA is freely available, but some of it is also occupied by the pre-initiation complexes as noted earlier. Therefore, the total concentration of mRNA in the cell includes the available mRNA, and the mRNA involved in the pre-initiation complexes, as represented in equation (2.2b). The final step where the translation competent ribosome (RIB) is produced is not reversible, therefore we do not track the fate of the RIB complex, and focus instead on the rate of initiation, $k_7[\text{RIB5B}]$.

By taking the above into consideration and applying the law of mass-action to the above model, the following set of ODEs results:

$$\frac{d[\text{PIC2}_{nc}]}{dt} = k_2[\text{PIC1}_{nc}][\text{mRNA}] - k_{-2}[\text{PIC2}_{nc}] - k_4[\text{PIC2}_{nc}][\text{TC}_{nc}] + k_{-4}[\text{PIC3}_{nc}], \quad (2.3a)$$

$$\frac{d[\text{PIC3}_{nc}]}{dt} = k_4[\text{PIC2}_{nc}][\text{TC}_{nc}] - k_{-4}[\text{PIC3}_{nc}] - k_5[\text{60S}][\text{PIC3}_{nc}] + k_{-5}[\text{PIC4}_{nc}], \quad (2.3b)$$

$$\frac{d[\text{PIC4}_{nc}]}{dt} = k_5[\text{60S}][\text{PIC3}_{nc}] - k_{-5}[\text{PIC4}_{nc}] - k_6[\text{PIC4}_{nc}], \quad (2.3c)$$

$$\frac{d[\text{RIB5B}]}{dt} = k_6[\text{PIC4}_{nc}] - k_7[\text{RIB5B}], \quad (2.3d)$$

At the steady-state, the rates of change of each species are 0, therefore the steady-state

equations for this model are:

$$0 = k_2[\text{PIC1}_{nc}][\text{mRNA}] - k_{-2}[\text{PIC2}_{nc}] - k_4[\text{PIC2}_{nc}][\text{TC}_{nc}] + k_{-4}[\text{PIC3}_{nc}], \tag{2.4a}$$

$$0 = k_4[\text{PIC2}_{nc}][\text{TC}_{nc}] - k_{-4}[\text{PIC3}_{nc}] - k_5[60\text{S}][\text{PIC3}_{nc}] + k_{-5}[\text{PIC4}_{nc}], \tag{2.4b}$$

$$0 = k_5[60\text{S}][\text{PIC3}_{nc}] - k_{-5}[\text{PIC4}_{nc}] - k_6[\text{PIC4}_{nc}], \tag{2.4c}$$

$$0 = k_6[\text{PIC4}_{nc}] - k_7[\text{RIB5B}], \tag{2.4d}$$

which correspond to setting the rates of the equations in equation set (2.3) to 0.

To summarize, the equations used in the analysis of this model are equations (2.2b), and (2.4) to solve for the variables mRNA, PIC2_{nc}, PIC3_{nc}, PIC4_{nc}, and RIB5B. The parameters used in the analysis are found in tables 2.2 and 2.3.

2.4 RIB5B dependence on eIF5B

As is obvious from the name of the pathway and the model constructed in this chapter, the RIB5B complex depends on the parameter, $[\text{eIF5B}]_\text{T}$. Therefore, we can do a parameter scan of eIF5B and examine its effects on the concentration of non-canonical RIB5B complexes.

We can represent the steady-state concentration of RIB5B complexes as a function of eIF5B, as shown by the following:

$$[\text{RIB5B}] = f([\text{eIF5B}]).$$

However, it is advantageous to look at the number of RIB5B complexes rather than their concentration in the cell, as one of the goals of this study is to limit the number of RIB5B complexes available to perform translation initiation using this eIF5B-dependent non-canonical pathway. Therefore, using Avagadro's number, and assuming the volume of the eukaryotic cell is 10^{-12} L [69, 70], we can transform the concentration of RIB5B complexes to the

number of RIB5B complexes present. Note this transformation does not impact its dependence on eIF5B, so therefore, the equation we can use to analyze RIB5B's dependence on the concentration of eIF5B is

$$\text{RIB5B} = f([\text{eIF5B}]). \tag{2.5}$$

This dependence is illustrated in figure 2.1. At total concentrations of eIF5B above $5\times10^{-3}\mu$M, the number of RIB5B complexes saturates at 1200 complexes. The region of sensitivity is between approximately $5\times10^{-5}\mu$M and $5\times10^{-3}\mu$M. In this region, the total concentration of eIF5B has a large effect on the number of RIB5B complexes assembled. This parameter scan is further discussed in chapter 3.

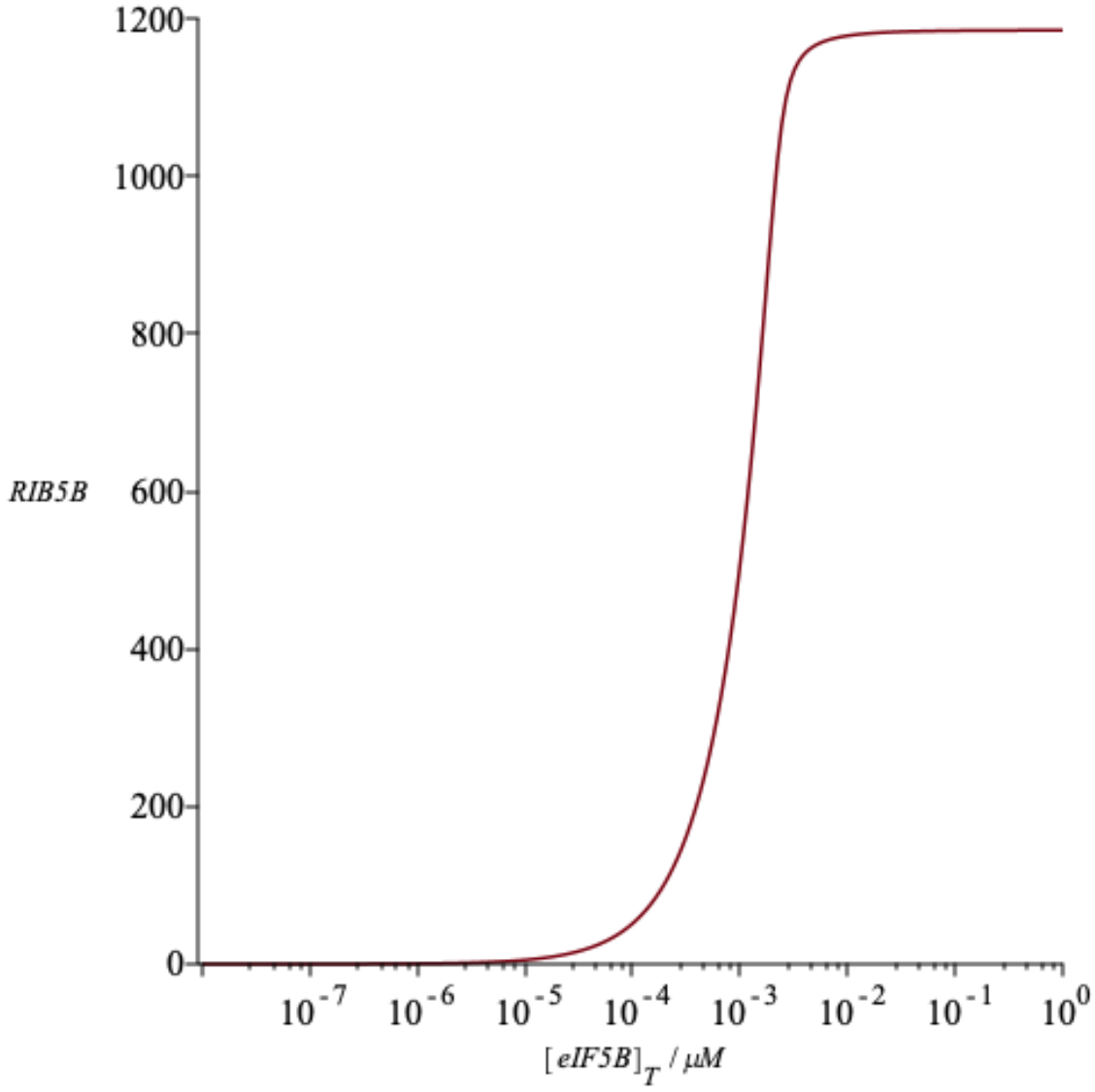

Figure 2.1: A parameter scan of eIF5B and its effects on the number of non-canonical RIB5B complexes in the cell. The complex reaches a saturation point of approximately 1200 complexes, which is a concentration of $1.7\times10^{-4}\,\mu$M, as the concentration of eIF5B varies from 0 – 1 μM. To convert from concentration of ribosomes to number of ribosomes, the volume of a eukaryotic cell was assumed to be 10^{-12} L [69, 70]. This figure was generated using Maple (2021).

Chapter 3

eIF5B-mediated translation initiation with a clearance delay

Previous research has indicated that clearance and synthesis delays are not negligible and result in dynamical behavioural differences [58]. The model described and analyzed in this chapter considers a clearance delay, namely the time it takes for the ribosome to move past the IRES structure on the mRNA. This delay is illustrated in figure 3.1.

Non-canonical translation initiation begins with the binding of eIF3 to the 40S subunit, which is then followed by the recruitment of the IRES-containing mRNA. Meanwhile, the ternary complex comprised of eIF5B, tRNA_i and a GTP molecule is formed, and subsequently binds to the pre-intiation complex. The 60S subunit then binds, followed by eIF3 and eIF5 dissociation, leaving the fully formed ribosome. The non-canonical eIF5B-mediated translation initiation pathway with a clearance delay is described below:

$$40\text{S} + \text{eIF3} \underset{k_{-1}}{\overset{k_1}{\rightleftharpoons}} \text{PIC1}_{nc} \tag{3.1a}$$

$$\text{PIC1}_{nc} + \text{mRNA} \underset{k_{-2}}{\overset{k_2}{\rightleftharpoons}} \text{PIC2} \tag{3.1b}$$

$$\text{eIF5B} \; + \; \text{tRNA}_\text{i} \underset{k_{-3}}{\overset{k_3}{\rightleftharpoons}} \text{TC}_{nc} \tag{3.1c}$$

$$\text{PIC2} + \text{TC}_{nc} \underset{k_{-4}}{\overset{k_4}{\rightleftharpoons}} \text{PIC3}_{nc} \tag{3.1d}$$

$$\text{PIC3}_{nc} + 60\text{S} \underset{k_{-5}}{\overset{k_5}{\rightleftharpoons}} \text{PIC4}_{nc} \tag{3.1e}$$

$$\text{PIC4}_{nc} \xrightarrow{k_6} \text{RIB5B} + \text{eIF3} \tag{3.1f}$$

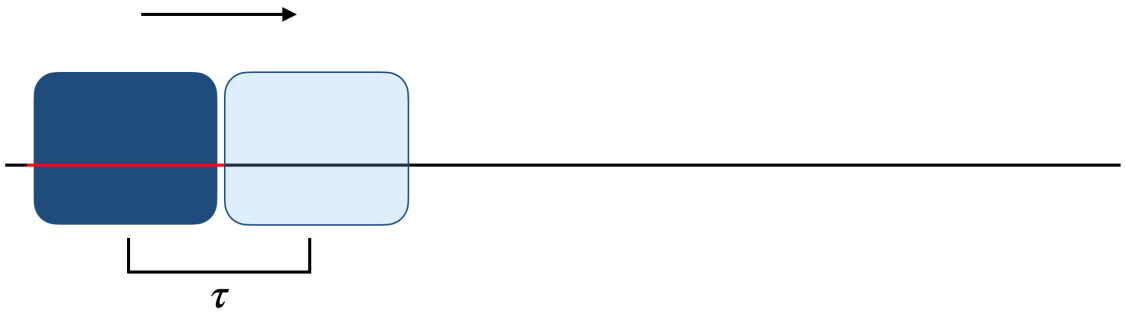

Figure 3.1: The clearance delay (τ) in the eIF5B-mediated non-canonical translation initiation pathway. τ is the time required for the ribosome to clear the IRES element so another ribosome can bind, illustrated by the movement to the second ribosome placement. The arrow shows the 5' to 3' movement of the ribosome, the black line represents the mRNA, the red line highlights the IRES element within the 5' UTR of the mRNA, and the blue boxes are ribosomes.

$$\text{RIB5B} \xrightarrow{k_7} \text{RIB} + \text{eIF5B} + \text{mRNA}(\text{t}+\tau) \tag{3.1g}$$

This delay is in the mRNA term, and therefore it will affect this differential equation. Steps (3.1b), (3.1d), (3.1e), and (3.1f) all occur without significant motion of the ribosome, which therefore blocks access to the binding site for other ribosomes. Once elongation starts following the formation of RIB5B, an additional time τ is required to clear the IRES. Additionally, if the IRES' structure is affected during translation initiation, the time it takes to reform the IRES structure would also be included in this delay. The mRNA will be available for another ribosome to bind at time $t+\tau$ following formation of RIB5B at time t. The rate at which the mRNA becomes available to another ribosome at time t thus depends on the rate of initiation at $t-\tau$. Therefore, the free mRNA is removed from the total mRNA pool at a rate $k_2[\text{PIC1}_{nc}][\text{mRNA}](t)$, and returned at a rate $k_7[\text{RIB5B}](t-\tau)$. This formalism was previously established [74], and is used throughout this thesis.

3.0.1 Constructing the eIF5B-dependent non-canonical translation initiation model with a clearance delay

By applying the delayed mass-action law to the non-canonical mechanism outlined earlier, we get the following DDEs:

$$\frac{d[\text{mRNA}]}{dt} = -k_2[\text{PIC1}_{nc}][\text{mRNA}] + k_{-2}[\text{PIC2}_{nc}] + k_7[\text{RIB5B}](t-\tau), \tag{3.2a}$$
$$\frac{d[\text{PIC1}_{nc}]}{dt} = k_1[\text{40S}][\text{eIF3}] - k_{-1}[\text{PIC1}_{nc}] - k_2[\text{PIC1}_{nc}][\text{mRNA}] + k_{-2}[\text{PIC2}_{nc}], \tag{3.2b}$$
$$\frac{d[\text{PIC2}_{nc}]}{dt} = k_2[\text{PIC1}_{nc}][\text{mRNA}] - k_{-2}[\text{PIC2}_{nc}] - k_4[\text{PIC2}_{nc}][\text{TC}_{nc}] + k_{-4}[\text{PIC3}_{nc}], \tag{3.2c}$$
$$\frac{d[\text{TC}_{nc}]}{dt} = k_3[\text{eIF5B}][\text{tRNA}_\text{i}] - k_{-3}[\text{TC}_{nc}] - k_4[\text{PIC2}_{nc}][\text{TC}_{nc}] + k_{-4}[\text{PIC3}_{nc}], \tag{3.2d}$$
$$\frac{d[\text{PIC3}_{nc}]}{dt} = k_4[\text{PIC2}_{nc}][\text{TC}_{nc}] - k_{-4}[\text{PIC3}_{nc}] - k_5[\text{60S}][\text{PIC3}_{nc}] + k_{-5}[\text{PIC4}_{nc}], \tag{3.2e}$$
$$\frac{d[\text{PIC4}_{nc}]}{dt} = k_5[\text{60S}][\text{PIC3}_{nc}] - k_{-5}[\text{PIC4}_{nc}] - k_6[\text{PIC4}_{nc}], \tag{3.2f}$$
$$\frac{d[\text{RIB5B}]}{dt} = k_6[\text{PIC4}_{nc}] - k_7[\text{RIB5B}]. \tag{3.2g}$$

Similarly to the model without delays, the total amount of mRNA must be conserved, and therefore a conservation relation must be accounted for. This is expressed by the following equation:

$$[\text{mRNA}]_\text{T} = [\text{mRNA}] + [\text{PIC2}_{nc}] + [\text{PIC3}_{nc}] + [\text{PIC4}_{nc}] + [\text{RIB5B}] + k_7 \int_{t-\tau}^{t} [\text{RIB5B}](\theta)\, d\theta, \tag{3.3}$$

where $[\text{mRNA}]_\text{T}$ is the total concentration of mRNA, [mRNA] is the available concentration of mRNA, and $k_7[\text{RIB5B}](\theta)$ is the rate at which the mRNA becomes available again at time $\theta \in [t-\tau, t]$. Therefore, the integral term in equation (3.3) represents the amount of mRNA unavailable due to ribosome binding between $t-\tau$ and t. Therefore the total amount of mRNA is accounted for by adding the free mRNA, and the occluded mRNA.

The total mRNA in the system should be constant. To prove this, using the fundamental theorem of calculus (FTC) we can take a time derivative of equation (3.3), which results in the following relationship:

$$\frac{d[\text{mRNA}]_\text{T}}{dt} = \frac{d[\text{mRNA}]}{dt} + \frac{d[\text{PIC2}_{nc}]}{dt} + \frac{d[\text{PIC3}_{nc}]}{dt} + \frac{d[\text{PIC4}_{nc}]}{dt} + \frac{d[\text{RIB5B}]}{dt} + k_7[\text{RIB5B}](t) - k_7[\text{RIB5B}](t-\tau).$$

We can then substitute equation set (3.2) into the above equation to show that $\frac{d[\text{mRNA}]_\text{T}}{dt} = 0$.

When the system reaches a steady-state, [RIB5B] is constant, which reduces equation (3.3) to

$$[\text{mRNA}]_\text{T} = [\text{mRNA}] + [\text{PIC2}_{nc}] + [\text{PIC3}_{nc}] + [\text{PIC4}_{nc}] + [\text{RIB5B}](1 + k_7\tau). \tag{3.4}$$

Like in the non-canonical model in chapter 2, there are other conservation relationships to consider, namely those for eIF3 and eIF5B, which are outlined in the following equations:

$$[\text{eIF3}]_\text{T} = [\text{eIF3}] + [\text{PIC1}_{nc}] + [\text{PIC2}_{nc}] + [\text{PIC3}_{nc}] + [\text{PIC4}_{nc}], \tag{3.5a}$$

$$[\text{eIF5B}]_\text{T} = [\text{eIF5B}] + [\text{TC}_{nc}] + [\text{PIC3}_{nc}] + [\text{PIC4}_{nc}] + [\text{RIB5B}]. \tag{3.5b}$$

At the steady-state, the rate of change of each species is assumed to be 0, therefore, steady-state equations for this model are:

$$0 = k_1[40\text{S}][\text{eIF3}] - k_{-1}[\text{PIC1}_{nc}] - k_2[\text{PIC1}][\text{mRNA}] + k_{-2}[\text{PIC2}_{nc}], \tag{3.6a}$$

$$0 = k_2[\text{PIC1}_{nc}][\text{mRNA}] - k_{-2}[\text{PIC2}_{nc}] - k_4[\text{PIC2}_{nc}][\text{TC}_{nc}] + k_{-4}[\text{PIC3}_{nc}], \tag{3.6b}$$

$$0 = k_3[\text{eIF5B}][\text{tRNA}_\text{i}] - k_{-3}[\text{TC}_{nc}] - k_4[\text{PIC2}_{nc}][\text{TC}_{nc}] + k_{-4}[\text{PIC3}_{nc}], \tag{3.6c}$$

$$0 = k_4[\text{PIC2}_{nc}][\text{TC}_{nc}] - k_{-4}[\text{PIC3}_{nc}] - k_5[60\text{S}][\text{PIC3}_{nc}] + k_{-5}[\text{PIC4}_{nc}], \tag{3.6d}$$

$$0 = k_5[60S][PIC3_{nc}] - k_{-5}[PIC4_{nc}] - k_6[PIC4_{nc}], \tag{3.6e}$$

$$0 = k_6[PIC4_{nc}] - k_7[RIB5B], \tag{3.6f}$$

which are closed by the conservation relations outlined in equations (3.4), (3.5a), and (3.5b), and where the concentrations of 40S, 60S, $tRNA_i$ are assumed to be constant. Therefore, the variables to be solved for in the numerical analysis include: eIF3, eIF5B, mRNA, $PIC1_{nc}$, $PIC2_{nc}$, TC_{nc}, $PIC3_{nc}$, $PIC4_{nc}$, and RIB5B.

Solving delay differential equations requires the specification of initial values of the state variables of the system and an initial function that recalls previous values of the delayed variable [75]. Initial values for these variables are provided in table 3.1. An initial function for the values of [RIB5B] is required since the forward time evolution of [mRNA] depends on past values of [RIB5B]. In this case, the initial function is [RIB5B] = 0 for $t \in [-\tau,0]$.

3.0.2 Parameters

The same parameter considerations and calculations that were described in chapter 2 were also used here. The table of parameters used in the calculations in this section are provided in table 3.1.

In this model, there is one delay that considers the time it takes to clear the IRES element on the mRNA so that another ribosome can bind to it. Unfortunately, no data on the clearance time was available in the literature to the best of my knowledge. Therefore, three sensitivity analyses at different magnitudes of delay times with respect to the canonical clearance delay were analyzed to determine the system's sensitivity to the delay, τ. The rationale behind these delay times and the analyses of the delays are discussed in section 3.2.1.

Table 3.1: Table of parameters in the non-canonical model with a clearance delay. [a] is approximated value. [c] is calculated value. Concentrations of translation initiation factors (μM) were calculated using the model provided by Firczuk *et al.* (2013) [56] via the procedure outlined in section 2.2.

Parameter	**Value**	**Source**
k_1	$1\,\mathrm{nM}^{-1}\mathrm{s}^{-1}$	[c][64]
k_{-1}	$6\,\mathrm{s}^{-1}$	[c][64]
k_2	$1\,\mathrm{nM}^{-1}\mathrm{s}^{-1}$	[c][71]
k_{-2}	$2\,\mathrm{s}^{-1}$	[c][71]
k_3	$0.01\,\mu\mathrm{M}^{-1}\mathrm{s}^{-1}$	[c][65]
k_{-3}	$0.027\,\mathrm{s}^{-1}$	[c][65]
k_4	$1\,\mathrm{nM}^{-1}\mathrm{s}^{-1}$	[a]
k_{-4}	$1\,\mathrm{s}^{-1}$	[a]
k_5	$0.81\,\mu\mathrm{M}^{-1}\mathrm{s}^{-1}$	[72]
k_{-5}	$1\,\mathrm{s}^{-1}$	[a]
k_6	$6\,\mathrm{s}^{-1}$	[a]
k_7	$0.035\,\mathrm{s}^{-1}$	[37]
$[\mathrm{eIF3}]_\mathrm{T}$	$0.21\,\mu\mathrm{M}$	[c][56]
$[\mathrm{eIF5B}]_\mathrm{T}$	$0.20\,\mu\mathrm{M}$	[c][56]
$[\mathrm{mRNA}]_\mathrm{T}$	$2.0\times10^{-3}\,\mu\mathrm{M}$	[a][19, 68]
$[\mathrm{tRNA_i}]$	$26\,\mu\mathrm{M}$	[c][56]
40S	$5.3\,\mu\mathrm{M}$	[c][56]
60S	$7.6\,\mu\mathrm{M}$	[c][56]
τ	$20\,\mathrm{s}$	[a][76]

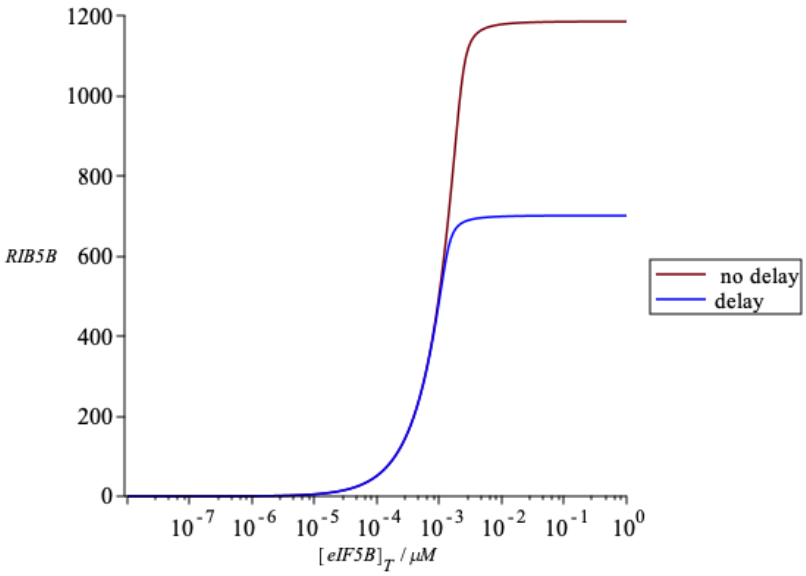

Figure 3.2: A parameter scan of the total concentration of eIF5B and its effect on the number of non-canonical RIB5B complexes in the cell for the models with the clearance delay and without the clearance delay. The total concentration of eIF5B when the number of RIB5B complexes is halved is $[\text{eIF5B}]_T$=0.69 nM, or approximately 4200 eIF5B molecules. This figure was generated using Maple (2021).

3.1 Differences in behaviour in the models with and without the delay

Again, RIB5B depends on the total concentration of eIF5B, therefore we can do a similar parameter scan to that in section 2.4. The effects of the parameter scan on the number of RIB5B complexes can be seen in figure 3.2. The RIB5B complex saturated around 1200 complexes in the model without delays, however we observe a much smaller saturation point in the model with the delay: approximately 700 complexes. This difference in complexes is due to the unavailable mRNA in the bridge between translation initiation and elongation. Recall that after the 80S ribosome has formed, it takes τ time units for the IRES to be available again for binding by another pre-initiation complex. Therefore, there are quantitative differences between the two models, despite their similar resulting sigmoidal curves.

To further analyze the differences between the model with the clearance delay and the one without, the models were assembled in Matlab. The same parameters as outlined in chapter 2 were considered. The time courses for all variables in the model without the

delay are found in figure 3.3.

Damped oscillations were present in the delay model at $\tau = 100\,\text{s}$, which were not present in the model without delays. These oscillations were present in the time courses for all five variables in the model: mRNA, PIC2_{nc}, PIC3_{nc}, PIC4_{nc}, and RIB5B. Time courses for all variables in the model with the delay are shown in figure 3.4. The inner panel of figure 3.4 zooms in on these oscillations present in mRNA, PIC2_{nc}, PIC3_{nc}, and PIC4_{nc}. The oscillations have a period of approximately 100 s, which is essentially the same as the delay. These oscillations result from step (3.1g), as there is a delay for when the IRES will be available again. This means that at the beginning of translation initiation, there will be a sharp decrease in the concentration of free mRNA available and a simultaneous increase in the concentrations of pre-initiation complexes formed. If we follow the evolution of the RIB5B complex in figure 3.4, we see this sharp increase, followed by a decrease that leads into the oscillations. The mRNA concentration increases when the rate at which the mRNA is made available again is greater than the rate at which it is converted to mRNA_c:

$$k_7[\text{RIB5B}](t-\tau) > k_2[\text{PIC1}][\text{mRNA}](t),$$

and decreases when the rate at which the mRNA is converted to mRNA_c is greater than the rate at which it becomes available again:

$$k_2[\text{PIC1}][\text{mRNA}](t) > k_7[\text{RIB5B}](t-\tau).$$

This qualitative difference in dynamic behaviour further outlines the importance of the inclusion of a delay in this model. Gene oscillations are frequently observed in living cells, and perhaps the most widely-known example is the circadian rhythm [77].

It should be noted that at least one maximum is observed after the transient given a delay of 20 s as well (figure 3.5). It is unclear as to whether true oscillations are present at this delay value based on inspection of the plots. To determine whether they are present,

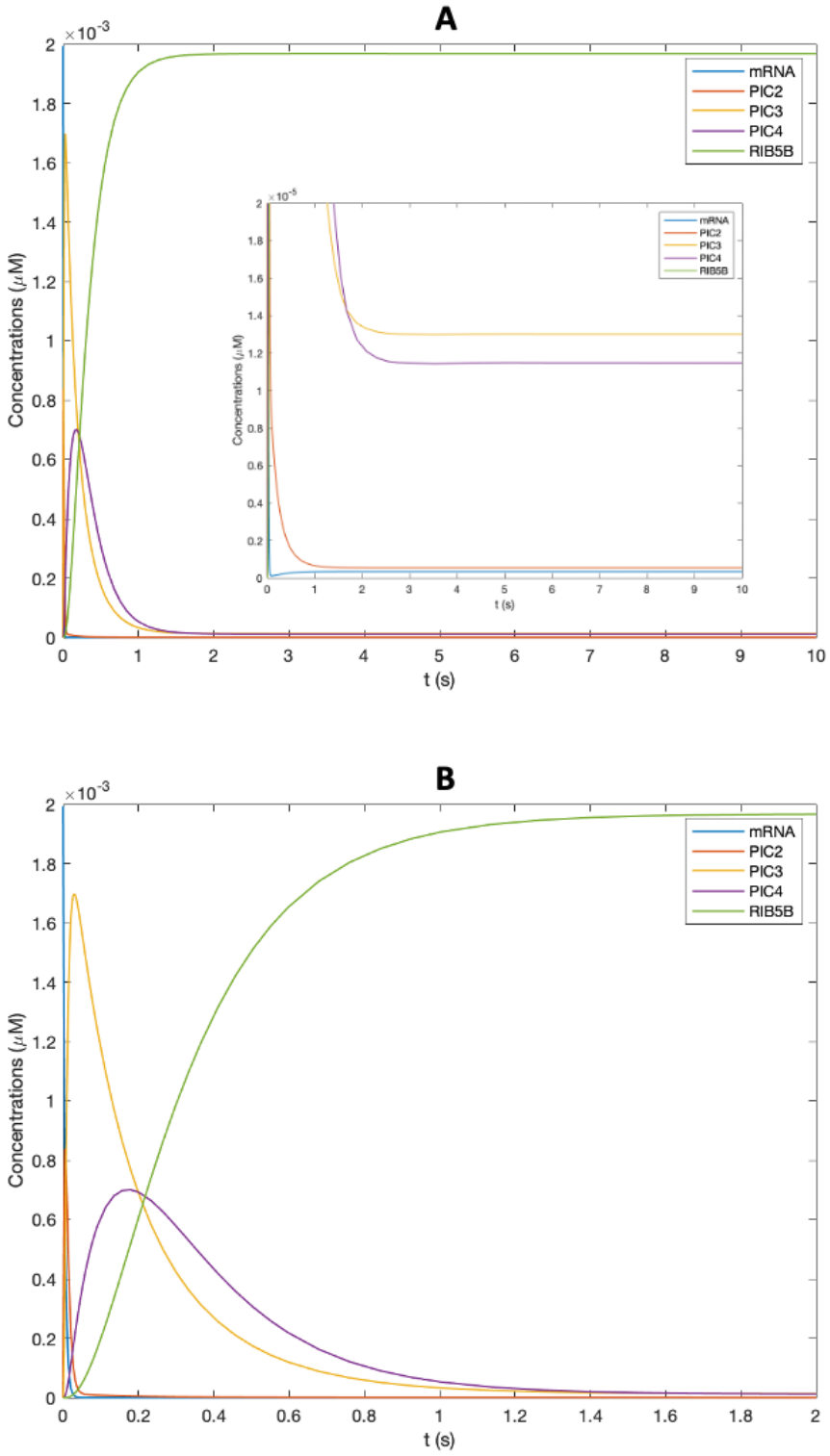

Figure 3.3: The evolution of the various pre-initiation complexes and mRNA over time in the model without a clearance delay. The inset in panel A highlights the species with smaller concentrations. Panel B highights the transients of the species before the steady-state is reached. These figures were generated using Matlab 2021.

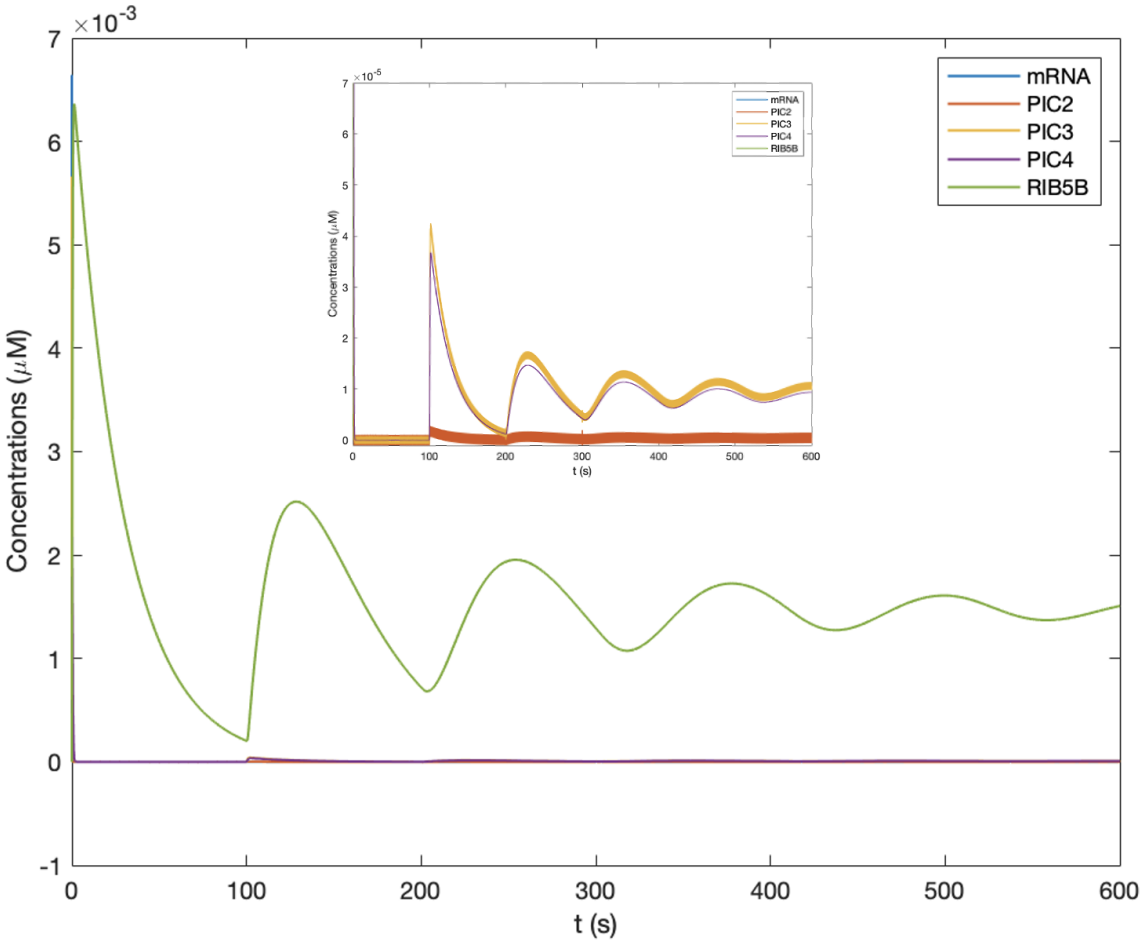

Figure 3.4: The progression of the various pre-initiation complexes and mRNA over time in the model with a clearance delay, where $\tau = 100$ s. A steep rise in concentration of RIB5B is observed at the beginning, followed by damped oscillations. The inner figure highlights the species at smaller concentrations. These figures were generated using Matlab 2021.

the eigenvalues for the characteristic equation would need to be calculated. In particular, if some of the eigenvalues are complex-valued, there is a potential for oscillations [75]. This analysis was not performed here due to the fact that oscillations are clearly observed in this model at larger delay values, thus the behavioural differences in the models with and without a delay were highlighted without the need for further analysis. The relevance of this 20 s delay is further discussed in section 3.2.1.

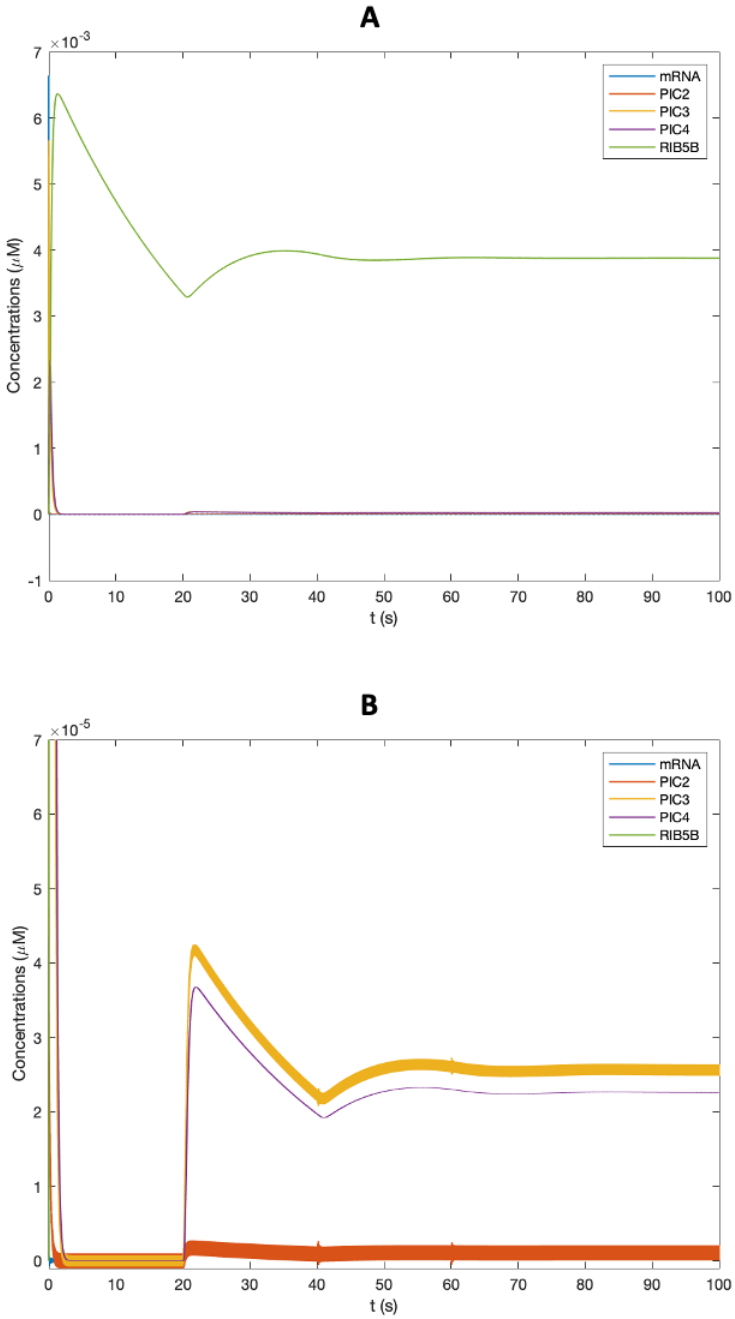

Figure 3.5: A: The progression of the various pre-initiation complexes and mRNA over time in the model with a clearance delay. A steep rise in concentration of RIB5B is observed in the transient (0–2 s), followed by one maximum around 30 s, where $\tau = 20$ s. B: This figure highlights the species at smaller concentrations from panel A. These figures were generated using Matlab 2021.

3.2 Sensitivity analysis

Before discussing any inhibition options, it is beneficial to examine the sensitivity of this model to some of its parameters, primarily the ones that have been assumed, as denoted by [a] in table 3.1; or calculated, as denoted by [c] in table 3.1; in addition to other parameters of interest such as the clearance delay, τ, the total eIF5B concentration, and the total mRNA concentration. Not only will the sensitivity analysis provide information on the parameters the system is most sensitive to, but this information may also be applied to develop some inhibition mechanisms that are outlined in the following section.

The calculation of absolute sensitivities at the steady-state is relatively straightforward. A system of equations, f_i, which depends on variables, x_m, and parameters, k_j, is represented by the following:

$$f_i\Big(x_1, x_2 ..., x_n; k_1, k_2, ..., k_p\Big) = 0, \tag{3.7}$$

where $i = 1, ..., n$. The equations, f_i, represent the system of equations for this model outlined in section 3.0.1, and the x_m represent the variables eIF3, eIF5B, PIC1$_{nc}$, PIC2$_{nc}$, PIC3$_{nc}$, PIC4$_{nc}$, TC$_{nc}$, mRNA, and RIB5B. To find the sensitivity of the steady-state solutions to a particular parameter, k_j, we apply the chain rule at the steady-state to establish

$$\frac{df_i}{dk_j} = \sum_{m=1}^{n} \frac{\partial f_i}{\partial x_m}\frac{\partial x_m}{\partial k_j} + \frac{\partial f_i}{\partial k_j} = 0, \tag{3.8}$$

for the n equations. This reduces to the linear equation

$$\sum_{m=1}^{n} \frac{\partial f_i}{\partial x_m}\frac{\partial x_m}{\partial k_j} = -\frac{\partial f_i}{\partial k_j}, \tag{3.9}$$

where $\left[\frac{\partial f_i}{\partial x_m}\right]$ is the Jacobian matrix of equations (3.7), $\left[\frac{\partial x_m}{\partial k_j}\right]$ is a vector of absolute sensitivities with respect to a single parameter, k_j, and $\left[\frac{\partial f_i}{\partial k_j}\right]$ is a vector of partial derivatives of the equations with respect to the single parameter, k_j. Note that the absolute sensitivities

are the unknowns in equation (3.9).

Solving linear systems is a well-developed area of mathematical and computational science [78]. To solve for the previously mentioned unknowns, we begin by calculating the Jacobian matrix as follows:

$$\mathbf{J} = \begin{bmatrix} \frac{\partial f_1}{\partial x_1} & \frac{\partial f_1}{\partial x_2} & \cdots & \frac{\partial f_1}{\partial x_q} \\ \frac{\partial f_2}{\partial x_1} & \frac{\partial f_2}{\partial x_2} & \cdots & \frac{\partial f_2}{\partial x_q} \\ \vdots & \vdots & \vdots & \vdots \\ \frac{\partial f_n}{\partial x_1} & \frac{\partial f_n}{\partial x_2} & \cdots & \frac{\partial f_n}{\partial x_q} \end{bmatrix}.$$

We now have the linear equation (3.8) we can solve. The result of this analysis is the the set of sensitivities of the n variables, x_m, with respect to a particular parameter, k_j, or $\frac{\partial x_m}{\partial k_j}$. To begin, we solve the system of equations for the steady state, substitute the parameters and steady-state concentrations into J and $\left[\frac{\partial f_i}{\partial k_j}\right]$, and then solve equation (3.9) for the sensitivities. However, the values resulting from this analysis are not dimensionless. For example, the variables in this thesis have concentrations in μM. Despite the consistency in concentrations, first-order and second-order rate constants have different units. Therefore, a vector of sensitivities calculated with respect to a first-order rate constant will differ from that of a second-order rate constant. The results of the analysis are therefore not only difficult to interpret, but also difficult to compare. Fortunately, there are methods to determine relative sensitivities, which alleviate this problem, as discussed below.

Relative sensitivities are precisely what the name implies. These values are dimensionless. Relative sensitivities are the most reported in the literature, and can help the researcher to understand the impact of approximating parameters in their models. For example, if a system is not sensitive to an approximated parameter, then the results do not depend on the value of the parameter. If the system is sensitive to an approximated or assumed parameter, then it is important to understand the implications that changes in the parameter may have

on the system. According to the above absolute sensitivity analysis, each element of the sensitivity matrix represents the absolute sensitivity of the steady-state concentration, x_m, with respect to a parameter, k_j. Therefore, if this element of the matrix is multiplied by the value of the parameter and divided by the variable concentration at the steady-state, this will yield a relative sensitivity of the variable with respect to the parameter. For a single sensitivity, this process is represented by the following:

$$RS_{k_j}^{x_m} = \frac{\partial x_m}{\partial k_j} \frac{k_j}{x_m*}, \tag{3.10}$$

where $RS_{k_j}^{x_m}$ is the relative sensitivity of a variable, x_m with respect to a parameter, k_j, $\left[\frac{\partial x_m}{\partial k_j}\right]$ is the sensitivity matrix evaluated at the steady-state, k_j is the value of the specific parameter of interest, and x_m* is the value of x_m at the steady-state.

3.2.1 Delay sensitivity analyses

Earlier, it was mentioned that the literature did not contain data on the value of τ. Typically, we can calculate clearance delays using the length of the RBS and the average translation rate. However, this approach cannot be used on IRES-containing mRNAs, as the IRES is a secondary structure of the mRNA that the ribosome likely does not scan. In chapter 4, the clearance delay time is calculated to be 2 s. The non-canonical clearance delay is expected to be slower than this for a number of reasons: binding the mRNA could be slow, for example, since it is not assisted by any of the initiation factors used in the canonical pathway; and moving past the IRES (which likely requires breaking up its secondary structure) is slow as well. Therefore, a series of sensitivity analyses were performed to determine the system's sensitivity to the clearance delay.

The results of this analysis in table 3.2 show a negligible relative sensitivity of the RIB5B complex to τ, regardless of its value. The RIB5B complex was chosen as the variable to analyze, as this represents the translation competent ribosomes in the cell, and therefore, if this variable is not sensitive to τ over several orders of magnitude, then the delay

Table 3.2: The relative sensitivity of RIB5B in the non-canonical model with respect to various τ values. This table of sensitivities was calculated using *XIAP* total mRNA concentration of $2.0\times10^{-3}\mu$M.

τ (s)	5	20	100
RIB5B	0.001	0.001	0.001

value chosen should not affect the results of the following analyses. The three τ values analyzed were chosen based on their order of magnitude with respect to the canonical delay of 2 s. $\tau_1 = 5\,s$, which is within an order of magnitude of the canonical delay, $\tau_2 = 20\,s$, which is an order of magnitude larger than the canonical delay, and $\tau_3 = 100\,s$, which is two orders of magnitude larger than the canonical delay. Based on the results of this analysis, the system is not sensitive to the value of the clearance delay, and therefore a delay value of 20 s was used throughout the rest of the chapter. This delay value was chosen because it is larger than that of the canonical delay, which is what we would expect from this pathway, but clearing the IRES should likely not take any longer than a few tens of seconds based on the fact that this mechanism is chosen by the cell under hypoxic conditions to produce XIAP and other IRES-containing anti-apoptotic proteins such as Bcl-XL and cIAP1 [42]. Therefore, a long delay (i.e. $\geq$100 s) may limit the cell's ability to synthesize these proteins, thus potentially affecting the cell's ability to protect itself from apoptosis, and a short delay (i.e. $\leq$ 2 s) may result in this pathway being chosen over the eIF2-mediated pathway to produce XIAP under healthy cell conditions, which is not true to scientific observations [18].

3.2.2 *XIAP* mRNA concentration analyses

The concentration of XIAP is greater in glioblastoma cells than in normal cells [19]. Therefore, it is beneficial for us to examine the local sensitivities of each species, with a particular focus on the RIB5B sensitivity, across a range of *XIAP* mRNA concentrations. Let us first consider normal cellular conditions. Under these conditions, we would expect the concentration of *XIAP* mRNA to be small, but nonzero. Therefore, an average of approximately 40 transcripts was used [68], which, considering a cellular volume

Table 3.3: The relative sensitivities of eIF5B, $PIC2_{nc}$, $PIC3_{nc}$, $PIC4_{nc}$, TC_{nc}, mRNA, and RIB5B in the non-canonical model with a clearance delay. This table of sensitivities was calculated using *XIAP* total mRNA concentration of $6.6\times10^{-5}\,\mu$M.

	k_3	k_{-3}	k_5	k_6	k_7	$[\text{mRNA}]_T$	$[\text{eIF5B}]_T$
eIF5B	-0.906	0.905	0.000	0.000	0.000	0.000	1.000
PIC2	-0.094	0.094	-0.155	-0.019	0.584	1.000	-1.000
$PIC3_{nc}$	0.000	0.000	-0.996	-0.139	0.584	1.000	0.000
$PIC4_{nc}$	0.000	0.000	0.004	-0.996	0.584	1.000	0.000
TC_{nc}	0.094	-0.094	0.000	0.000	0.000	0.000	1.000
mRNA	-0.001	0.001	-0.001	0.004	0.584	1.000	-0.015
RIB5B	0.000	0.000	0.004	0.004	-0.416	1.000	0.000

Table 3.4: The relative sensitivities of eIF5B, $PIC2_{nc}$, $PIC3_{nc}$, $PIC4_{nc}$, TC_{nc}, mRNA, and RIB5B in the non-canonical model with a clearance delay. This table of sensitivities was calculated using *XIAP* total mRNA concentration of $6.6\times10^{-4}\,\mu$M.

	k_3	k_{-3}	k_5	k_6	k_7	$[\text{mRNA}]_T$	$[\text{eIF5B}]_T$
eIF5B	-0.906	0.906	0.000	0.000	0.003	0.001	1.000
$PIC2_{nc}$	-0.094	0.095	-0.155	-0.019	0.583	1.003	-1.002
$PIC3_{nc}$	0.000	0.000	-0.996	-0.139	0.584	1.000	0.000
$PIC4_{nc}$	0.000	0.000	0.004	-0.996	0.584	1.000	0.000
TC_{nc}	0.094	-0.095	0.000	0.000	0.001	-0.003	1.003
mRNA	-0.001	0.001	0.001	0.004	0.584	1.000	-0.015
RIB5B	0.000	0.000	0.004	0.004	-0.416	1.000	0.000

of 10^{-12} L [69, 70], is $6.6\times10^{-5}\,\mu$M. The sensitivities at this concentration of *XIAP* mRNA are found in table 3.3.

The RIB5B complex was consistently sensitive to the total concentration of *XIAP* mRNA at each of the three mRNA concentrations analyzed in tables 3.3 – 3.5. At none of these concentrations was the RIB5B complex sensitive to the total concentration of eIF5B or any of the other parameters examined, with the exception of k_7, which is the rate constant that describes the transition from initiation to elongation in step (3.1g), and the total mRNA concentration. The RIB5B complex remained consistently sensitive to k_7 and the total mRNA concentration across the three mRNA concentrations analyzed.

The RIB5B complex is sensitive to the k_7 parameter due to the fact that step (3.1g) bridges translation initiation and elongation. Therefore, an increase in k_7 will directly neg-

Table 3.5: The relative sensitivities of eIF5B, $PIC2_{nc}$, $PIC3_{nc}$, $PIC4_{nc}$, TC_{nc}, mRNA, and RIB5B in the non-canonical model with a clearance delay. This table of sensitivities was calculated using *XIAP* total mRNA concentration of $2.0\times10^{-3}\,\mu$M.

	k_3	k_{-3}	k_5	k_6	k_7	$[\text{mRNA}]_\text{T}$	$[\text{eIF5B}]_\text{T}$
eIF5B	-0.906	0.897	0.000	0.000	0.008	0.002	0.998
$PIC2_{nc}$	-0.095	0.094	-0.155	-0.019	0.582	1.008	-1.008
$PIC3_{nc}$	0.000	0.000	-0.996	-0.139	0.584	1.000	0.000
$PIC4_{nc}$	0.000	0.000	0.001	-0.996	0.584	1.000	0.000
TC_{nc}	0.095	-0.094	0.000	0.000	0.002	-0.008	1.008
mRNA	-0.001	0.001	0.001	0.004	0.584	1.000	-0.015
RIB5B	0.000	0.000	0.004	0.004	-0.416	1.000	0.000

atively affect the RIB5B concentration. Additionally, at an eIF5B concentration of $0.2\,\mu$M, the number of RIB5B complexes is saturated, as is observed in figure 3.2, which is not in the region of sensitivity (i.e. between $[\text{eIF5B}]_\text{T} = 1.0\times10^{-5} - 1.0\times10^{-2.5}\,\mu$M). This is why RIB5B is not sensitive to $[\text{eIF5B}]_\text{T}$ in tables 3.3–3.5. Moreover, RIB5B is sensitive to the total mRNA concentration across all mRNA concentrations. This is due to the fact that the mRNA concentration is the limiting reagent in this mechanism, and therefore it directly affects the number of potential RIB5B complexes.

Although all of the parameters and variables of the model were analyzed, not all of them are included in the tables. Some less interesting sets of sensitivity coefficients were omitted from the table for brevity. The only variable sensitive to parameters k_1 and k_{-1} was eIF3, and therefore these parameters were excluded from this table. eIF3 was only sensitive to parameters k_1 and k_{-1}, and therefore it was also excluded. The only variable sensitive to k_2 and k_{-2} was free mRNA, and therefore these parameters were excluded from the table. Additionally, the only species sensitive to k_4 was free eIF5B, and therefore, k_4 was excluded. None of the variables were sensitive to parameters k_{-3}, k_{-4}, k_{-5} or τ, and therefore these were also excluded from the sensitivities table. Finally, $PIC1_{nc}$ was not sensitive to any of the parameters examined here, and therefore, it was excluded from the table.

As mentioned previously, in glioblastoma cells, the expression of XIAP is much greater

than it is in normal cells. The median expression of XIAP in glioblastoma cells is approximately 10-fold higher than that in normal cells [19]. Therefore, this was simulated with a 10-fold increase in the concentration of *XIAP* mRNA. The table of sensitivities at this concentration is found in table 3.4. The same variables and parameters that were excluded from table 3.3 were excluded from table 3.4 for the same reasons.

If the concentration of XIAP is increased 30-fold to $2.0\times10^{-3}\mu$M (the highest observed increase in expression [19]), RIB5B's relative sensitivities to the total mRNA concentration and total eIF5B concentration are still unchanged. This confirms the results we observe in figure 3.2, as the total eIF5B concentration considered in these analyses ($0.20\,\mu$M) is in a region in which the RIB5B concentration is insensitive to $[\text{eIF5B}]_\text{T}$. The relative sensitivities at a total mRNA concentration of $2.0\times10^{-3}\,\mu$M are shown in table 3.5. The same variables and parameters that were excluded from table 3.3 were excluded from table 3.5 for the same reasons.

Interestingly, the results obtained from the sensitivity analyses presented above show essentially the same sensitivities regardless of the total mRNA concentration used. Therefore, the total mRNA concentration has very little effect on the analysis. A similar statement is true of the other parameters and variables, including the calculated and assumed values.

3.3 Inhibition

LWW31 is a previously developed drug that has proven to induce apoptosis and interfere with translation [31]. This drug was hypothesized to bind to the N-terminal region of eIF5B, which is believed to be involved in the stabilization of the canonical TC in the canonical translation pathway. However, recent studies indicate that LWW31 likely interacts with the C-terminus region [79]. Although this drug has been effective in inducing apoptosis and perturbing translation initiation, it is only cytotoxic at very high concentrations ($40\,\mu$M). To put this in perspective, only 13 out of the 141 small molecule drugs approved for oncology indications were above a maximum plasma concentration of $40\,\mu$M in 2017 [80].

There are a few different ways we could think about inhibiting the non-canonical pathway, which are listed below[3]. Additionally, the number transcript copies for *XIAP* is typically lower than that of some important canonically translated proteins such as type-1 collagen and β-actin (both of which are examined in chapter 4) particularly under unstressed conditions. We would expect an inhibitor that targets the RIB5B complex to affect the canonical mechanism as well. However, as there are more transcript copies available and therefore more RIB5B complexes, it may be useful to examine the degree to which such an inhibition mechanism would affect the canonical mechanism as well. For that reason, the RIB5B inhibition mechanisms are considered in this thesis. The different ways we could inhibit the non-canonical pathway are:

- target eIF5B such that it cannot bind to the Met-tRNA$_i$, consequently limiting the number of non-canonical ternary complexes available;
- target PIC2 such that TC$_{nc}$ is unable to bind to the interface;
- target TC$_{nc}$ such that it inhibits its ability to bind to PIC2;
- target the RIB5B complex thereby creating translation incompetent ribosomes where eIF5B cannot leave the complex, thus reducing its ability to move from initiation to elongation.

It should be noted that the last 3 proposed modes of inhibition are biologically expensive. That is, the cell would use a lot of energy to create the ternary complex, and the pre-initiation complexes. Moreover, creating translation incompetent ribosomes would be not only expensive biologically, but may also be toxic for the cells, which is explored in more detail in chapter 4.

The remainder of this chapter focuses on the development of the inhibition models for each potential target, and includes discussions on the resulting properties of the inhibitors

[3]Earlier, it was noted that eIF5B does not have a GEF due to its similar affinities for GTP and GDP [44]. Therefore, there is no GEF protein to target to inhibit this pathway.

that should be considered in future experiments.

3.3.1 Inhibition mechanism I_{5B}

In figure 3.2, we see that when the total concentration of eIF5B is $6.9\times10^{-4}\mu$M in the delay curve, this results in a total of 350 RIB5B complexes. If, under hypoxic conditions, the total concentration of eIF5B is assumed to be $0.20\,\mu$M, such as is used in this thesis, then this means we need to inhibit approximately 99% of the eIF5B in the cell in order to impact the number of translation competent ribosomes available to perform translation of the *XIAP* mRNA. This is very similar to what has been observed in current experimental data (Thakor, unpublished). At least 90% depletion of eIF5B is required to observe an effect on cell death under TRAIL treatment conditions. Earlier it was mentioned that the total concentration of eIF5B under hypoxic conditions was not known, so it was calculated using the model by Firczuk *et al.* (2013). As the results obtained in this study are confirmed by the experimental data, this approximation regarding the concentration of eIF5B is justified.

A number of inhibition possibilities were outlined above. The first one mentioned was disturbing eIF5B's ability to bind to the Met-tRNA$_\mathrm{i}$. This will essentially limit the number of ternary complexes available for the cell to use in this pathway, thus decreasing the amount of XIAP synthesized to help the cancer cell survive. To describe this, we take the mechanism outlined in equations (3.1), and add the following step:

$$\mathrm{eIF5B} \;+\; \mathrm{I_{5B}} \underset{k_{-5Bi}}{\overset{k_{5Bi}}{\rightleftharpoons}} \mathrm{eIF5B_i}, \tag{3.11}$$

where the subscript i denotes the inhibited form of the species, and $\mathrm{I_{5B}}$ denotes the eIF5B inhibitor.

This would add the following differential equations:

$$\begin{aligned}\frac{d[\mathrm{I_{5B}}]}{dt} &= -k_{5B_i}[\mathrm{eIF5B}][\mathrm{I_{5B}}] + k_{-5B_i}[\mathrm{eIF5B_i}],\\ \frac{d[\mathrm{eIF5B_i}]}{dt} &= k_{5B_i}[\mathrm{eIF5B}][\mathrm{I_{5B}}] - k_{-5B_i}[\mathrm{eIF5B_i}],\end{aligned}$$

which we can see will cancel each other out if we add them. Knowing this, we will keep the [eIF5B$_{\text{i}}$] differential equation. If we divide this equation by k_{5B_i} at the steady-state, we get

$$0 = [\text{eIF5B}][\text{I}_{5\text{B}}] - K_{D_{5B_i}}[\text{eIF5B}_{\text{i}}]. \tag{3.13}$$

We also add the following conservation equation for the inhibitor:

$$[\text{I}_{5\text{B}}]_{\text{T}} = [\text{I}_{5\text{B}}] + [\text{eIF5B}_{\text{i}}], \tag{3.14}$$

and we change the eIF5B conservation equation to

$$[\text{eIF5B}] = [\text{eIF5B}]_{\text{T}} - \Big([\text{TC}_{nc}] + [\text{PIC3}_{nc}] + [\text{PIC4}_{nc}] + [\text{RIB5B}] + [\text{eIF5B}_{\text{i}}]\Big). \tag{3.15}$$

There are two parameters of interest to scan and analyze their effects on the number of RIB5B complexes: the K_D of the inhibitor, and the concentration of the inhibitor. These are explored in the following subsection.

Inhibitor properties

It is imperative that we understand the properties of the inhibitors. For example, a primary question we should ask is: what concentration and value of K_{D} is necessary for inhibition to limit the concentration of ribosomes translating a message via the non-canonical pathway to a given extent? To determine the properties of the inhibitor, we vary the K_{D} of the inhibitor, as well as its total concentration and analyze the number of RIB5B complexes predicted by the model.

To help determine the dissociation constant of an effective inhibitor as well as a dosage concentration, a 3D plot was constructed that shows the concentration of ribosomes represented by RIB5B vs $\text{K}_{\text{D}_{5\text{B}_{\text{i}}}}$ and $\text{I}_{5\text{B}}$. This plot is shown in figure 3.6.

Although it is helpful to visualize the range of inhibitor properties necessary to limit the number of RIB5B complexes through a surface plot, such as that provided in figure 3.6, it is

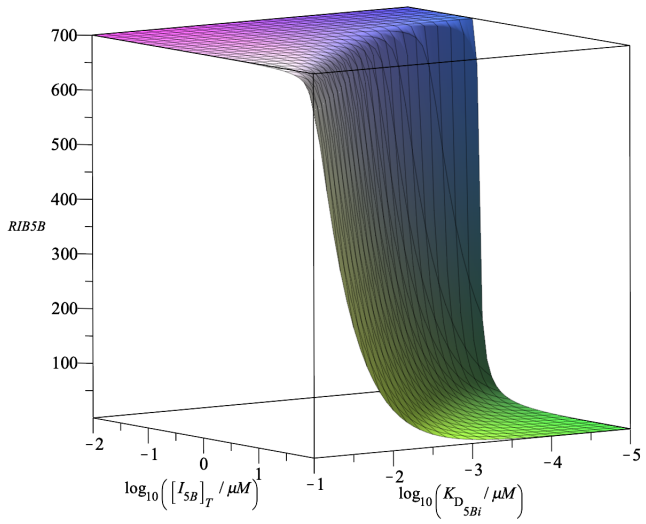

Figure 3.6: A 3-D surface plot of the number of RIB5B complexes in the cell as the total concentration of the inhibitor ($[I_{I5B}]_T$) and the dissociation constant of the inhibitor ($K_{D_{5Bi}}$) are varied. The green part of this plot is representative of the lowest number of RIB5B complexes. At smaller concentrations of inhibitor (10^{-1} – $10^{-2}\mu$M), there is no effect on the number of RIB5B complexes, regardless of the K_D value.

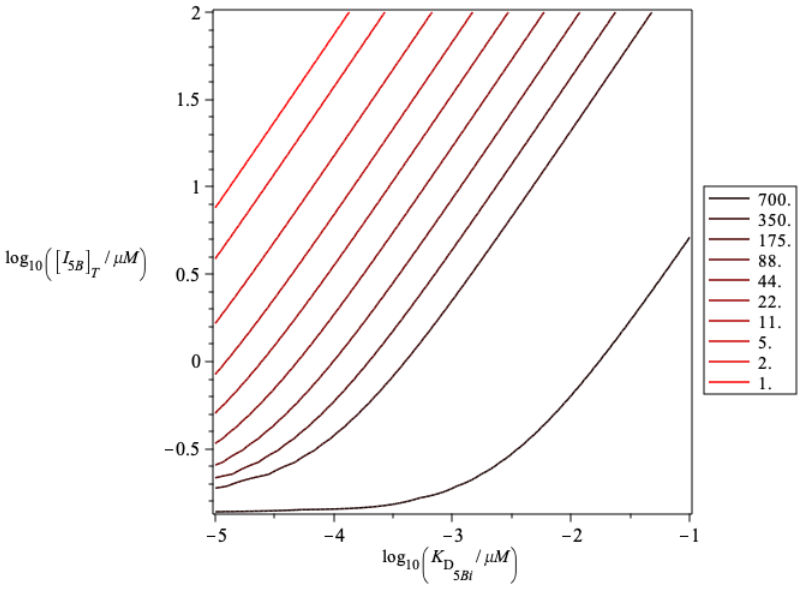

Figure 3.7: A contour plot of the inhibition of eIF5B in non-canonical translation initiation. The contour lines represent the number of RIB5B complexes assembled on the *XIAP* mRNA, where the black line represents the largest possible whole number of ribosomes (700), and the red represents the fewest (1). The IC_{50} is $\sim 2\,\mu$M when the K_D is 1 nM. A combination of inhibitor concentration and K_D values that result in a 2-fold reduction of RIB5B complexes are provided on the second darkest contour line.

not obvious from this figure what the precise values are. Therefore, throughout this thesis, surface and contour plots are provided in tandem to facilitate the extraction of data. The contour plots present curves in the $K_D \times$ [I] space on which the same degree of inhibition is obtained. The contour lines are presented at logarithmic intervals, with each contour line representing a decrease in the number of RIB5B complexes by a factor or 2 relative to the previous one. Some rounding was required during this process when the answer was not a round number. Throughout the rest of this thesis, the contour plots are presented this way.

As the K_D of the inhibitor increases, so does the concentration of inhibitor required to maintain a given number of RIB5B complexes. The black line in figure 3.7 represents the greatest whole number of ribosomes possible in the presence of an inhibitor. To decrease the number of RIB5B complexes by half, the IC_{50} is $\sim 2\,\mu$M, when the K_D of the inhibitor is 1 nM. To decrease the number of RIB5B complexes by a factor of 4 at the same K_D, a concentration of $\sim 4\,\mu$M is required.

As mentioned above, to successfully inhibit the eIF5B-mediated non-canonical translation initiation pathway through the direct inhibition of eIF5B, approximately 99% inhibition is necessary. If we consult figure 3.7, we see that the IC_{50} at a K_D of 1 nM is $2\,\mu$M. However, any pairing of concentration and K_D value will achieve the same number of RIB5B complexes along the second darkest contour line in figure 3.7.

Clearly, according to figures 3.6 and 3.7, the number of RIB5B complexes available to perform translation of the *XIAP* mRNA can be limited within a reasonable biological range of concentrations and K_D values of the potential inhibitor.

Sensitivity Analysis

Earlier it was noted that the non-canonical model was not locally sensitive to fluctuations in the total eIF5B concentration. However, experiments have indicated that silencing or knocking out/down eIF5B reduces cell viability in gliomas [20, 81], and therefore, the system is likely globally sensitive to eIF5B.

The same process that was described in section 3.2 was used to conduct this analysis. At an inhibitor concentration of $2\,\mu$M, and a dissociation constant value of 1 nM, the number of RIB5B complexes is halved, as is observed in figure 3.7. In other words, at a K_D value of 1 nM, the IC_{50} is $\sim 2\,\mu$M. Therefore, these conditions were chosen for this analysis. At these conditions, the system becomes sensitive to fluctuations in the total eIF5B concentration. The results of this sensitivity analysis are provided in table 3.6. The sensitivity coefficients presented in this table can be interpreted as multiplication factors. For example, RIB5B has a relative sensitivity of 1.04 to the total available eIF5B concentration. Therefore, a 1% increase in eIF5B concentration would lead to a 1.04% increase in the RIB5B concentration. There are some large sensitivity coefficients reported in table 3.6 such as the one previously mentioned. These large sensitivity coefficients are present in the total concentration of available eIF5B column. This is not surprising, as the non-canonical mechanism is dependent on eIF5B, which is inherent from the mechanism, and also due to the fact that this inhibition mechanism targets eIF5B directly. Particularly at the conditions at which this analysis was performed, the number of RIB5B complexes is halved. If we refer to the delay curve in figure 3.2, the number of RIB5B complexes is halved when $[\text{eIF5B}]_\text{T} = 6.9 \times 10^{-4}\,\mu$M. This is within the region of sensitivity for RIB5B, and at this point, the concentration of eIF5B has been reduced by 99%. Therefore, the large sensitivity coefficients observed in table 3.6 are consistent with the other data presented in this chapter.

Only species and parameters displaying large sensitivities in important variables were included in table 3.6. The full table of sensitivities can be found in Appendix C (see table C.1). One notable difference from sensitivity tables 3.3–3.5 is the sensitivity of RIB5B to k_3. Recall that k_3 is the rate constant for TC_{nc} formation (see step (3.1c)). As this parameter affects TC_{nc} formation, and the RIB5B complex relies on TC_{nc}, it is not surprising to see a large RIB5B sensitivity to k_3 in table 3.6. Interestingly, the sensitivity of RIB5B to $[\text{mRNA}]_\text{T}$ significantly decreases when the eIF5B inhibitor is applied to the model. This is due to $[\text{eIF5B}]_\text{T}$ becoming the limiting reagent in the system, which is confirmed through

Table 3.6: Table of selected sensitivities for non-canonical direct eIF5B inhibition. The total concentration of mRNA used in this analysis was assumed to be $2.0 \times 10^{-3}\mu$M, the total inhibitor concentration used was $2\,\mu$M, and the K_D of the inhibitor was 1nM.

	k_3	k_7	$[\text{mRNA}]_T$	$[\text{eIF5B}]_T$	$[I_{5B}]_T$	$K_{D_{5Bi}}$
eIF5B	-0.005	0.004	0.000	1.091	-1.086	0.995
$PIC2_{nc}$	-1.228	0.715	2.189	-1.346	1.340	-1.227
$PIC3_{nc}$	0.951	0.030	0.079	1.043	-1.038	0.951
$PIC4_{nc}$	0.951	0.030	0.079	1.043	-1.038	0.951
TC_{nc}	2.179	-0.685	-2.110	2.389	-2.378	2.178
mRNA	-1.204	0.709	2.171	-1.320	1.314	-1.204
I_{5B}	0.000	0.000	0.000	-0.092	1.091	0.000
RIB5B	0.951	-0.970	0.079	1.043	-1.038	0.951

the comparison of their concentrations during the analysis: $[\text{eIF5B}]_T = 6.9 \times 10^{-4}\,\mu$M, $[\text{mRNA}]_T = 2.0 \times 10^{-3}\,\mu$M. Finally, the system is sensitive to the total inhibitor concentration and the K_D of the inhibitor, as these directly impact the number of potential RIB5B complexes, which is further illustrated in figures 3.6 and 3.7.

3.3.2 Inhibition mechanism I_{P2}

Another possibility is to use an inhibitor that disrupts the TC_{nc}–PIC2 interface such that TC_{nc} cannot bind to the pre-initiation complex. This would essentially produce a buildup of TC_{nc} in the cell, as well as translation incompetent ribosome complexes, thus decreasing the amount of XIAP synthesized to help the cancer cell survive. This is a potentially dangerous inhibition mechanism, as it may slow down global translation depending on the specificity of the inhibitor. For example, one possible $PIC2_{nc}$ inhibitor affects the pre-initiation complex–$tRNA_i$ interface, which may impact the canonical TC's ability to bind to the PIC in the canonical model. This is further discussed in section 4.3.1. Again, using equations (3.1), we can add the following step to describe this inhibition mechanism:

$$\text{PIC2} \;+\; \text{I}_{\text{P2}} \underset{k_{-P2_i}}{\overset{k_{P2_i}}{\rightleftharpoons}} \text{PIC2}_\text{i}, \tag{3.16}$$

where the subscript i denotes the inhibited form of the species, and I_{P2} denotes the PIC2 inhibitor.

The [PIC2] rate equation is then modified to

$$\frac{d[\text{PIC2}_{nc}]}{dt} = k_2[\text{PIC1}_{nc}][\text{mRNA}] - k_{-2}[\text{PIC2}_{nc}] - k_4[\text{PIC2}_{nc}][\text{TC}_{nc}] + k_{-4}[\text{PIC3}_{nc}] - k_{P2_i}[\text{PIC2}_{nc}][\text{I}_{P2}] + k_{-P2_i}[\text{PIC2}_{\text{i}}], \quad (3.17a)$$

which may be problematic, since we have no knowledge of the rate constants or binding properties of this theoretical inhibitor. Therefore, we will factor out k_{P2_i} from the inhibition parts of the equation, resulting in the following:

$$\frac{d[\text{PIC2}_{nc}]}{dt} = k_2[\text{PIC1}_{nc}][\text{mRNA}] - k_{-2}[\text{PIC2}_{nc}] - k_4[\text{PIC2}_{nc}][\text{TC}_{nc}] + k_{-4}[\text{PIC3}_{nc}] + k_{P2_i}\Big(K_{D_{P2_i}}[\text{PIC2}_{\text{i}}] - [\text{PIC2}_{nc}][\text{I}_{P2}]\Big). \quad (3.17b)$$

This inhibition step also adds the following differential equations:

$$\frac{d[\text{I}_{P2}]}{dt} = -k_{P2_i}[\text{PIC2}_{nc}][\text{I}_{P2}] + k_{-P2_i}[\text{PIC2}_{\text{i}}], \quad (3.18a)$$

$$\frac{d[\text{PIC2}_{\text{i}}]}{dt} = k_{P2_i}[\text{PIC2}_{nc}][\text{I}_{P2}] - k_{-P2_i}[\text{PIC2}_{\text{i}}], \quad (3.18b)$$

which again will cancel each other out if we add them. Knowing this, we will keep equation (3.18b). Again, if we divide this equation by k_{P2_i}, at the steady-state, we get

$$0 = [\text{PIC2}_{nc}][\text{I}_{P2}] - K_{D_{P2_i}}[\text{PIC2}_{\text{i}}]. \quad (3.19)$$

We also add the following conservation equation for the inhibitor:

$$[\text{I}_{P2}]_{\text{T}} = [\text{I}_{P2}] + [\text{PIC2}_{\text{i}}]. \quad (3.20)$$

If we combine equation (3.17b) with (3.19), then only the terms in the first line survive. If we solve (3.17b) numerically with (3.19), the effect will be that the solutions do not depend on k_{P2_i} at all. Therefore, the first line of equation (3.17b) along with equation (3.19) were used in the calculations.

Unlike the eIF5B inhibition mechanism, we have more than one other conservation equation to amend, namely, the eIF3 and mRNA conservation equations, as these include PIC2 species. Taking this into account, the eIF3 and mRNA conservation equations become

$$[\text{eIF3}] = [\text{eIF3}]_\text{T} - \Big([\text{PIC1}_{nc}] + [\text{PIC2}_{nc}] + [\text{PIC2}_\text{i}] + [\text{PIC3}_{nc}] + [\text{PIC4}_{nc}]\Big), \quad (3.21a)$$

$$[\text{mRNA}] = [\text{mRNA}]_\text{T} - \Big([\text{PIC2}_{nc}] + [\text{PIC2}_\text{i}] + [\text{PIC3}_{nc}] + [\text{PIC4}_{nc}] + [\text{RIB5B}](1 + k_7\tau)\Big), \quad (3.21b)$$

The results of the numerical analysis of the above equations and the inhibitor properties are discussed below.

Inhibitor properties

To understand the dissociation constant and concentration of an effective PIC2 inhibitor, we can analyze the contour plot shown in figure 3.8. The surface plot has the same general appearance as figure 3.7, and is therefore not shown here. For the reader's reference, it is provided in Appendix A (figure A.1).

The black line in figure 3.8 represents the greatest whole number of ribosomes (i.e. 700). As we can see from figure 3.8, the parameter region at which the number of RIB5B complexes is minimized in the PIC2 inhibition mechanism is very small. Once again, effective inhibition is obtained where the concentration of the inhibitor is very large, and the K_D is very small. To reduce the number of RIB5B complexes by half, the IC_{50} is $\sim 5\,\mu$M at a K_D of 1 nM. To decrease the number of RIB5B complexes by a factor of 4 at the same

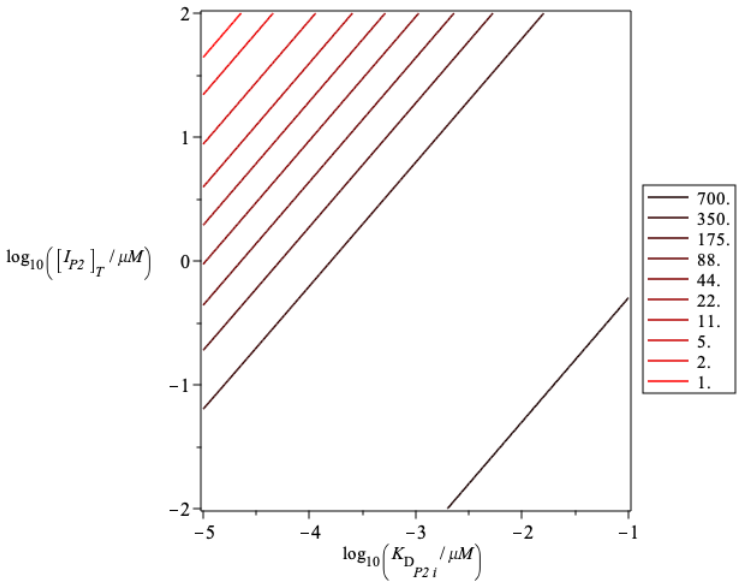

Figure 3.8: A contour plot of the inhibition of PIC2 in non-canonical translation initiation. The contour lines represent the number of RIB5B complexes, where the black line represents the largest whole number of ribosomes (700), and the red represents the fewest (1). The IC_{50} is $\sim 5\,\mu$M when the K_D is 1 nM. A combination of inhibitor concentration and K_D values that result in a 2-fold reduction of RIB5B complexes are provided on the second darkest contour line.

K_D, the concentration of inhibitor required is $\sim 16\,\mu$M.

Although the concentration of inhibitor necessary to decrease the number of ribosomes by half is smaller in the PIC2 inhibition mechanism compared to the eIF5B inhibition mechanism, the concentration required to limit the number of RIB5B complexes to 1 is much higher, and the K_D is much lower. This may be more toxic to the patient. Among other things, high concentrations of drugs often have hepatotoxic or nephrotoxic effects [82, 83, 84, 85].

Sensitivity Analysis

A sensitivity analysis for this inhibition mechanism was also conducted. The IC_{50} at a K_D of 1 nM is $\sim 5\,\mu$M, as is observed in figure 3.8. Under these conditions, we see that the RIB5B complex becomes more sensitive to fluctuations in the total eIF5B concentration. This is observed in table 3.7. Unsurprisingly, the RIB5B complex is sensitive to the total

Table 3.7: Table of selected sensitivities for non-canonical PIC2 inhibition. The total concentration of mRNA used in this analysis was assumed to be $2.0 \times 10^{-3}\mu$M, the total inhibitor concentration used was $5\,\mu$M, and the K_D of the inhibitor was 1 nM.

	k_4	k_5	k_7	$[\text{mRNA}]_T$	$[\text{eIF5B}]_T$	$[I_{P2}]_T$	$K_{D_{P2i}}$
$PIC2_{nc}$	-0.554	-0.086	0.323	1.003	-0.557	-0.446	0.446
$PIC3_{nc}$	0.444	-0.927	0.325	0.998	0.446	-0.444	0.444
$PIC4_{nc}$	0.444	0.073	0.325	0.998	0.446	-0.444	0.444
mRNA	0.426	0.070	0.327	1.003	0.428	-0.442	0.442
$PIC2_i$	-0.554	-0.086	0.323	1.002	-0.556	0.554	-0.554
RIB5B	0.444	0.073	-0.675	0.998	0.446	-0.444	0.444

mRNA concentration and k_7, which is similar to what is observed in tables 3.3 – 3.5, and it is also sensitive to fluctuations in the inhibitor concentration and K_D value. Interestingly, applying an inhibitor at a concentration and K_D value which decreases the number of RIB5B complexes by half results in an increased sensitivity to parameters k_4, k_5 and $[\text{eIF5B}]_T$.

Only species and parameters displaying large sensitivities in important variables were included in table 3.7. The full table of sensitivities can be found in Appendix C (see table C.2).

3.3.3 Inhibition mechanism I_{TC}

Along the same idea as the above, we can also inhibit the TC_{nc} from binding to PIC2 using the following additional step:

$$\text{TC} \; + \; \text{I}_{\text{TC}} \underset{k_{-TC_i}}{\overset{k_{TC_i}}{\rightleftharpoons}} \text{TC}_\text{i}., \tag{3.22}$$

where the subscript i denotes the inhibited form of the species, and I_{TC} denotes the TC_{nc} inhibitor.

This will modify the TC_{nc} differential equation to

$$\frac{d[\text{TC}_{nc}]}{dt} = k_3[\text{eIF5B}][\text{tRNA}_\text{i}] - k_{-3}[\text{TC}_{nc}] - k_4[\text{PIC2}_{nc}][\text{TC}_{nc}] + k_{-4}[\text{PIC3}_{nc}]$$
$$- k_{TC_i}[\text{TC}_{nc}][\text{I}_{\text{TC}}] + k_{-TC_i}[\text{TC}_\text{i}]. \tag{3.23a}$$

Just like we saw above in the inhibition of the PIC2 interface, we have no knowledge of the rate constants or binding properties of this theoretical inhibitor. Therefore, we will factor out k_{TC_i} from the inhibition parts of the equation, resulting in the following:

$$\frac{d[\mathrm{TC}_{nc}]}{dt} = k_3[\mathrm{eIF5B}][\mathrm{tRNA_i}] - k_{-3}[\mathrm{TC}_{nc}] - k_4[\mathrm{PIC2}_{nc}][\mathrm{TC}_{nc}] + k_{-4}[\mathrm{PIC3}_{nc}] + k_{TC_i}\Big(K_{D_{TC_i}}[\mathrm{TC_i}] - [\mathrm{TC}_{nc}][\mathrm{I_{TC}}]\Big). \quad (3.23b)$$

This inhibition step also adds the following differential equations:

$$\frac{d[\mathrm{I_{TC}}]}{dt} = -k_{TC_i}[\mathrm{TC}_{nc}][\mathrm{I_{TC}}] + k_{-TC_i}[\mathrm{TC_i}], \quad (3.24a)$$

$$\frac{d[\mathrm{TC_i}]}{dt} = k_{TC_i}[\mathrm{TC}_{nc}][\mathrm{I_{TC}}] - k_{-TC_i}[\mathrm{TC_i}], \quad (3.24b)$$

which again cancel each other out. Knowing this, we will keep equation (3.24b). If we divide this equation by k_{TC_i} at the steady-state, we get

$$0 = [\mathrm{TC}_{nc}][\mathrm{I_{TC}}] - K_{D_{TC_i}}[\mathrm{TC_i}]. \quad (3.25)$$

We also add the following conservation equation for the inhibitor:

$$[\mathrm{I_{TC}}]_\mathrm{T} = [\mathrm{I_{TC}}] + [\mathrm{TC_i}]. \quad (3.26)$$

If we solve equations (3.23b) and (3.25) numerically, the solutions do not depend on k_{TC_i}. Therefore, the first line of equation (3.23b) along with equation (3.25) were used in the calculations.

Like the eIF5B inhibition mechanism, we only need to modify the eIF5B conservation equation. Taking this into account, the new eIF5B conservation equation becomes

$$[\mathrm{eIF5B}] = [\mathrm{eIF5B}]_\mathrm{T} - \Big([\mathrm{TC}_{nc}] + [\mathrm{TC_i}] + [\mathrm{PIC3}_{nc}] + [\mathrm{PIC4}_{nc}] + [\mathrm{RIB5B}]\Big). \quad (3.27)$$

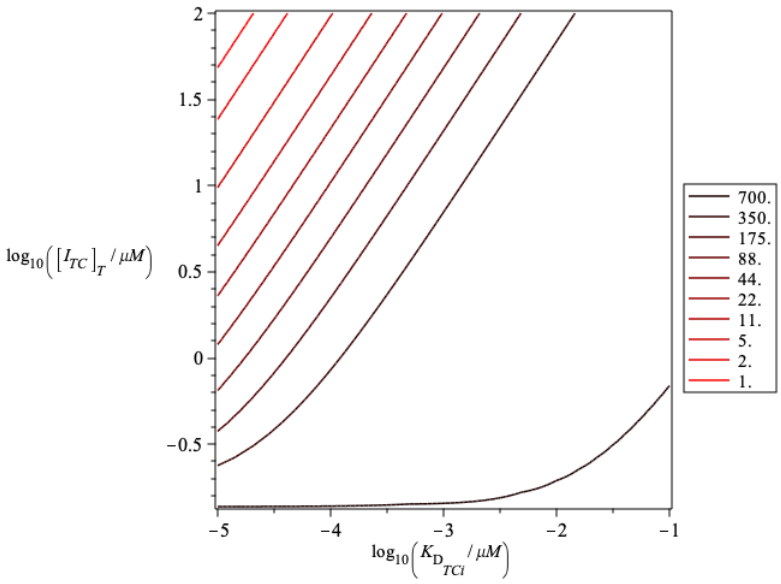

Figure 3.9: A contour plot of the inhibition of the TC_{nc} in non-canonical translation initiation. The contour lines represent the number of RIB5B complexes, where the black line represents the largest whole number of ribosomes (700), and the red represents the fewest (1). The IC_{50} is $\sim 5\,\mu$M when the K_D is 1 nM. A combination of inhibitor concentration and K_D values that result in a 2-fold reduction of RIB5B complexes are provided on the second darkest contour line.

The concentration and K_D of the inhibitor are varied in the contour plot provided in figure 3.9.

Inhibitor properties

To understand the properties of an effective inhibitor, the contour plot is provided in figure 3.9. The surface plot is similar in appearance to figure 3.7, and is therefore not shown here. For the reader's reference, it is provided in Appendix A.

The black line in figure 3.9 represents the greatest whole number of ribosomes (i.e. 700). To decrease the number of RIB5B complexes by half, the IC_{50} is $\sim 5\,\mu$M at a K_D value of 1 nM. To decrease the number of RIB5B complexes by a factor of 4 at the same K_D, the concentration of inhibitor required is $\sim 20\,\mu$M.

Similarly to the above two inhibition mechanisms, the total concentration of the TC_{nc} inhibitor decreases as the K_D decreases. The concentration of inhibitor necessary to de-

crease the number of ribosomes by half in the TC_{nc} inhibition mechanism is similar to both the eIF5B and PIC2 inhibitors. However, to limit the number of RIB5B complexes to 1, the inhibitor properties are more similar to that of the PIC2 inhibitor. As was mentioned with the PIC2 inhibitor, the conditions required to limit the number of RIB5B complexes to 1 may be toxic to the patient. However, it is not likely these conditions are necessary to promote apoptosis. Further studies should be pursued to examine the switch-like behaviour of cell fates with respect to XIAP expression.

Mechanistically, and through potential biological implications, it is easier to imagine a ternary complex inhibitor having less of an effect (or no effect at all) on the canonical mechanism at high concentrations than the direct eIF5B inhibitor. This is further discussed in chapter 4.

Sensitivity Analysis

Like directly inhibiting eIF5B, inhibiting the ternary complex limits the amount of eIF5B available. Therefore, the system becomes more locally sensitive to fluctuations in the total eIF5B concentration. The results of this sensitivity analysis are provided in table 3.8. Only species and parameters displaying large sensitivities in important variables, and specific sensitivities for discussion were included in the table. The full table of sensitivities can be found in Appendix C (see table C.3).

As was expected, the RIB5B complex was sensitive to the total eIF5B concentration when the TC inhibition mechanism was applied. The IC_{50} at a K_D of 1 nM is $\sim 5\,\mu$M as is observed in figure 3.9. Interestingly, the complex's sensitivity is less in the TC inhibition mechanism than in the direct eIF5B inhibition mechanism, despite the fact that the number of RIB5B complexes are still reduced by half at these inhibition conditions.

3.3.4 Inhibition mechanism I_{R5B}

Like inhibiting the PIC2 interface, this is also a dangerous inhibition mechanism, as this too may slow down global translation. Essentially, we could also think about inhibiting

Table 3.8: Table of selected sensitivities for non-canonical TC_{nc} inhibition. The total concentration of mRNA used in this analysis was assumed to be $2.0 \times 10^{-3}\mu$M, the total inhibitor concentration used was 5μM, and the K_D of the inhibitor was 1nM.

	k_4	k_{-4}	k_5	k_7	$[\text{mRNA}]_\text{T}$	$[\text{eIF5B}]_\text{T}$	$[\text{I}_\text{TC}]_\text{T}$	$K_{D_{TCi}}$
eIF5B	0.398	-0.063	0.065	0.330	0.960	0.453	-0.450	0.435
$PIC2_{nc}$	-0.585	0.093	-0.091	0.341	1.003	-0.608	0.605	-0.584
$PIC3_{nc}$	0.413	-0.066	-0.932	0.343	0.998	0.430	-0.428	0.413
$PIC4_{nc}$	0.413	-0.066	0.068	0.343	0.998	0.430	-0.428	0.413
TC_{nc}	-0.002	0.000	0.000	0.003	-0.005	1.037	-1.032	0.998
mRNA	-0.573	0.091	-0.089	0.342	1.007	-0.595	0.592	-0.572
TC_i	-0.002	0.000	0.000	0.002	-0.005	1.003	0.002	-0.002
RIB5B	0.413	-0.066	0.068	-0.657	0.998	0.430	-0.428	0.413

eIF5B's hydrolysis, therefore accumulating pre-initiation complexes in the cell. This adds the following step:

$$\text{RIB5B} + \text{I}_\text{R5B} \underset{\text{k}_{-\text{R5B}_\text{i}}}{\overset{\text{k}_{\text{R5B}_\text{i}}}{\rightleftharpoons}} \text{RIB5B}_\text{i}, \tag{3.28}$$

where the subscript i denotes the inhibited form of the species, and I_R5B denotes the RIB5B inhibitor.

This will modify the RIB5B differential equation to

$$\frac{d[\text{RIB5B}]}{dt} = k_6[\text{PIC4}_{nc}] - k_7[\text{RIB5B}] - k_{R5B_i}[\text{RIB5B}][\text{I}_\text{R5B}] + k_{-R5B_i}[\text{RIB5B}_\text{i}]. \tag{3.29a}$$

Just as we have done with the previous examples, we may factor out k_{R5B_i} from the inhibition terms to arrive at our final differential equation for RIB5B:

$$\frac{d[\text{RIB5B}]}{dt} = k_6[\text{PIC4}_{nc}] - k_7[\text{RIB5B}] + k_{R5B_i}\Big(K_{D_{R5B_i}}[\text{RIB5B}_\text{i}] - [\text{RIB5B}][\text{I}_\text{R5B}]\Big). \tag{3.29b}$$

This inhibition step also adds the following differential equations:

$$\frac{d[\text{I}_\text{R5B}]}{dt} = -k_{R5B_i}[\text{RIB5B}][\text{I}_\text{R5B}] + k_{-R5B_i}[\text{RIB5B}_\text{i}], \tag{3.30a}$$

$$\frac{d[\text{RIB5B}_\text{i}]}{dt} = k_{R5B_i}[\text{RIB5B}][\text{I}_\text{R5B}] - k_{-R5B_i}[\text{RIB5B}_\text{i}], \tag{3.30b}$$

which once again cancel each other if we add them. We will keep equation (3.30b). If we divide this equation by k_{R5B_i}, we get

$$0 = [\text{RIB5B}][\text{I}_{\text{R5B}}] - K_{D_{R5B_i}}[\text{RIB5B}_\text{i}]. \tag{3.31}$$

We also add the following conservation equation for the inhibitor:

$$[\text{I}_{\text{R5B}}]_\text{T} = [\text{I}_{\text{R5B}}] + [\text{RIB5B}_\text{i}]. \tag{3.32}$$

We also need to consider the effect of this mechanism on the eIF5B and mRNA conservation equations, which change to the following:

$$[\text{eIF5B}] = [\text{eIF5B}]_\text{T} - \Big([\text{TC}_{nc}] + [\text{PIC3}_{nc}] + [\text{PIC4}_{nc}] + [\text{RIB5B}] + [\text{RIB5B}_\text{i}]\Big), \tag{3.33a}$$

$$[\text{mRNA}] = [\text{mRNA}]_\text{T} - \Big([\text{PIC2}_{nc}] + [\text{PIC3}_{nc}] + [\text{PIC4}_{nc}] + [\text{RIB5B}_\text{i}] + [\text{RIB5B}](1 + k_7\tau)\Big), \tag{3.33b}$$

If we solve equations (3.29b) and (3.31) numerically, the solutions do not depend on k_{R5B_i}. Therefore, the first two terms of equation (3.29b) along with equation (3.31) were used in the calculations.

The concentration and K_D of the inhibitor are varied in the 3D surface and contour plots provided in figures 3.10 and 3.11.

Inhibitor properties

Once again, we compute a contour plot of this inhibition mechanism. The 3D surface plot is shown in figure 3.10, and the contour plot is is provided in figure 3.11.

Unlike the last three inhibition mechanisms explored, there is a much larger parameter region in which the number of RIB5B complexes is limited. The contour plot in figure 3.11 shows that any combination of inhibitor properties that resides in the region about the red line will result in only 1 RIB5B complex. To decrease the number of RIB5B complexes by

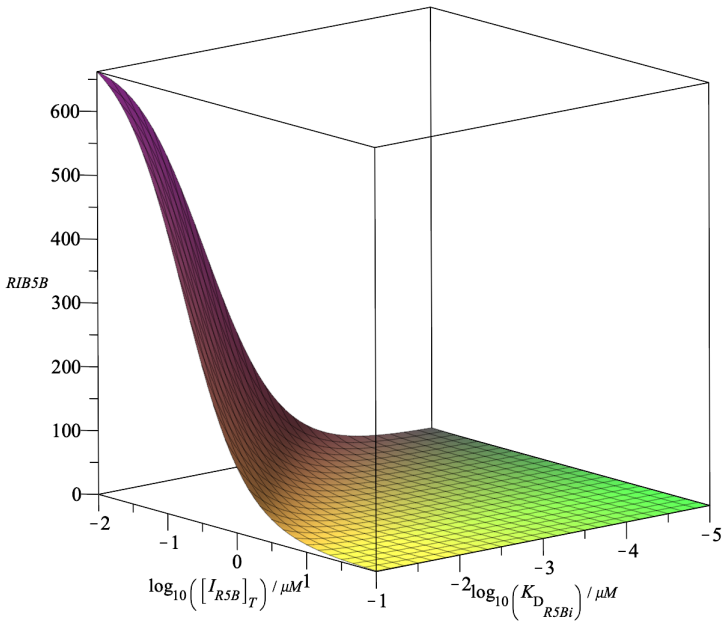

Figure 3.10: A 3-D surface plot of the number of RIB5B complexes in the cell as the total concentration of the inhibitor ($[I_{R5B}]_T$) and the dissociation constant of the inhibitor ($K_{D_{R5Bi}}$) are varied. Compared to the other inhibition mechanisms, the area in which the lowest number of RIB5B complexes are present is much greater, covering nearly all of the parameter values.

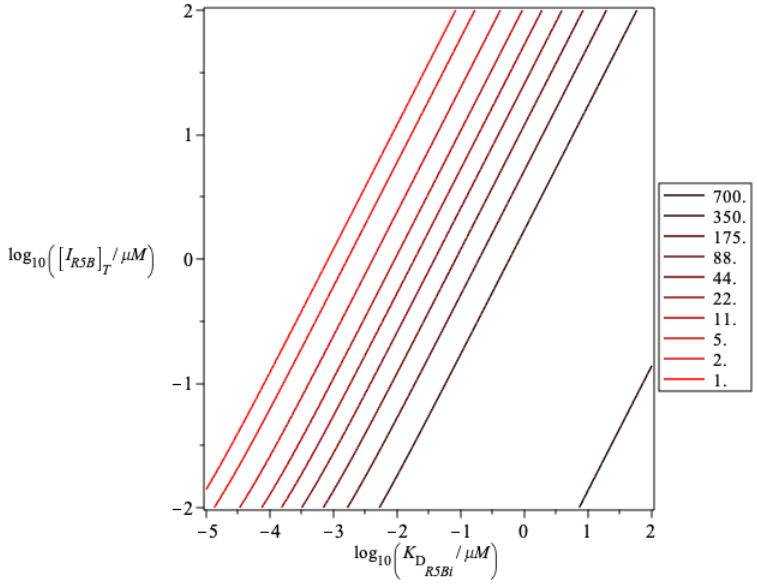

Figure 3.11: A contour plot of the inhibition of RIB5B in the non-canonical translation initiation mechanism. The contour lines represent the number of RIB5B complexes, where the black line represents the largest whole number of ribosomes (700), and the red represents the fewest (1). By extrapolation, the IC_{50} is $\sim 3\times10^{-3}$ μM at a K_D of 1 nM. A combination of inhibitor concentration and K_D values that result in a 2-fold reduction of RIB5B complexes are provided on the second darkest contour line.

half, the IC_{50} is ~ 3 nM at a K_D of 1 nM. To decrease the number of RIB5B complexes by a factor of 4 at the same K_D value, the concentration of inhibitor required is ~ 6 nM.

Although this inhibition mechanism appears to be promising due to the properties necessary to limit the number of RIB5B complexes, it is important to consider that the RIB5B complex is also present in the canonical mechanism, and therefore, the effects should be analyzed in this mechanism before any conclusions are made regarding the most promising inhibitor option.

At first glance, the RIB5B inhibitor seems to be promising. The 3D surface plot provided in figure 3.10 shows a large parameter region where the number of RIB5B complexes is small. Indeed, even at low concentrations of inhibitor considering a 1 nM K_D, the number of RIB5B complexes is still very small (i.e. less than 44). This is perhaps seen more obviously in the contour plot provided in figure 3.11, where even at low concentrations and large values of K_D, the number of RIB5B complexes are still greatly limited.

However, although this may seem promising, we must recall that the RIB5B complex is present in both the canonical and non-canonical models, and therefore, we need to consider the effects this inhibition mechanism may have on canonical translation initiation as well. These effects are explored in chapter 4.

Sensitivity Analysis

The IC_{50} at a K_D of 1 nM is $\sim 3\times10^{-3}\,\mu$M as is observed in figure 3.11, therefore these values were chosen for the sensitivity analysis. Only species and parameters displaying large sensitivities in important variables, and specific sensitivities for discussion were included in table 3.9. The full table of sensitivities can be found in Appendix C (table C.4).

Interestingly, despite RIB5B being an eIF5B-containing complex, it is not locally sensitive to fluctuations in the total eIF5B concentration. Unsurprisingly, RIB5B is sensitive to the total inhibitor concentration and K_D of the inhibitor. RIB5B remains sensitive to the total mRNA concentration, however its sensitivity to k_7 is decreased compared to the sen-

Table 3.9: Table of selected sensitivities for non-canonical RIB5B inhibition. The total concentration of mRNA used in this analysis was $2.0\times10^{-3}\,\mu$M. This analysis was performed at an inhibitor concentration of $3\times10^{-3}\,\mu$M, and a K_D value of 1 nM.

	k_7	$[\text{mRNA}]_\text{T}$	$[\text{eIF5B}]_\text{T}$	$[\text{I}_{5\text{B}}]_\text{T}$	$K_{D_{5Bi}}$
PIC2	0.769	1.185	-1.010	-0.963	0.623
PIC3	0.771	1.175	0.000	-0.965	0.624
PIC4	0.771	1.175	0.000	-0.965	0.624
mRNA	0.771	1.176	-0.016	-0.965	0.624
I_{R5B}	0.064	-0.330	0.000	1.816	-0.175
RIB5B_i	-0.165	0.845	0.000	0.851	-0.551
RIB5B	-0.229	1.175	0.000	-0.965	0.624

Table 3.10: Summary of approximate IC_{50} values and their respective K_D values for each non-canonical inhibition target.

Inhibition Target	**IC_{50} (μM)**	**K_D (nM)**
eIF5B	2	1
PIC2	5	1
TC	5	1
RIB5B	0.003	1

sitivity analyses presented in tables 3.3–3.5. It takes approximately 30 s to hydrolyze the GTP on eIF5B and transition from translation initiation to elongation [37]. Therefore, small changes in this time may be less critical to the system than changes to the rate constants for RIB5B inhibition. Additionally, RIB5B_i acts as a reservoir for RIB5B, and thus Le Chatellier's principle will have a strong effect on this mechanism since step (3.1g) is irreversible. Thus the reverse binding step of the inhibitor will compensate for the RIB5B transformed into RIB. This explains why RIB5B's sensitivity to k_7 is smaller than what we observed in tables 3.3– 3.5, and is also small compared to the sensitivity of RIB5B to $K_{D_{R5BI}}$.

3.4 Effects of Inhibition Mechanisms

Although the greatest level of inhibition occurs at high concentrations of inhibitor and low values of K_D across the inhibition options presented here, it is likely not necessary to limit the number of RIB5B complexes to 1 to promote apoptosis of the cancerous cell.

Therefore, it may be of interest to study the switch-like behaviour of cell fates with respect to XIAP expression before determining which is the best of the inhibitor options.

A summary of the IC_{50} values and their respective K_D values for each non-canonical inhibition target is provided in table 3.10. It is important to consider not only the mathematics behind the properties of the inhibitors, but also the possible biological consequences of the inhibitors. Although we observe similar behaviours across all of the inhibition mechanisms, we should consider the mechanism of inhibition. In particular, the inhibitor discussed and outlined in the PIC2 and RIB5B inhibition subsections would bind directly to the PIC interface, which could cause some biological problems when applied to the canonical pathway. Again, the purpose of these potential inhibitors is to inhibit the non-canonical mechanism with minimal toxicity to the patient. For this reason, the effects of each inhibition mechanism on the canonical model which are explored in the next chapter, and further discussed in chapter 5.

Chapter 4

Canonical translation initiation

A critical component of this study was to analyze the effects of the non-canonical inhibition mechanisms on the canonical model to determine whether the hypothesized therapy would be toxic (i.e. significantly reduce the number of canonically assembled RIB5B complexes) to the patient. Type-1 collagen (Uniprot ID: P02452) and β-actin (Uniprot ID: P60709) were chosen for analysis for a number of reasons. Both proteins are highly abundant, and perform important maintenance roles within cells. Additionally, diseases such as osteoporosis have been associated with chemotherapy due to improper gene expression of type-1 collagen, and β-actin [86]. Therefore, it is important to ensure the gene expression of essential proteins such as type-1 collagen and β-actin are not too strongly affected by the above proposed inhibition mechanisms.

Canonical translation initiation is comprised of four main steps: assembly of the 43S pre-initiation complex, recruitment of the mRNA to the 43S pre-initiation complex, scanning to find the AUG start codon, and final assembly of the 80S ribosome. The biological process of these steps is provided in the model below. This model also contains a clearance delay that again represents the time required for the RIB5B complex to clear the RBS and move into the elongation phase of translation.

Recall from figure 1.1: canonical translation initiation begins via eIFs 1, 3, and 5 binding to the 40S ribosomal subunit. The ternary complex comprised of eIF2, $tRNA_i$ and a GTP molecule (not shown in the mechanism) is formed. After it has been assembled, the TC then binds, establishing the 43S pre-intiation complex. Up until this point, these have

been generic steps that involve the cellular pool of initiation factors. In other words, these steps are required to prepare any canonically assembled ribosome for translation. The cellular pool begins to affect the translation of specific mRNAs when eIF4E and eIF4G bind to the 5' cap of the mRNA, creating an mRNA complex (denoted mRNA_c in the model). The mRNA complex then binds to the previously assembled 43S pre-initiation complex, establishing the 48S complex. The 48S then scans for the AUG codon. Once the start codon has been reached, eIF5 hydrolyzes the GTP on eIF2 prompting eIF2 dissociation, which is followed by eIF5B recruitment to the pre-intiation complex. After eIF5B has bound, eIFs 1, 3, and 5 then dissociate. The 60S ribosomal subunit is then recuited to the pre-initiation complex, which promotes the dissociation of eIFs 4E and 4G. Finally, eIF5B dissociates, leaving the translation competent 80S ribosome. The canonical model is as follows:

$$40\text{S} + \text{eIF3} \underset{k_{-1}}{\overset{k_1}{\rightleftharpoons}} \text{PIC1} \tag{4.1a}$$

$$\text{PIC1} + \text{eIF5} \underset{k_{-2}}{\overset{k_2}{\rightleftharpoons}} \text{PIC2} \tag{4.1b}$$

$$\text{PIC2} + \text{eIF1} \underset{k_{-3}}{\overset{k_3}{\rightleftharpoons}} \text{PIC3} \tag{4.1c}$$

$$\text{eIF2} + \text{tRNA}_\text{i} \underset{k_{-4}}{\overset{k_4}{\rightleftharpoons}} \text{TC} \tag{4.1d}$$

$$\text{PIC3} + \text{TC} \underset{k_{-5}}{\overset{k_5}{\rightleftharpoons}} \text{PIC4} \tag{4.1e}$$

$$\text{eIF4E} + \text{eIF4G} \underset{k_{-6}}{\overset{k_6}{\rightleftharpoons}} \text{eIF4}_\text{c} \tag{4.1f}$$

$$\text{eIF4}_\text{c} + \text{mRNA}_\text{f} \underset{k_{-7}}{\overset{k_7}{\rightleftharpoons}} \text{mRNA}_\text{c} \tag{4.1g}$$

$$\text{PIC4} + \text{mRNA}_\text{c} \underset{k_{-8}}{\overset{k_8}{\rightleftharpoons}} \text{PIC5} \tag{4.1h}$$

$$\text{PIC5} \xrightarrow{k_9} \text{PIC6} + \text{eIF2} \tag{4.1i}$$

$$\text{PIC6} + \text{eIF5B} \underset{k_{-10}}{\overset{k_{10}}{\rightleftharpoons}} \text{PIC7} \tag{4.1j}$$

Table 4.1: Abbreviations for the biochemical complexes present in the canonical model of eukaryotic translation initiation.

Biological Complex	Abbreviation
$40S \cdot eIF3$	PIC1
$40S \cdot eIF3 \cdot eIF5$	PIC2
$40S \cdot eIF3 \cdot eIF5 \cdot eIF1$	PIC3
$40S \cdot eIF3 \cdot eIF5 \cdot eIF1 \cdot TC$	PIC4
$40S \cdot eIF3 \cdot eIF5 \cdot eIF1 \cdot TC \cdot mRNA_c$	PIC5
$40S \cdot eIF3 \cdot eIF5 \cdot eIF1 \cdot tRNA_i \cdot mRNA_c$	PIC6
$40S \cdot eIF3 \cdot eIF5 \cdot eIF1 \cdot tRNA_i \cdot mRNA_c \cdot eIF5B$	PIC7
$40S \cdot tRNA_i \cdot mRNA_c \cdot eIF5B$	PIC8
$40S \cdot tRNA_i \cdot mRNA_c \cdot eIF5B \cdot 60S$	PIC9
$80S \cdot eIF5B$	RIB5B
$eIF2 \cdot tRNA_i$	TC
$mRNA \cdot eIF4E \cdot eIF4G$	$mRNA_c$
$eIF4E \cdot eIF4G$	$eIF4_c$

$$\text{PIC7} \xrightarrow{k_{11}} \text{PIC8} + \text{eIF1} + \text{eIF3} + \text{eIF5} \tag{4.1k}$$

$$\text{PIC8} + 60S \underset{k_{-12}}{\overset{k_{12}}{\rightleftharpoons}} \text{PIC9} \tag{4.1l}$$

$$\text{PIC9} \xrightarrow{k_{13}} \text{RIB5B} + \text{eIF4E} + \text{eIF4G} \tag{4.1m}$$

$$\text{RIB5B} \xrightarrow{k_{14}} \text{RIB} + \text{eIF5B} + \text{mRNA}_f(t+\tau) \tag{4.1n}$$

where the $eIF4_c$, $mRNA_f$ and $mRNA_c$ denote the 5' cap complex, and free and complexed state of the mRNA, respectively. Note that the fate of the RIB complex (80S ribosome) is ignored due to the fact that the last step in the canonical mechanism is irreversible. Abbreviations for the complexes are described in table 4.1.

One of the primary differences between the canonical mechanism described in this chapter, and the non-canonical mechanism described in chapters 2 and 3 is that the canonical ternary complex uses eIF2 as the delivery initiation factor for the initiator tRNA, whereas the non-canonical ternary complex uses eIF5B. Additionally, the mechanistic assembly of the 80S ribosomes differ. In non-canonical translation initiation, the mRNA is recruited before the eIF5B-ternary complex binds to the pre-initiation complex. In canoni-

cal translation initiation, the mRNA is recruited *after* the eIF2-ternary complex has bound to the pre-initiation complex. Finally, canonical translation is, by definition, cap-dependent. eIFs 4E and 4G bind to the 5' cap of the mRNA before it is recruited to the pre-initiation complex. The non-canonical mechanism described earlier in chapters 2 and 3 is cap-independent (but IRES-dependent).

As the canonical mechanism encompasses general eukaryotic translation initiation, we will look at a number of different essential mRNAs and determine whether the inhibition mechanisms affect their translation. These mechanisms are applied to type-1 collagen and β-actin in section 4.3.

4.1 Parameters

Many rate constants were borrowed from the previously published canonical model by Firczuk *et al.* (2013) [56]. The K_D of eIF3 interacting with the 40S subunit in humans is 6 nM [64]. The K_D for the ternary complex binding to the 40S subunit is 2.9 nM [87]. The rate constant for 60S binding to the 48S is $0.81\,\mu\text{M}^{-1}\text{s}^{-1}$ [72]. Finally, after the 80S ribosome has been assembled in the canonical pathway, eIF5B takes approximately 29.1 s to hydrolyze GTP and dissociate from the complex [37], which was also used in the non-canonical model as they share this terminal step in eukaryotic translation initiation. The values used for k_3, k_{-3}, k_4, and k_{-4} were adopted from Firczuk *et al.* (2013) [56] as measured rate constants were not available in the literature to the best of my knowledge. The rate constants and concentrations of species used in the canonical model can be found in table 4.2.

On average, a eukaryotic ribosome occupies 12 codons on an mRNA or 30–35 nucleotides [89]. The average translation rate in human is approximately 5 amino acids per second [90]. We can calculate a value for τ using this information: the time it takes for the ribosome to clear its initial binding site is approximately 2 seconds.

Table 4.2: Parameters, species and their corresponding sources used in the canonical model with a clearance delay under hypoxic conditions. [a] denotes an assumed value, and [c] denotes a calculated value.

Parameters / Species	**Value**	**Source**
k_1	$1\,\mathrm{nM^{-1}s^{-1}}$	[c][64]
k_{-1}	$6\,\mathrm{s^{-1}}$	[c][64]
k_2	$20\,\mu\mathrm{M^{-1}s^{-1}}$	[56]
k_{-2}	$0.41\,\mathrm{s^{-1}}$	[56]
k_3	$0.81\,\mu\mathrm{M^{-1}s^{-1}}$	[56]
k_{-3}	$1\,\mathrm{s^{-1}}$	[a]
k_4	$0.11\,\mu\mathrm{M^{-1}s^{-1}}$	[56]
k_{-4}	$6.3\,\mathrm{s^{-1}}$	[56]
k_5	$0.34\,\mathrm{nM^{-1}s^{-1}}$	[c][87]
k_{-5}	$1\,\mathrm{s^{-1}}$	[c][87]
k_6	$43\,\mu\mathrm{M^{-1}s^{-1}}$	[56]
k_{-6}	$2.0\times10^{3}\,\mathrm{s^{-1}}$	[56]
k_7	$58\,\mu\mathrm{M^{-1}s^{-1}}$	[56]
k_{-7}	$2.7\,\mathrm{s^{-1}}$	[56]
k_8	$1\,\mathrm{nM^{-1}s^{-1}}$	[a]
k_{-8}	$1\,\mathrm{s^{-1}}$	[a]
k_9	$13\,\mathrm{s^{-1}}$	[88]
k_{10}	$1\,\mathrm{nM^{-1}s^{-1}}$	[a]
k_{-10}	$1\,\mathrm{s^{-1}}$	[a]
k_{11}	$1\,\mathrm{s^{-1}}$	[a]
k_{12}	$0.81\,\mu\mathrm{M^{-1}s^{-1}}$	[72]
k_{-12}	$1\,\mathrm{s^{-1}}$	[a]
k_{13}	$1\,\mathrm{s^{-1}}$	[a]
k_{14}	$0.035\,\mathrm{s^{-1}}$	[37]
[40S]	$5.3\,\mu\mathrm{M}$	[c][56]
[60S]	$7.6\,\mu\mathrm{M}$	[56]
$[\mathrm{eIF3}]_\mathrm{T}$	$0.21\,\mu\mathrm{M}$	[c][56]
$[\mathrm{eIF5}]_\mathrm{T}$	$0.083\,\mu\mathrm{M}$	[c][56]
$[\mathrm{eIF1}]_\mathrm{T}$	$1.5\,\mu\mathrm{M}$	[c][56]
$[\mathrm{eIF2}]_\mathrm{T}$	$0.035\,\mu\mathrm{M}$	[c][56]
$[\mathrm{eIF4E}]_\mathrm{T}$	$2.6\,\mu\mathrm{M}$	[c][56]
$[\mathrm{eIF4G}]_\mathrm{T}$	$0.27\,\mu\mathrm{M}$	[c][56]
$[\mathrm{eIF5B}]_\mathrm{T}$	$0.20\,\mu\mathrm{M}$	[c][56]
$[\mathrm{mRNA}]_\mathrm{T}$	Variable	
$[\mathrm{tRNA_i}]$	$26\,\mu\mathrm{M}$	[56]
τ	$2\,\mathrm{s}$	[c]

4.2 Analytical solution

In this model, we have one clearance delay which describes the amount of time it takes for the mRNA to become available again for another 40S ribosome to bind to it. The mRNA will be available for binding again at time $t+\tau$. The rate at which the mRNA becomes available to another ribosome at time t depends on the rate of initation at $t-\tau$. Therefore, the free mRNA is removed from the total mRNA at a rate $k_7[\text{eIF4}_\text{c}][\text{mRNA}_\text{f}]$ and returned at a rate $k_{14}[\text{RIB5B}](t-\tau)$. We can apply this reasoning to derive the following DDEs for the canonical model. Note that the 40S, 60S, and Met-tRNA$_\text{i}$ concentrations are held constant in this model, as their concentrations are much higher than those of the other species in this model, and therefore their decrease in concentration when participating in the reactions will be negligible compared to their initial concentrations. There is no equation for RIB, as its synthesis step is irreversible.

If we apply the delayed mass-action law to this canonical model, the following DDEs result:

$$\frac{d[\text{PIC1}]}{dt} = k_1[\text{40S}][\text{eIF3}] - k_{-1}[\text{PIC1}] - k_2[\text{PIC1}][\text{eIF5}] + k_{-2}[\text{PIC2}], \tag{4.2a}$$

$$\frac{d[\text{PIC2}]}{dt} = k_2[\text{PIC1}][\text{eIF5}] - k_{-2}[\text{PIC2}] - k_3[\text{PIC2}][\text{eIF1}] + k_{-3}[\text{PIC3}], \tag{4.2b}$$

$$\frac{d[\text{PIC3}]}{dt} = k_3[\text{PIC2}][\text{eIF1}] - k_{-3}[\text{PIC3}] - k_5[\text{PIC3}][\text{TC}] + k_{-5}[\text{PIC4}], \tag{4.2c}$$

$$\frac{d[\text{TC}]}{dt} = k_4[\text{eIF2}][\text{tRNAi}] - k_{-4}[\text{TC}] - k_5[\text{PIC3}][\text{TC}] + k_{-5}[\text{PIC4}], \tag{4.2d}$$

$$\frac{d[\text{PIC4}]}{dt} = k_5[\text{PIC3}][\text{TC}] - k_{-5}[\text{PIC4}] - k_8[\text{PIC4}][\text{mRNA}_\text{c}] + k_{-8}[\text{PIC5}], \tag{4.2e}$$

$$\frac{d[\text{eIF4}_\text{c}]}{dt} = k_6[\text{eIF4E}][\text{eIF4G}] - k_{-6}[\text{eIF4}_\text{c}] - k_7[\text{eIF4}_\text{c}][\text{mRNA}_\text{f}] + k_{-7}[\text{mRNA}_\text{c}], \tag{4.2f}$$

$$\frac{d[\text{mRNA}_\text{f}]}{dt} = -k_7[\text{eIF4}_\text{c}][\text{mRNA}_\text{f}] + k_{-7}[\text{mRNA}_\text{c}] + k_{14}[\text{RIB5B}](t-\tau), \tag{4.2g}$$

$$\frac{d[\text{mRNA}_\text{c}]}{dt} = k_7[\text{eIF4}_\text{c}][\text{mRNA}_\text{f}] - k_{-7}[\text{mRNA}_\text{c}] - k_8[\text{PIC4}][\text{mRNA}_\text{c}] + k_{-8}[\text{PIC5}], \tag{4.2h}$$

$$\frac{d[\text{PIC5}]}{dt} = k_8[\text{PIC4}][\text{mRNA}_\text{c}] - k_{-8}[\text{PIC5}] - k_9[\text{PIC5}] \tag{4.2i}$$

$$\frac{d[\text{PIC6}]}{dt} = k_9[\text{PIC5}] - k_{10}[\text{PIC6}][\text{eIF5B}] + k_{-10}[\text{PIC7}], \tag{4.2j}$$

$$\frac{d[\text{PIC7}]}{dt} = k_{10}[\text{PIC6}][\text{eIF5B}] - k_{-10}[\text{PIC7}] - k_{11}[\text{PIC7}] \tag{4.2k}$$

$$\frac{d[\text{PIC8}]}{dt} = k_{11}[\text{PIC7}] - k_{12}[\text{PIC8}][\text{60S}] + k_{-12}[\text{PIC9}] \tag{4.2l}$$

$$\frac{d[\text{PIC9}]}{dt} = k_{12}[\text{PIC8}][\text{60S}] - k_{-12}[\text{PIC9}] - k_{13}[\text{PIC9}], \tag{4.2m}$$

$$\frac{d[\text{RIB5B}]}{dt} = k_{13}[\text{PIC9}] - k_{14}[\text{RIB5B}]. \tag{4.2n}$$

Additionally, we must consider the conservation relationships in this model which are represented by the following equations:

$$[\text{eIF3}]_\text{T} = [\text{eIF3}] + [\text{PIC1}] + [\text{PIC2}] + [\text{PIC3}] + [\text{PIC4}] + [\text{PIC5}] + [\text{PIC6}] + [\text{PIC7}], \tag{4.3a}$$

$$[\text{eIF5}]_\text{T} = [\text{eIF5}] + [\text{PIC2}] + [\text{PIC3}] + [\text{PIC4}] + [\text{PIC5}] + [\text{PIC6}] + [\text{PIC7}], \tag{4.3b}$$

$$[\text{eIF1}]_\text{T} = [\text{eIF1}] + [\text{PIC3}] + [\text{PIC4}] + [\text{PIC5}] + [\text{PIC6}] + [\text{PIC7}], \tag{4.3c}$$

$$[\text{eIF2}]_\text{T} = [\text{eIF2}] + [\text{TC}] + [\text{PIC4}] + [\text{PIC5}], \tag{4.3d}$$

$$[\text{eIF4E}]_\text{T} = [\text{eIF4E}] + [\text{eIF4}_\text{c}] + [\text{mRNA}_\text{c}] + [\text{PIC5}] + [\text{PIC6}] + [\text{PIC7}] + [\text{PIC8}] + [\text{PIC9}], \tag{4.3e}$$

$$[\text{eIF4G}]_\text{T} = [\text{eIF4G}] + [\text{eIF4}_\text{c}] + [\text{mRNA}_\text{c}] + [\text{PIC5}] + [\text{PIC6}] + [\text{PIC7}] + [\text{PIC8}] + [\text{PIC9}], \tag{4.3f}$$

$$[\text{eIF5B}]_\text{T} = [\text{eIF5B}] + [\text{PIC7}] + [\text{PIC8}] + [\text{PIC9}] + [\text{RIB5B}]. \tag{4.3g}$$

As was the case in the non-canonical model, the total amount of mRNA is conserved, and therefore a conservation relation must be accounted for. This is expressed by the following equation:

$$[\text{mRNA}]_\text{T} = [\text{mRNA}_\text{f}] + [\text{mRNA}_\text{c}] + [\text{PIC5}] + [\text{PIC6}] + [\text{PIC7}] + [\text{PIC8}] + [\text{PIC9}] + k_{14}\int_{t-\tau}^{t} [\text{RIB5B}](\theta)d\theta, \quad (4.4)$$

where $[\text{mRNA}]_\text{T}$ is the constant amount of mRNA, $[\text{mRNA}_\text{f}]$ is the free mRNA and the term $k_{14}[\text{RIB5B}](\theta)$ is the rate at which the translation moves into the early elongation phase at time $\theta \in [t-\tau, t]$. The integral term in equation (4.4) represents the amount of mRNA unavailable due to ribosome binding between $t-\tau$ and t. The free mRNA, occluded mRNA, and mRNA within pre-initiation complexes 5 – 9 comprise the total mRNA in the system, and is constant. We can take a time derivative of equation (4.4) which results in the following:

$$\frac{[\text{mRNA}]_\text{T}}{dt} = \frac{d[\text{mRNA}_\text{f}]}{dt} + \frac{d[\text{mRNA}_c]}{dt} + \frac{d[\text{PIC5}]}{dt} + \frac{d[\text{PIC6}]}{dt} + \frac{d[\text{PIC7}]}{dt} + \frac{d[\text{PIC8}]}{dt} + \frac{d[\text{PIC9}]}{dt} + k_{14}[\text{RIB5B}](t) - k_{14}[\text{RIB5B}](t-\tau).$$

We can then substitute equation set (4.2) into the above equation to show that $\frac{d[\text{mRNA}]_\text{T}}{dt} = 0$ at the steady-state. This proves that, at the steady-state, the total mRNA given by equation (4.4) is constant. When the system reaches a steady-state, [RIB5B] is constant, which reduces equation (4.4) to

$$[\text{mRNA}]_\text{T} = [\text{mRNA}_\text{f}] + [\text{mRNA}_c] + [\text{PIC5}] + [\text{PIC6}] + [\text{PIC7}] + [\text{PIC8}] + [\text{PIC9}] + [\text{RIB5B}](1 + k_{14}\tau). \quad (4.5)$$

Once again, an initial function for the values of [RIB5B] is required since the forward time evolution of $[\text{mRNA}_\text{f}]$ depends on past values of [RIB5B]. In this case, the initial function is $[\text{RIB5B}] = 0$ for $t \in [-\tau, 0]$.

4.3 Essential protein analysis – hypoxic conditions

It is important to consider the effects of the inhibition mechanisms on the canonical model. One of the objectives of this study was to determine therapeutic options while managing the possible negative effects on the patient. Therefore, it would be remiss of us not to consider the effects of the inhibition mechanisms on other proteins translated canonically.

Although cancer cells are subjected to hypoxic conditions due to their rapid growth and proliferation, stromal cells can also be subjected to hypoxic microenvironments, particularly in cancer-infected organs and tissues [91]. Stromal cells sense pathogens and tissue damage, and promote immune response and tissue repair [92]. Two important proteins involved in stromal cell maintenance and structure include type-1 collagen and β-actin, both of which are canonically translated. For the rest of this chapter, these two proteins and the effects of the previously derived inhibition mechanisms are analyzed.

4.3.1 Type-1 Collagen

Type-1 collagen (COL1A1) is a ubiquitous maintenance protein involved in wound healing [93], blood vessel development [94], and muscle and bone strength [95, 96]. On average, there are 589 $\pm$ 178 collagen mRNAs per cell [68] which, assuming the volume of the eukaryotic cell is 10^{-12} L [69, 70], is $9.8\times10^{-4}\,\mu$M. The translation initiation of *COL1A1* dependence on eIF5B is presented in figure 4.1. According to the calculations from Firczuk *et al.* (2013) [56], the total free concentration of eIF5B in the cell is $0.20\,\mu$M under hypoxic conditions. Earlier it was noted that eIF5B is over-expressed in malignancies and drives non-canonical translation of several proto-oncogenes [22, 23, 24], however no data on the level of up-regulation was available to the best of my knowledge. As we can see from figure 4.1, at a concentration of mRNA of $9.8\times10^{-4}\,\mu$M, RIB5B$_{COL1A1}$ saturates at 490 complexes. This reaches a saturation point when the total available concentration of eIF5B is greater than $0.01\,\mu$M. Therefore, reducing the eIF5B concentration similar to the

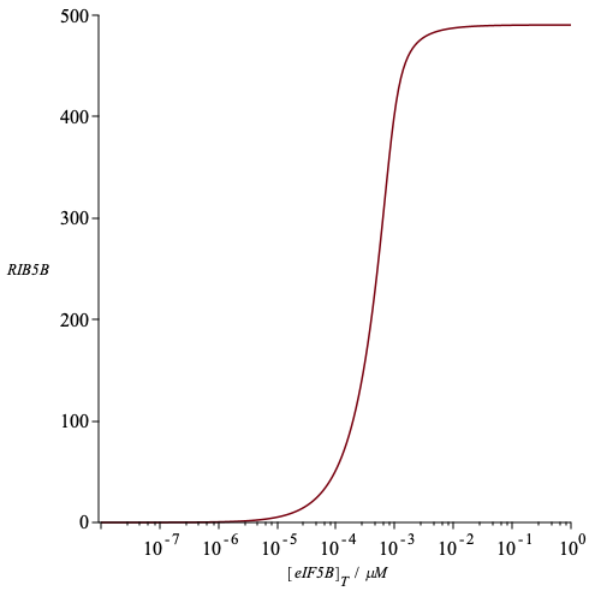

Figure 4.1: A parameter scan of RIB5B$_{COL1A1}$ vs the total eIF5B concentration in canonical *COL1A1* translation initiation under hypoxic conditions. The system reaches a saturation point of 490 RIB5B$_{COL1A1}$ complexes. In order to reduce the number of RIB5B$_{COL1A1}$ complexes by half, the total concentration of eIF5B must be $5.0 \times 10^{-4} \mu$M.

non-canonical mechanism will decrease the number of RIB5B$_{COL1A1}$ complexes as well. This is not desirable in a chemotherapy, however, it must be noted that the mechanism presented here is one mode of canonical translation, as reducing the concentration of eIF5B in the cell has been shown to not impact cell viability, and therefore there must be a mode of translation initiation that is eIF5B-independent [81]. Although eIF5B is not essential for cell viability in *in cellulo* experiments, it is clear that eIF5B makes canonical translation initiation much more efficient [37]. Therefore, if eIF5B is available, the cell will elect to use this eIF5B-dependent translation initiation pathway. Understanding the effects of the non-canonical inhibition mechanisms as they are applied to the eIF5B-dependent canonical translation initiation mechanism will allow us to determine the combinations of inhibitor properties at their highest end (i.e. highest inhibitor concentration and lowest values of K_D) to provide future researchers with potential limits for their experiments. These combinations of inhibitor properties are elucidated throughout the rest of the chapter.

Table 4.3: Selected relative sensitivities of variables in the canonical model analyzing the translation initiation for *COL1A1* under hypoxic conditions. $RIB5B_{COL1A1}$ is not strongly locally sensitive to any of the parameters examined, including the total concentration of eIF5B, and the clearance delay, τ. The total concentration of *COL1A1* mRNA in this analysis was $9.8\times10^{-4}\mu$M.

	k_{11}	k_{13}	$[eIF5B]_T$	$[mRNA_T]$
eIF5B	0.000	0.000	1.000	-0.005
PIC5	0.029	0.034	0.000	1.000
PIC6	-0.471	0.034	-1.000	1.005
PIC7	-0.971	0.034	0.000	1.000
PIC8	0.029	-0.466	0.000	1.000
PIC9	0.029	-0.966	0.000	1.000
$RIB5B_{COL1A1}$	0.029	0.034	0.000	1.000

Sensitivity Analysis

As mentioned previously, some of the rate constants were calculated or assumed, therefore, it was necessary to conduct a sensitivity analysis on the model to understand the effect of approximating these unknown parameters on the model.

In addition to the unknown parameters listed above in table 4.2, sensitivity analysis was also performed for the total eIF5B concentration in the cell, and τ, the clearance delay. It was necessary to study the total eIF5B concentration in the cell, as this concentration varies in the cell depending on the conditions. Additionally, translation rates vary from about 3 codons/s to approximately 11.5 codons/s, depending on the stage of translation [97]. For example, translation is slower at first, during a period called the 5' translational ramp [97]. Therefore, the clearance delay, τ, was chosen for analysis as it depends on how fast the ribosome makes the transition from initiation to elongation.

The same method of calculations that was described in section 3.2 was used here to perform a local relative sensitivity analysis. Some less interesting sets of sensitivity coefficients were omitted from the table for brevity. A complete sensitivity table is provided in Appendix C (table C.5).

It is beneficial to examine the sensitivity of this model to some of its parameters, primarily the ones that have been assumed, as denoted by [a] in table 4.2; or calculated, as

denoted by [c] in table 4.2; in addition to other parameters of interest such as the clearance delay, τ, and the total eIF5B concentration. According to the data presented in tables 4.3 and C.5, RIB5B$_{COL1A1}$ shows little-to-no sensitivity to any of the parameters considered in this analysis, with the exception of the total mRNA concentration. Of particular interest was RIB5B$_{COL1A1}$'s sensitivity to eIF5B, since this is a potential therapeutic target. As seen in table 4.3, RIB5B$_{COL1A1}$ is not sensitive to the total concentration of eIF5B. This is consistent with results from previous experimental studies, in which eIF5B was decreased, and no significant decrease in high molecular weight polysomes was observed [18]. This is fortunate for our study, as the approximated values used in this model should not have a significant impact on the model's behaviour or outputs. Therefore, eIF5B is a plausible therapeutic target.

Direct eIF5B inhibition

The first inhibition mechanism noted in chapter 3 was that of direct eIF5B inhibition. The purpose of this inhibition mechanism was to limit the number of ternary complexes available to deliver the initiator tRNA to the pre-initiation complex. However, eIF5B is involved in both mechanisms, and therefore, it is important to consider the effects on the canonical mechanism with respect to some structural proteins such as type-1 collagen and β-actin.

One more step must be considered in addition to the mechanism outlined in equations (4.1):

$$\text{eIF5B} \; + \; \text{I}_{5\text{B}} \underset{k_{-5Bi}}{\overset{k_{5Bi}}{\rightleftharpoons}} \text{eIF5B}_\text{i}, \tag{4.6}$$

again, where the subscript i denotes the inhibited form of the species, and $\text{I}_{5\text{B}}$ denotes the eIF5B inhibitor. The same notation is used through the rest of the section.

As was observed with the inhibition mechanisms in section 3.3, equation (4.6) results in a pair of differential equations for $\text{I}_{5\text{B}}$ and eIF5B_i that cancel each other out when added.

Therefore, we keep the eIF5B_i differential equation

$$\frac{d[\text{eIF5B}_\text{i}]}{dt} = k_{5B_i}[\text{eIF5B}][\text{I}_{5\text{B}}] - k_{-5B_i}[\text{eIF5B}_\text{i}],$$

and divide it by k_{5B_i} at the steady-state to get

$$0 = [\text{eIF5B}][\text{I}_{5\text{B}}] - K_{D_{5B_i}}[\text{eIF5B}_\text{i}]. \tag{4.7}$$

The conservation equation for the inhibitor is also added to the equation set for this model:

$$[\text{I}_{5\text{B}}]_\text{T} = [\text{I}_{5\text{B}}] + [\text{eIF5B}_\text{i}], \tag{4.8}$$

and the eIF5B conservation equation is modified to

$$[\text{eIF5B}] = [\text{eIF5B}]_\text{T} - \Big([\text{PIC7}] + [\text{PIC9}] + [\text{RIB5B}] + [\text{eIF5B}_\text{i}]\Big). \tag{4.9}$$

Figure 4.2 shows a 3D surface plot of the number of RIB5B_{COL1A1} complexes as the concentration of inhibitor and the K_D of the inhibitor are varied. Figure 4.3 shows the same data presented as a contour plot.

The black line in the contour plot provided in figure 4.3 represents the greatest whole number of RIB5B_{COL1A1} complexes possible in this model with the inhibitor present (i.e. 490). To reduce the number of RIB5B_{COL1A1} complexes by half, we consult the next contour line. As we can see, at a K_D of 1 nM, the IC_{50} is $\sim 3\,\mu$M. In section 3.3.1, it was noted that at the same K_D, the IC_{50} was $\sim 2\,\mu$M. Therefore, it is likely that a direct eIF5B inhibitor will affect the canonical translation of *COL1A1* under hypoxic conditions. It should also be noted once again that eIF5B is not essential for cell viability [81]. This suggests that proteins are able to be canonically translated in the absence of eIF5B, which still makes this a potential therapeutic target.

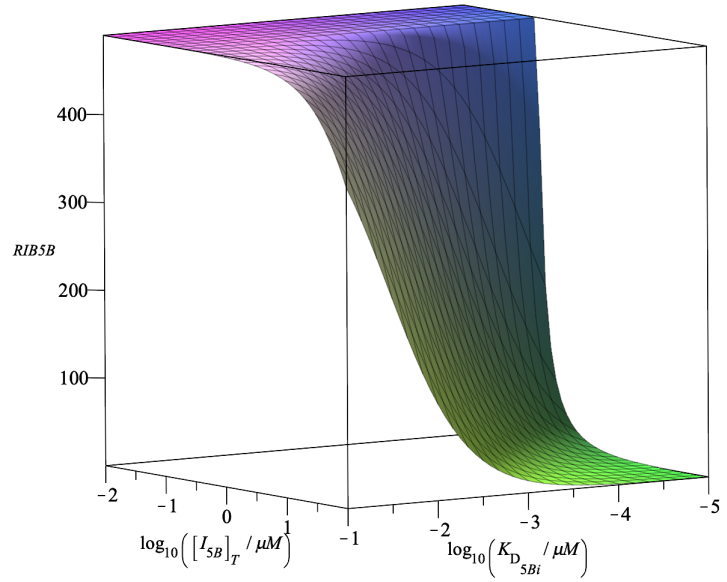

Figure 4.2: A 3D surface plot of direct eIF5B inhibition in the canonical model for *COL1A1* translation initiation under hypoxic conditions. At smaller concentrations of inhibitor (10^{-1} – $10^{-2}\mu$M), there is no effect on the number of RIB5B$_{COL1A1}$ complexes regardless of the K_D value. The region of complete inhibition is similar to that observed in figure 3.6.

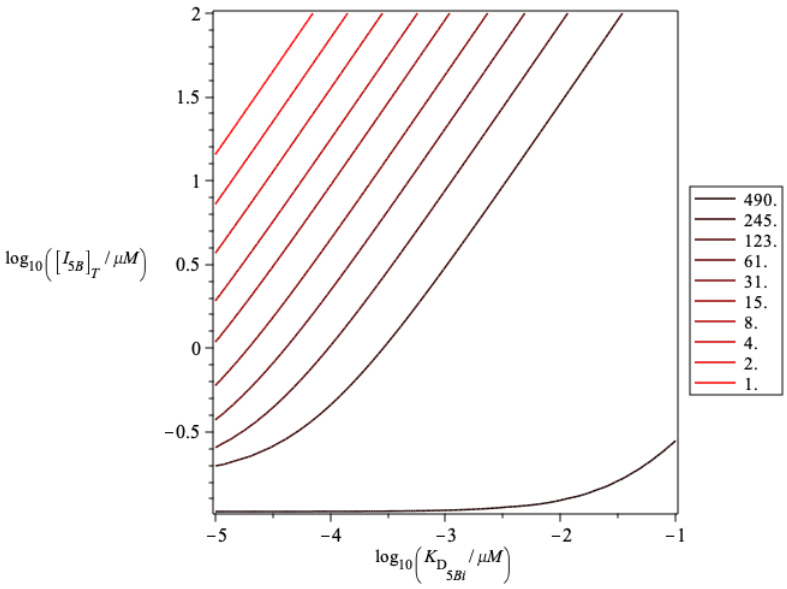

Figure 4.3: A contour plot of the direct inhibition of eIF5B in the *COL1A1* canonical translation initiation model under hypoxic conditions. The contour lines represent the number of RIB5B$_{COL1A1}$ complexes, where the black line represents the largest whole number of ribosomes (490), and the red the fewest (1). The IC$_{50}$ is $\sim 3\,\mu$M when the K_D is 1 nM. A combination of inhibitor concentration and K_D values that result in a 2-fold reduction of RIB5B$_{COL1A1}$ complexes are provided on the second darkest contour line.

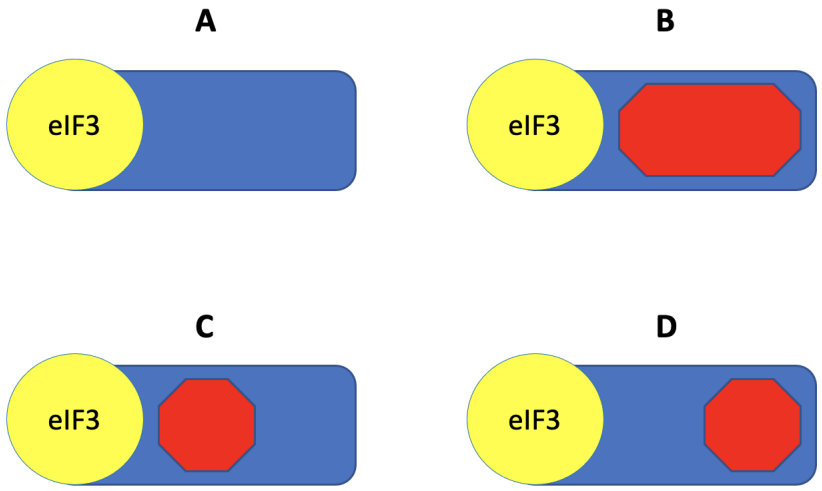

Figure 4.4: $PIC2_{nc}$ inhibition possibilities. Panel A shows a top-down view onto the $PIC2_{nc}$–TC_{nc} interface. Panel B shows a potential inhibitor across the entire interface, while panels C and D show potential inhibitors across the tRNA and eIF5B binding sites, respectively.

PIC interface inhibition

In section 3.3, one of the proposed inhibition mechanisms is to interfere with the PIC2–TC interface. In other words, we proposed an inhibitor that would bind to the pre-initiation complex before the ternary complex, such that it would disrupt this interface.

There are a few ways we could think about inhibiting this complex:

- target the entire PIC2–TC interface,
- target the $tRNA_i$ binding site, or
- target the eIF5B binding site.

The inhibition options provided in this list are illustrated in figure 4.4. The first option in the above list will have no effect on the canonical mechanism, as the non-canonical TC is different from the canonical TC in its composition. However, the latter two points may affect the canonical mechanism, so this is what is considered in this section.

As is obvious from the mechanisms outlined in (3.1) and (4.1), the pre-initiation complexes do not contain the same initiation factors. For example, PIC2 in the non-canonical

model is comprised of the 40S subunit, eIF3, and the IRES-containing mRNA. PIC2 in the canonical model outlined above is comprised of the 40S subunit, eIF3 and eIF5. Therefore, we should not consider the effect of inhibiting PIC2 literally in the canonical model, but rather the complex before ternary complex binding, which, according to the model presented in equations 4.1, is PIC3.

To simulate this inhibition mechanisms, one more step must be considered in addition to the mechanism outlined in equations (4.1):

$$\text{PIC3} \ + \ \text{I}_{\text{P3}} \underset{k_{-P3i}}{\overset{k_{P3i}}{\rightleftharpoons}} \text{PIC3}_{\text{i}}, \tag{4.10}$$

again, where the subscript i denotes the inhibited form of the species, and I_{P3} denotes the PIC inhibitor.

The addition of this step will change the PIC3 differential equation to

$$\frac{d[\text{PIC3}]}{dt} = k_3[\text{PIC2}][\text{eIF1}] - k_{-3}[\text{PIC3}] - k_5[\text{PIC3}][\text{TC}] + k_{-5}[\text{PIC4}] \\ - k_{P3i}[\text{PIC3}][\text{I}_{\text{P3}}] + k_{-P3i}[\text{PIC3}_{\text{i}}]. \tag{4.11a}$$

If we factor out k_{P3i} from the inhibition parts of this equation, we get

$$\frac{d[\text{PIC3}]}{dt} = k_3[\text{PIC2}][\text{eIF1}] - k_{-3}[\text{PIC3}] - k_5[\text{PIC3}][\text{TC}] + k_{-5}[\text{PIC4}] \\ + k_{P3i}\Big(K_{D_{P3i}}[\text{PIC3}_{\text{i}}] - [\text{PIC3}][\text{I}_{\text{P3}}]\Big). \tag{4.11b}$$

Treating the equations as we did previously, we get

$$\frac{d[\text{PIC3}_{\text{i}}]}{dt} = k_{P3_i}[\text{PIC3}][\text{I}_{\text{P3}}] - k_{-P3_i}[\text{PIC3}_{\text{i}}], \tag{4.12a}$$

and divide it by k_{5B_i} at the steady-state to get

$$0 = [\text{PIC3}][\text{I}_{\text{P3}}] - K_{D_{P3_i}}[\text{PIC3}_\text{i}]. \tag{4.12b}$$

The conservation equation for the inhibitor is also added to the equation set for this model:

$$[\text{I}_{\text{P3}}]_\text{T} = [\text{I}_{\text{P3}}] + [\text{PIC3}_\text{i}]. \tag{4.13}$$

This will also impact the conservation equations for eIF3, eIF5, and eIF1, which all include PIC3 terms. These new equations are:

$$[\text{eIF3}] = [\text{eIF3}]_\text{T} - \Big([\text{PIC1}] + [\text{PIC2}] + [\text{PIC3}] + [\text{PIC3}_\text{i}] + [\text{PIC4}] + [\text{PIC5}] + [\text{PIC6}] + [\text{PIC7}]\Big), \tag{4.14a}$$

$$[\text{eIF5}] = [\text{eIF5}]_\text{T} - \Big([\text{PIC2}] + [\text{PIC3}] + [\text{PIC3}_\text{i}] + [\text{PIC4}] + [\text{PIC5}] + [\text{PIC6}] + [\text{PIC7}]\Big), \tag{4.14b}$$

$$[\text{eIF1}] = [\text{eIF1}]_\text{T} - \Big([\text{PIC3}] + [\text{PIC3}_\text{i}] + [\text{PIC4}] + [\text{PIC5}] + [\text{PIC6}] + [\text{PIC7}]\Big). \tag{4.14c}$$

If we solve equations (4.11b) and (4.12b) numerically, the solutions do not depend on k_{P3_i}. Therefore, the first line of equation (4.11b) along with equation (4.12b) were used in the calculations.

Figure 4.5 shows the contour plot of the number of RIB5B_{COL1A1} complexes as the concentration of inhibitor and the K_D of the inhibitor are varied. The surface plot showed the same general trend observed in figure 4.2, and is therefore not shown here. For the reader's reference, it is provided in Appendix A (see figure A.3). As we can see from figure 4.5, at a K_D of 1 nM, the IC_{50} is $\sim 2\,\mu$M. The IC_{50} at the same K_D value in the non-canonical model was 5 μM. Therefore, implementing a PIC2 inhibitor to the non-canonical model may affect the canonical translation initiation of *COL1A1* under hypoxic conditions.

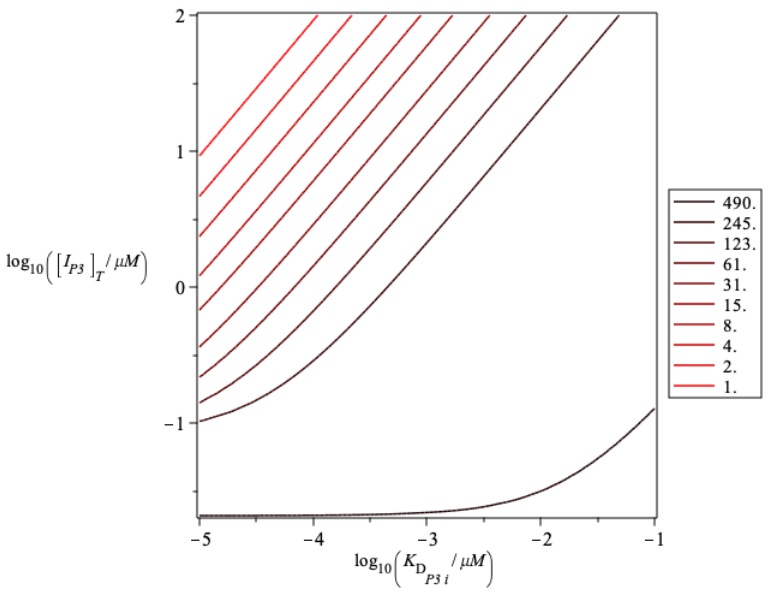

Figure 4.5: A contour plot of the inhibition of PIC3 in the *COL1A1* canonical translation initiation model under hypoxic conditions. The contour lines represent the number of RIB5B$_{COL1A1}$ complexes, where the black line represents the largest whole number of ribosomes (490), and the red the fewest (1). The IC$_{50}$ is $\sim 2\,\mu$M when the K_D is 1 nM. A combination of inhibitor concentration and K_D values that result in a 2-fold reduction of RIB5B$_{COL1A1}$ complexes are provided on the second darkest contour line.

TC inhibition

Before any equations for this inhibition mechanism are established, we must first consider what part of the ternary complex is being inhibited in order to interfere with the PIC2–TC interface of the non-canonical model. There are a few options:

- the inhibitor targets eIF5B once it has bound to the Met-tRNA$_i$,
- the inhibitor targets Met-tRNA$_i$ of the ternary complex so that it cannot bind to the pre-initiation complex, or
- the inhibitor targets the ternary complex as a whole to disrupt its binding potential to the pre-initiation complex.

The inhibition options provided in this list are illustrated in figure 4.6. Only one out of the above list has a corresponding process in the canonical mechanism. If the inhibitor targets eIF5B once it has bound to the initiator tRNA, then we do not need to consider its

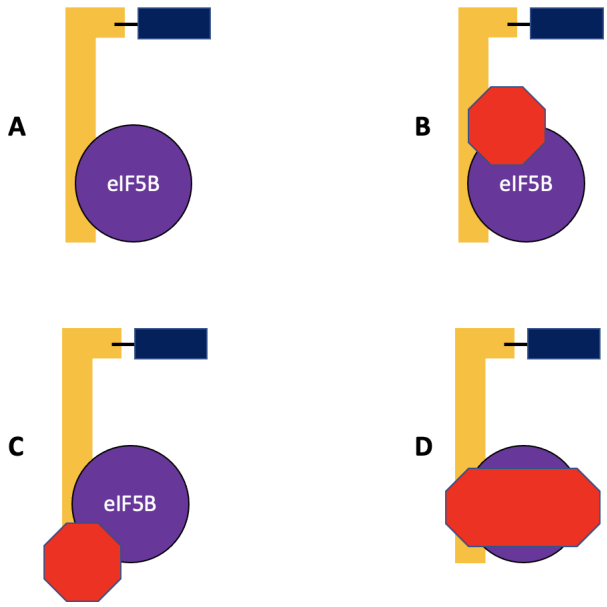

Figure 4.6: TC_{nc} inhibition possibilities. Panel A shows the TC_{nc}. Panels B–D show inhibitor possibilities that target eIF5B after it has bound to the $tRNA_i$, the $tRNA_i$, and the entire TC_{nc}, respectively.

effects to the canonical mechanism, since the eIF5B-ternary complex is not relevant in the canonical initiation pathway. For the same reason, if the inhibitor targets the eIF5B-ternary complex as a whole, once again we do not have to consider its effect. However, if the inhibitor targets the initiator tRNA such that it cannot bind to the pre-initiation complex, then this will impact the canonical mechanism as well. This is the case we will consider here.

We add the following additional step to be considered in addition to the mechanism outlined in equations (4.1):

$$\mathrm{TC} + \mathrm{I_{TC}} \underset{k_{-TCi}}{\overset{k_{TC_i}}{\rightleftharpoons}} \mathrm{TC_i}, \tag{4.15}$$

where the subscript i denotes the inhibited form of the species, and I_{TC} denotes the TC inhibitor. Note that we are inhibiting the $tRNA_i$ of the ternary complex, but assuming it can only be inhibited after the ternary complex is formed, which is why the TC is inhibited in this mechanism.

The addition of this step changes the TC differential equation to

$$\frac{d[\mathrm{TC}]}{dt} = k_4[\mathrm{eIF2}][\mathrm{tRNAi}] - k_{-4}[\mathrm{TC}] - k_5[\mathrm{PIC3}][\mathrm{TC}] + k_{-5}[\mathrm{PIC4}] - k_{TC_i}[\mathrm{TC}][\mathrm{I_{TC}}] + k_{-TCi}[\mathrm{TC_i}]. \quad (4.16a)$$

If we factor out k_{TC_i} from the inhibition parts of this equation, we get

$$\frac{d[\mathrm{TC}]}{dt} = k_4[\mathrm{eIF2}][\mathrm{tRNAi}] - k_{-4}[\mathrm{TC}] - k_5[\mathrm{PIC3}][\mathrm{TC}] + k_{-5}[\mathrm{PIC4}] + k_{TC_i}\Big(K_{D_{TCi}}[\mathrm{TC_i}] - [\mathrm{TC}][\mathrm{I_{TC}}]\Big). \quad (4.16b)$$

Treating the equations as we did previously, we get

$$\frac{d[\mathrm{TC_i}]}{dt} = k_{TC_i}[\mathrm{TC}][\mathrm{I_{TC}}] - k_{-TC_i}[\mathrm{TC_i}], \quad (4.17a)$$

and divide it by k_{TC_i} at the steady-state to get

$$0 = [\mathrm{TC}][\mathrm{I_{TC}}] - K_{D_{TC_i}}[\mathrm{TC_i}]. \quad (4.17b)$$

The conservation equation for the inhibitor is also added to the equation set for this model:

$$[\mathrm{I_{TC}}]_\mathrm{T} = [\mathrm{I_{TC}}] + [\mathrm{TC_i}], \quad (4.18)$$

and the eIF2 conservation equation is modified to

$$[\mathrm{eIF2}] = [\mathrm{eIF2}]_\mathrm{T} - \Big([\mathrm{TC}] + [\mathrm{TC_i}] + [\mathrm{PIC4}] + [\mathrm{PIC5}]\Big). \quad (4.19)$$

If we solve equations (4.16b) and (4.17b) numerically, the solutions do not depend on k_{TC_i}. Therefore, the first line of equation (4.16b) along with equation (4.17b) were used

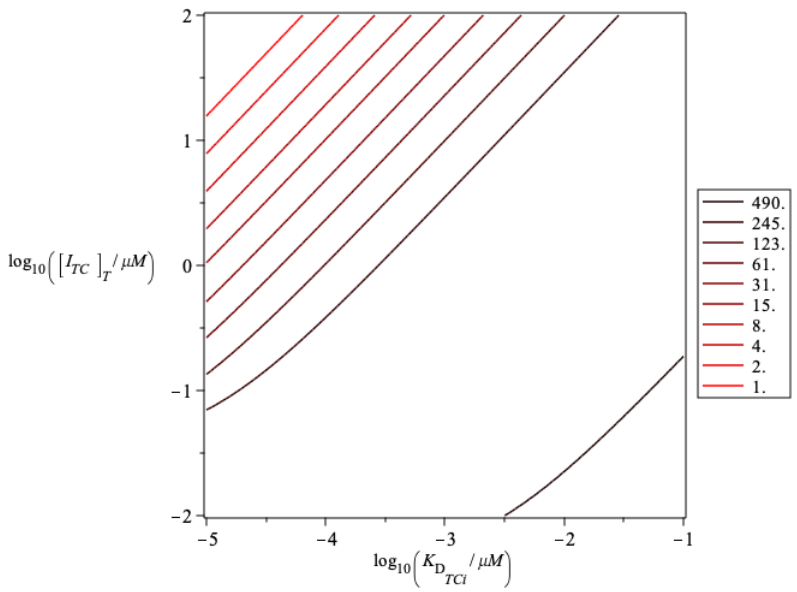

Figure 4.7: A contour plot of the direct inhibition of the ternary complex in the *COL1A1* canonical translation initiation model under hypoxic conditions. The contour lines represent the number of RIB5B$_{COL1A1}$ complexes, where the black line represents the largest whole number of ribosomes (490), and the red the fewest (1). The IC$_{50}$ is $\sim 3\,\mu$M when the K_D is 1 nM. A combination of inhibitor concentration and K_D values that result in a 2-fold reduction of RIB5B$_{COL1A1}$ complexes are provided on the second darkest contour line.

in the calculations.

Figure 4.7 shows the contour plot of the number of RIB5B$_{COL1A1}$ complexes as the concentration of inhibitor and the K_D of the inhibitor are varied. The surface plot is similar in appearance to figure 4.2, and is therefore not shown here. For the reader's reference, it is provided in Appendix A (see figure A.4). As we can see from figure 4.7, at a K_D of 1 nM, the IC$_{50}$ is $\sim 3\,\mu$M. The IC$_{50}$ at the same K_D value in the non-canonical model was $5\,\mu$M. Therefore, implementing a inhibitor that targets the initiator tRNA of the ternary complex in the non-canonical model may affect the canonical translation initiation of *COL1A1* under hypoxic conditions.

RIB5B Inhibition

The final inhibition possibility is to target the RIB5B complex such that the GTP on eIF5B cannot be hydrolyzed and therefore cannot dissociate from the complex. However,

as this hydolysis step is thought to be the rate-determining step in canonical translation initiation [37], this may impact global translation initiation, and should be approached with caution.

If we are to inhibit the RIB5B complex, one more step must be considered in addition to the mechanism outlined in equations (4.1):

$$\text{RIB5B} \; + \; \text{I}_{\text{R5B}} \underset{k_{-R5Bi}}{\overset{k_{R5Bi}}{\rightleftharpoons}} \text{RIB5B}_\text{i}, \tag{4.20}$$

again, where the subscript i denotes the inhibited form of the species, and I_{R5B} denotes the RIB5B inhibitor.

The addition of this step changes the RIB5B differential equation to

$$\frac{d[\text{RIB5B}]}{dt} = k_{13}[\text{PIC9}] - k_{14}[\text{RIB5B}] - k_{R5Bi}[\text{RIB5B}][\text{I}_{\text{R5B}}] + k_{-R5Bi}[\text{RIB5B}_\text{i}]. \tag{4.21a}$$

If we factor out k_{R5Bi} from the inhibition parts of this equation, we get

$$\frac{d[\text{RIB5B}]}{dt} = k_{13}[\text{PIC9}] - k_{14}[\text{RIB5B}] + k_{R5Bi}\Big(K_{D_{R5Bi}}[\text{RIB5B}_\text{i}] - [\text{RIB5B}][\text{I}_{\text{R5B}}]\Big). \tag{4.21b}$$

Treating the equations as we did previously, we get

$$\frac{d[\text{RIB5B}_\text{i}]}{dt} = k_{R5B_i}[\text{RIB5B}][\text{I}_{\text{R5B}}] - k_{-R5B_i}[\text{RIB5B}_\text{i}], \tag{4.22a}$$

and divide it by k_{R5B_i} at the steady-state to get

$$0 = [\text{RIB5B}][\text{I}_{\text{R5B}}] - K_{D_{R5B_i}}[\text{RIB5B}_\text{i}]. \tag{4.22b}$$

The conservation equation for the inhibitor is also added to the equation set for this model:

$$[\text{I}_{\text{R5B}}]_\text{T} = [\text{I}_{\text{R5B}}] + [\text{RIB5B}_\text{i}], \tag{4.23}$$

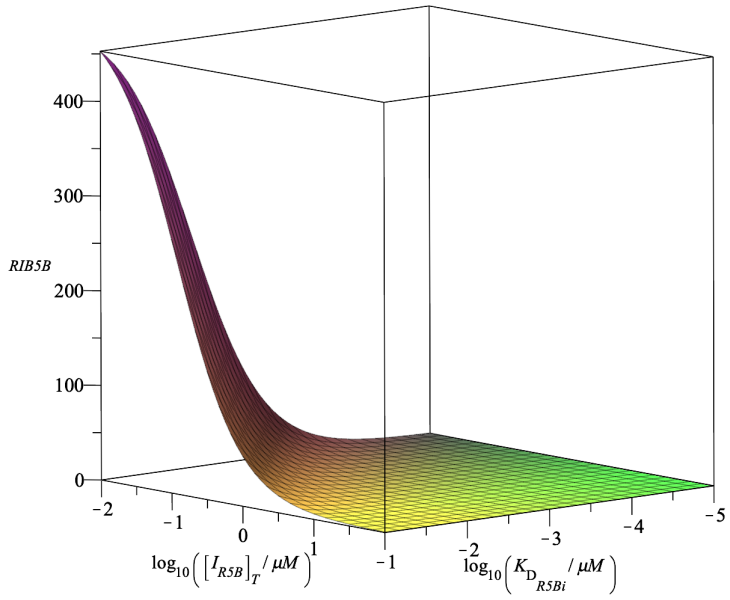

Figure 4.8: A 3D surface plot of RIB5B inhibition in the canonical model for *COL1A1* translation initiation under hypoxic conditions. The region of minimal RIB5B$_{COL1A1}$ complexes is greater than that of figures 4.2, A.3, and A.4. Only at the smallest concentration of inhibitor ($10^{-2}\mu$M) and highest value of K_D considered ($10^{1}\mu$M) does the number of RIB5B$_{COL1A1}$ complexes approach the maximum (490 ribosomes; figure 4.1).

and the eIF5B and mRNA conservation equations are modified to

$$[\text{eIF5B}] = [\text{eIF5B}]_\text{T} - \Big([\text{PIC7}] + [\text{PIC9}] + [\text{RIB5B}] + [\text{RIB5B}_\text{i}]\Big), \tag{4.24a}$$

$$[\text{mRNA}_\text{f}] = [\text{mRNA}]_\text{T} - \Big([\text{mRNA}_\text{c}] + [\text{PIC5}] + [\text{PIC6}] + [\text{PIC7}] + [\text{PIC9}] + [\text{RIB5B}_\text{i}] + [\text{RIB5B}](1 + \text{k}_{14}\tau)\Big). \tag{4.24b}$$

If we solve equations (4.21b) and (4.22b) numerically, the solutions do not depend on k_{R5B_i}. Therefore, the first two terms of equation (4.21b) along with equation (4.22b) were used in the calculations.

Figures 4.8 and 4.9 show the 3D surface and contour plots of the number of RIB5B$_{COL1A1}$ complexes as the concentration of inhibitor and the K_D of the inhibitor are varied. Based on figure 4.9, the IC$_{50}$ for COL1A1 RIB5B inhibition under hypoxic conditions is $\sim 1\times10^{-3}\,\mu$M, which is 3-fold smaller than the concentration required for the non-canonical model. There-

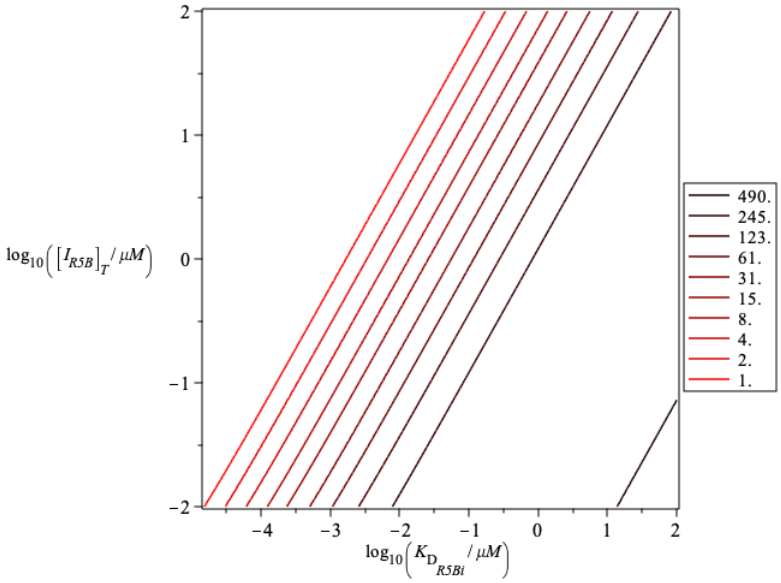

Figure 4.9: A contour plot of the inhibition of RIB5B in the *COL1A1* canonical translation initiation model under hypoxic conditions. The contour lines represent the number of RIB5B$_{COL1A1}$ complexes, where the black line represents the largest whole number of ribosomes (490), and the red the fewest (1). By extrapolation, the IC$_{50}$ is $\sim 1 \times 10^{-3}\,\mu$M when the K_D is 1 nM. A combination of inhibitor concentration and K_D values that result in a 2-fold reduction of RIB5B$_{COL1A1}$ complexes are provided on the second darkest contour line. The region of inhibition is slightly larger than that in figure 3.11.

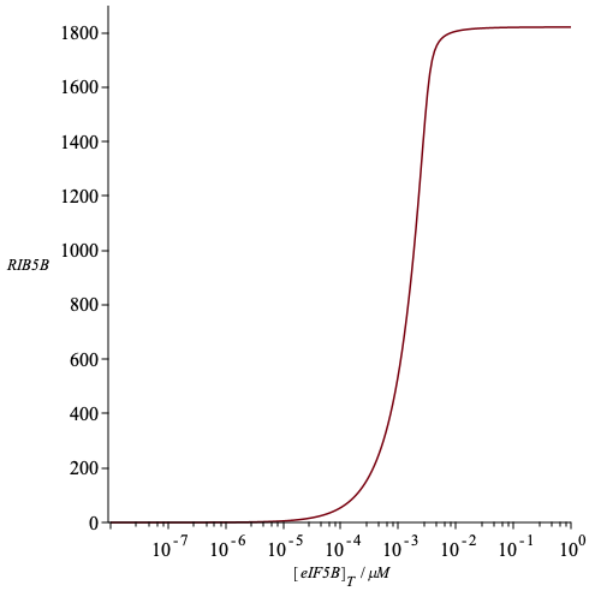

Figure 4.10: A parameter scan of $\text{RIB5B}_{\beta-actin}$ vs the total eIF5B concentration in canonical β-*actin* translation initiation under hypoxic conditions. The system reaches a saturation point of 1820 $\text{RIB5B}_{\beta-actin}$ complexes. When the number of $\text{RIB5B}_{\beta-actin}$ complexes is halved, the total eIF5B concentration is $1.7 \times 10^{-3}\mu$M.

fore, implementing a RIB5B inhibitor to the non-canonical model may affect the canonical translation initiation of *COL1A1* under hypoxic conditions.

4.3.2 β-actin

β-actin is a ubiquitous, endogenous protein that is essential for cell growth and migration. β-actin is involved in a number of cellular processes including nitric-oxide synthase binding [98], and protein kinase binding [99], as well as cell cycle regulation [100], and maintenance of the blood-brain barrier [101], among others. On average, the concentration of β-*actin* mRNA in the cell is approximately $3.6\times10^{-3}\mu$M, which represents 2187 ± 210 copies of β-*actin* mRNA in the cell [68]. This concentration is approximately 3.7 times larger than *COL1A1*. The translation initiation of β-*actin* dependence on eIF5B is presented in figure 4.10.

Table 4.4: Selected relative sensitivities of variables in the canonical model analyzing the translation initiation for β-*actin* under hypoxic conditions. $RIB5B_{\beta-actin}$ is not locally sensitive to any of the parameters examined, with the exception of the total concentration of mRNA. The total concentration of β-*actin* mRNA in this analysis was $3.6\times10^{-3}\mu$M.

	k_{-3}	k_{11}	k_{-12}	k_{13}	$eIF5B_T$	τ	$[mRNA_T]$
PIC6	-0.001	-0.471	0.012	0.034	-1.000	-0.059	1.020
PIC7	-0.001	-0.971	0.012	0.034	0.000	-0.058	1.000
PIC8	-0.001	0.029	-1.223	-0.466	0.000	-0.058	1.000
PIC9	-0.001	0.029	0.012	-0.966	0.000	-0.058	1.000
$mRNA_c$	0.110	0.029	0.012	0.034	0.000	-0.058	1.003
$RIB5B_{\beta-actin}$	-0.001	0.029	0.012	0.034	0.000	-0.058	1.000

Sensitivity Analysis

The same mechanism that was used for type-1 collagen was also considered for β-actin. The parameters used in this analysis are the same as those outlined in table 4.2, with the exception of the total mRNA concentration, which was noted above.

The same method of calculations that was described in section 3.2 was used here to perform a local relative sensitivity analysis. The results of the relative sensitivity analysis for β-actin are found in table 4.4, which highlights no strong sensitivity of $RIB5B_{\beta-actin}$ to the parameters evaluated in this study, with the exception of the total mRNA concentration. Some less interesting sensitivities were omitted for brevity. A complete sensitivity table is provided in Appendix C (table C.6).

Direct eIF5B inhibition

The same methods that were described for COL1A1 in subsection 4.3.1 were applied to the β-actin inhibition mechanisms here. However, like mentioned above, the total mRNA concentration used was $3.6\times10^{-3}\mu$M.

Figures 4.11 and 4.12 show the 3D surface and contour plots for the number of canonical $RIB5B_{\beta-actin}$ complexes as the concentration and K_D of the eIF5B inhibitor are varied. We observe a similar reduction in $RIB5B_{\beta-actin}$ complexes as we approach the effective parameter region to inhibit the number of non-canonical RIB5B complexes. If we compare

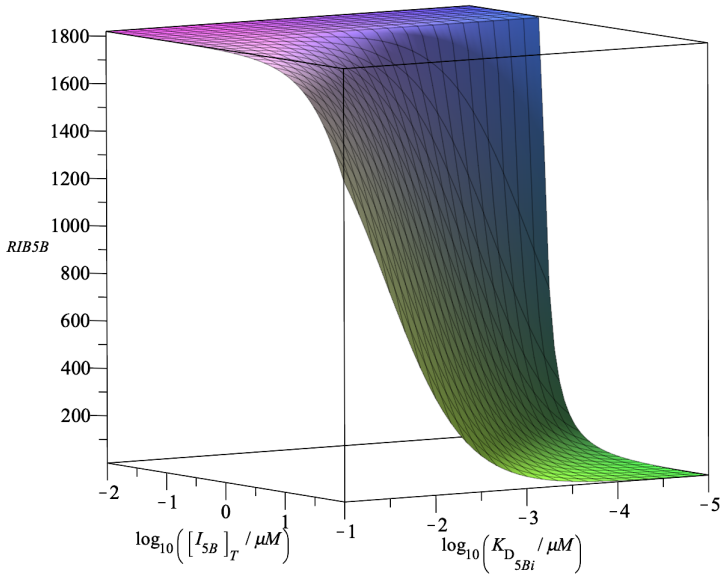

Figure 4.11: A 3D surface plot of direct eIF5B inhibition in the canonical model for β-*actin* translation initiation under hypoxic conditions. At smaller concentrations of inhibitor ($\sim 10^{-1}$ – $10^{-2}\mu$M), there is no effect on the number of RIB5B$_{\beta-actin}$ complexes regardless of the K_D value. The region of minimal RIB5B$_{\beta-actin}$ complexes is smaller than that of the COL1A1 model under the same conditions in figure 4.2.

figure 3.6 to figures 4.2 and 4.11, we see that the parameter region that results in the fewest number of RIB5B complexes ($K_D = 10^{-3}$ – 10^{-5} and $[I_{5B}]_T = 10^1$ – 10^2) is the same parameter region which limits the number of RIB5B complexes for the canonical *COL1A1* and β-*actin* translation initiation mechanisms. This is further exemplified in their respective contour plots illustrated in figures 3.7, 4.3 and 4.12.

Under hypoxic conditions, both COL1A1 and β-actin expression are impacted when subjected to a direct eIF5B inhibitor. As was noted in section 3.3.1, to decrease the number of non-canonical RIB5B complexes by half, the IC_{50} is $\sim 3\,\mu$M at a K_D value of 1 nM. If we consult figures 4.3 and 4.12, we see that similar conditions are required to reduce the number of canonical RIB5B complexes by half as well. Therefore the structural integrity and maintenance of stromal cells, which may be under hypoxic conditions, may be impacted, which could have a deleterious effect, particularly on any rapidly renewed tissues or brain cells after resection surgery.

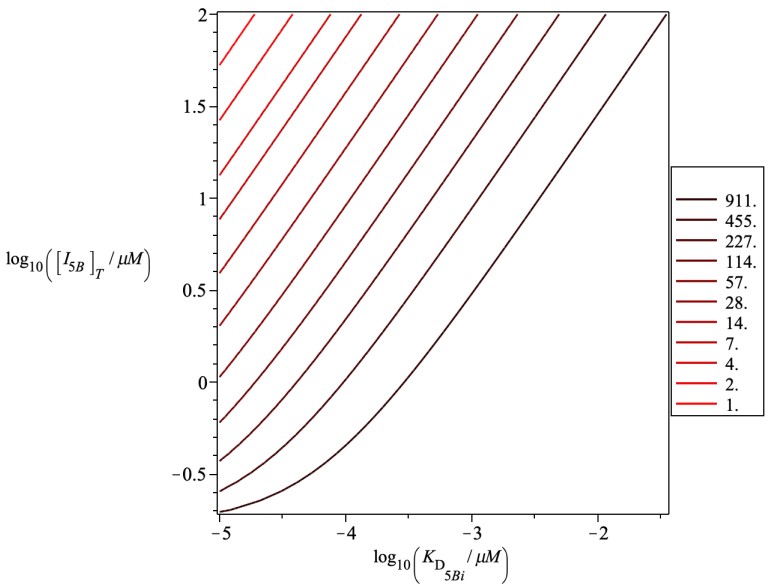

Figure 4.12: A contour plot of the direct inhibition of eIF5B in the β-actin canonical translation initiation model under hypoxic conditions. The contour lines represent the number of RIB5B$_{\beta-actin}$ complexes, where the darkest line represents the combinations of inhibitor properties that result in IC$_{50}$ values (911 RIB5B$_{\beta-actin}$ complexes), and the red line represents the fewest number of RIB5B$_{\beta-actin}$ complexes (1). The IC$_{50}$ is $\sim 3\,\mu$M when the K_D is 1 nM. A combination of inhibitor concentration and K_D values that result in a 2-fold reduction of RIB5B$_{\beta-actin}$ complexes are provided on the darkest contour line. The region of inhibition is similar to that observed in figure 3.7.

Therefore, if this inhibitor is applied directly to brain tissue during surgery for tumour resection, for example, it is possible the patient may experience side effects linked to COL1A1 and β-actin depletion. These side effects could include inefficient wound healing which could lead to infections, or increased porousness of the blood-brain barrier, which can lead to the infection of brain tissue, inflammation, or death. Therefore, it is important to consider the repercussions of instituting such a therapy.

It should be noted that eIF5B knock-down experiments have reported no decrease in cell viability [20, 81]. The results reported here do not indicate cell viability, or organism health, but rather protein expression if the alternative pathway is not considered.

PIC interface inhibition

Figure 4.13 shows the contour plot for the number of $\text{RIB5B}_{\beta-actin}$ complexes as the concentration and K_D of the eIF5B inhibitor are varied. The surface plot showed the same general trend observed in figure 4.11, and is therefore not shown here. For the reader's reference, it is provided in Appendix A (see figure A.5).

In section 4.3.1, it was noted that there are several ways we could inhibit the PIC–TC interface, which include targeting the entire PIC–TC interface, targeting the tRNA_i binding site, or targeting the eIF5B binding site. The former option will have no effect on the canonical mechanism, or should not, as the non-canonical TC has a different composition from the canonical TC. Should either of the latter two approaches be taken however, they may impact the canonical mechanism, and therefore they were analyzed in section 4.3.1.

In order to decrease the number of non-canonical RIB5B complexes by half, the IC_{50} is $\sim 5\,\mu$M at a K_D value of 1 nM, as was presented in figure 3.8. When a PIC inhibitor is applied to the canonical model for *COL1A1* and β-*actin* translation initiation, we see that, under hypoxic conditions, the IC_{50} is $\sim 2\,\mu$M, when the K_D of the inhibitor is 1nM (see figures 4.5 and 4.13). This means that the PIC inhibitor may affect the expression of β-actin under hypoxic conditions.

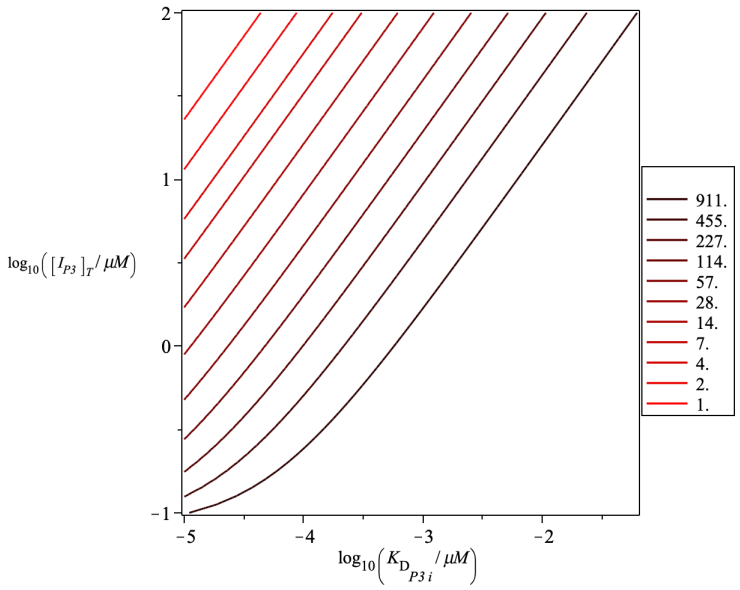

Figure 4.13: A contour plot of the inhibition of PIC3 in the β-*actin* canonical translation initiation model under hypoxic conditions. The contour lines represent the number of RIB5B$_{\beta-actin}$ complexes. A combination of inhibitor concentration and K_D values that result in a 2-fold reduction of RIB5B$_{\beta-actin}$ complexes are provided on the darkest contour line. The IC$_{50}$ is $\sim 2\,\mu$M when the K_D is 1 nM. The region of inhibition is slightly larger than that observed in figure 3.8.

TC inhibition

As was mentioned in the type-1 collagen analysis, there are a number of ways we could inhibit the ternary complex, however, only one of them transfers to the canonical mechanism. This is the mechanism in which the initiator tRNA is targeted on the ternary complex such that it is unable to bind to the pre-initiation complex.

Figure 4.14 shows the contour plot for the number of RIB5B$_{\beta-actin}$ complexes as the concentration and K_D of the eIF5B inhibitor are varied. The surface plot is similar in appearance to figure 4.11, and is therefore not shown here. For the reader's reference, it is provided in Appendix A (figure A.6).

Like the non-canonical PIC2 inhibition mechanism impacts, we observe similar results in the TC inhibition mechanism. This is perhaps the most obvious if we compare figure 3.9 to figures 4.7 and 4.14. The parameter region in which the number of RIB5B complexes are fewest in the non-canonical model is smaller than that of the canonical models for *COL1A1*

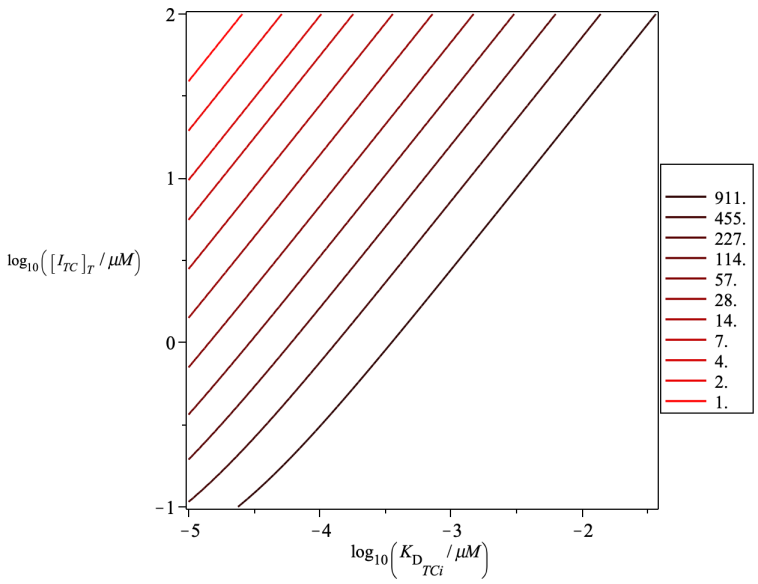

Figure 4.14: A contour plot of the inhibition of TC in the β-*actin* canonical translation initiation model under hypoxic conditions. The contour lines represent the number of $\text{RIB5B}_{\beta-actin}$ complexes. A combination of inhibitor concentration and K_D values that result in a 2-fold reduction of $\text{RIB5B}_{\beta-actin}$ complexes are provided on the darkest contour line. The IC_{50} is $\sim 3\,\mu$M when the K_D is 1 nM. The region of inhibition is similar to that observed in figure 3.9.

and β-*actin* translation initiation.

As we can see from figure 3.9, to decrease the number of non-canonical RIB5B complexes by half, the IC_{50} is $\sim 5\,\mu$M, when the K_D of the inhibitor is 1 nM. There are also several ways we could implement a TC inhibitor, only one of which is relevant to the canonical mechanism: targeting the tRNA_i such that it cannot bind to the pre-initiation complex. If such an inhibitor is applied to the canonical mechanism under hypoxic conditions, the number of *COL1A1* and β-*actin* RIB5B complexes will be reduced by half at an IC_{50} value of $3\,\mu$M, when the K_D of the inhibitor is 1 nM (see figures 4.7 and 4.14). Therefore, the effective concentration and K_D region to reduce the number of RIB5B complexes by half in the non-canonical model may affect the expression of canonically translated proteins such as COL1A1 and β-actin under hypoxic conditions.

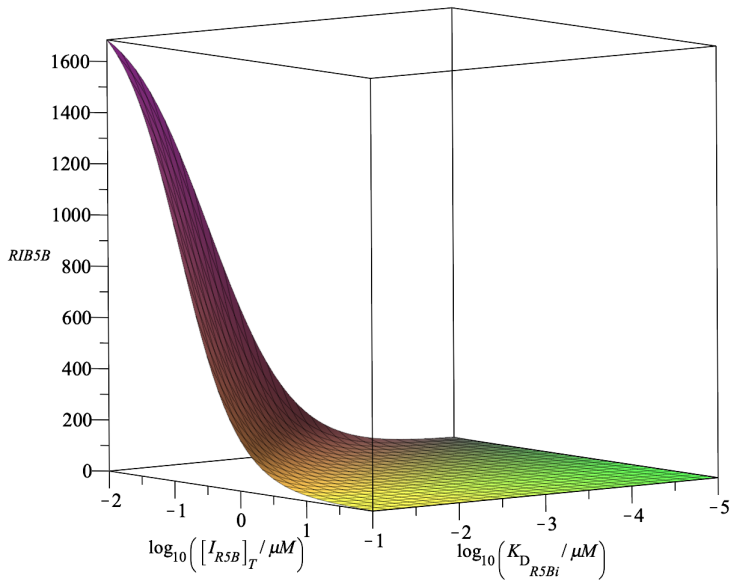

Figure 4.15: A 3D surface plot of RIB5B inhibition in the canonical model for β-*actin* translation initiation under hypoxic conditions. Only at the smallest concentration of inhibitor ($10^{-2}\mu$M) and highest value of K_D considered ($10^{-1}\mu$M) does the number of RIB5B$_{\beta-actin}$ complexes approach the maximum (1820 ribosomes via figure 4.10). The region of minimal RIB5B$_{\beta-actin}$ complexes is greater than that in figures 4.11, A.5 and A.6, and smaller than that in the COL1A1 model under the same conditions in figure 4.8.

RIB5B inhibition

Figures 4.15 and 4.16 show the 3D surface and contour plots for the number of canonical RIB5B complexes for β-actin as the concentration and K_D of the RIB5B inhibitor are varied.

As was expected, applying the RIB5B inhibition mechanism to the canonical model resulted in a large parameter area where the number of RIB5B complexes were decreased significantly. In fact, according to figures 4.8 and 4.15, even at low concentrations of inhibitor and relatively large values of K_D, there is still a large decrease in the number of RIB5B complexes. This is further exemplified in the contour plots provided in figures 4.9 and 4.16.

The IC_{50} is the same for RIB5B inhibition for β-actin under hypoxic conditions as RIB5B inhibition in the non-canonical model. Recall the IC_{50} at the same K_D value in the non-canonical model was $\sim 3\times10^{-3}\,\mu$M. Therefore, the effective concentration and K_D region to reduce the number of RIB5B complexes by half in the non-canonical model may

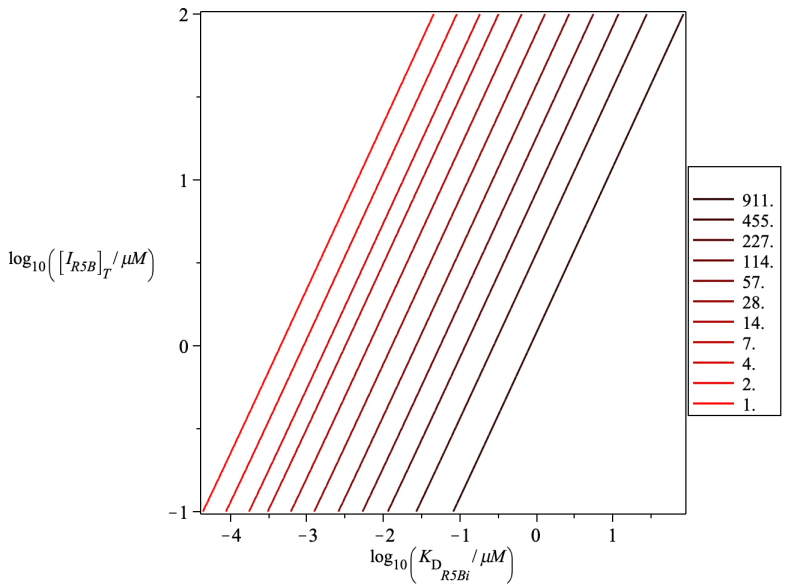

Figure 4.16: A contour plot of the inhibition of RIB5B in the β-*actin* canonical translation initiation model under hypoxic conditions. A combination of inhibitor concentration and K_D values that result in a 2-fold reduction of $\text{RIB5B}_{\beta-actin}$ complexes are provided on the darkest contour line. By extrapolation, the IC_{50} is $\sim 3 \times 10^{-3}$ μM when the K_D is 1 nM. The region of inhibition is similar to that observed in figure 3.11.

affect the expression of COL1A1 under hypoxic conditions. A summary of the IC_{50} values discussed in this section are provided in table 4.5.

4.4 Essential protein analysis – unstressed conditions

The previous section analyzed the effects of the inhibition mechanisms on collagen and β-actin in hypoxic cells. However, it is perhaps more important to analyze the effects of these inhibition mechanisms on healthy cells under unstressed conditions. Since glioblastoma is a form of brain cancer, it would be detrimental to the patient if the chemotherapy was also having a significant effect on otherwise healthy brain cells.

To determine the parameter values at unstressed conditions, a similar approach to that described in section 2.2 was used. The model provided by Firczuk *et al.* (2013) [56] was consulted, and a steady-state calculation was performed. When the cell is under hypoxic conditions, eIF2-α is phosphorylated, as was previously described in section 2.2. How-

Table 4.5: Summary of approximate IC_{50} values and their respective K_D values for COL1A1 and β-actin inhibition targets under hypoxic conditions.

	Inhibition Target	**IC_{50} (μM)**	**K_D (nM)**
COL1A1	eIF5B	3	1
	$PIC2_{nc}$	2	1
	TC_{nc}	3	1
	RIB5B	0.001	1
β-actin	eIF5B	3	1
	$PIC2_{nc}$	2	1
	TC_{nc}	3	1
	RIB5B	0.003	1

Table 4.6: Species and their corresponding concentrations and sources used in the canonical model with a clearance delay under unstressed conditions. All rate constants and the clearance delay are unchanged from table 4.2.

Species	**Concentrations (μM)**	**Source**
[40S]	4.6	[c][56]
[60S]	6.7	[56]
$[eIF3]_T$	0.25	[c][56]
$[eIF5]_T$	0.13	[c][56]
$[eIF1]_T$	1.4	[c][56]
$[eIF2]_T$	0.58	[c][56]
$[eIF4E]_T$	3.0	[c][56]
$[eIF4G]_T$	0.63	[c][56]
$[eIF5B]_T$	0.14	[c][56]
$[tRNA_i]$	26	[56]

ever, under unstressed conditions, eIF2-α is not phosphorylated, so therefore no *ad hoc* adjustments to eIF2 and eIF2B are necessary. The steady-state calculation resulted in parameter values for the total free concentrations of the eIFs, and $tRNA_i$ available to perform translation initiation. The parameters used in this analysis are provided in table 4.6.

4.4.1 Results of analyses under unstressed conditions

The parameter scans of eIF5B vs RIB5B for both COL1A1 and β-actin are similar to their respective plots under hypoxic conditions found in figures 4.1 and 4.10. For the reader's reference, the parameter scans under unstressed conditions can be found in Ap-

Table 4.7: Summary of saturation and IC_{50} values for COL1A1 and β-actin under hypoxic and unstressed conditions, where S. P. is the saturation point in number of complexes.

mRNA	**Conditions**	**S. P. (no. complexes)**	**IC_{50} (μM)**
COL1A1	Hypoxic	490	5.0×10^{-4}
	Unstressed	503	5.1×10^{-4}
β-*actin*	Hypoxic	1820	1.7×10^{-3}
	Unstressed	1860	1.8×10^{-3}

pendix D (see figures D.1 and D.2). A comparison of their saturation and IC_{50} points are provided in table 4.7, where the saturation point is the greatest whole number of RIB5B complexes present when the total concentration of eIF5B is 1 μM, similar to the upper horizontal, insensitive region in figure 4.10.

The results for eIF5B and RIB5B inhibition for both COL1A1 and β-actin are similar to what was observed in section 4.3.1. Similar surface and contour plots, as well as similar IC_{50} values were obtained. Therefore, these are not reported here. For the reader's reference, the surface plots are provided in Appendix A, and the contour plots in Appendix B. Additionally, the results of the sensitivity analyses performed for both COL1A1 and β-actin were almost identical to the results obtained from the analyses in sections 4.3.1 and 4.3.2 so they are not provided in this section. The sensitivity tables that contain all of the parameters analyzed in this study under unstressed conditions are provided in Appendix C (tables C.7 and C.8).

There are notable differences between the results of the two conditions in the surface and contour plots for the PIC3 and TC inhibition mechanisms. As we can see in figures 4.17 and 4.19, the effective parameter region of inhibition is much smaller than what was observed under hypoxic conditions (see figures A.3 and A.4). Interestingly, the IC_{50} values at a K_D of 1 nM are similar for both COL1A1 and β-actin. A summary of the IC_{50} values under unstressed conditions are provided in table 4.8.

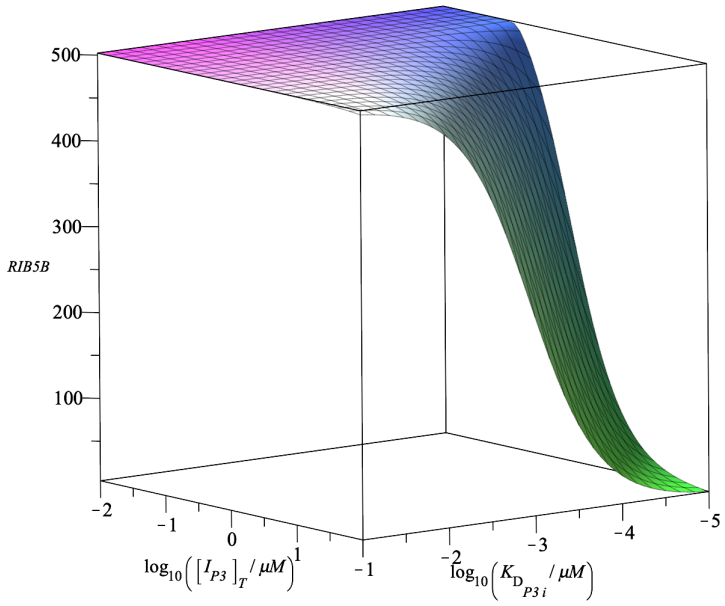

Figure 4.17: A 3D surface plot of PIC3 inhibition in the canonical model for *COL1A1* translation initiation under unstressed conditions. At smaller concentrations of inhibitor ($10^{-0.5}$ – $10^{-2}\mu$M), there is no effect on the number of RIB5B$_{COL1A1}$ complexes regardless of the K_D value. The number of RIB5B$_{COL1A1}$ complexes decreases as the concentration of the inhibitor increases, and the K_D decreases. Only at the highest inhibitor concentration ($10^2\mu$M) and lowest K_D value ($10^{-5}\mu$M) considered does the number of RIB5B$_{COL1A1}$ complexes approach a minimum. The region of inhibition is much smaller than that observed for the eIF5B inhibition mechanism in figure 4.2.

Table 4.8: Summary of approximate IC$_{50}$ values and their respective K_D values for COL1A1 and β-actin inhibition targets under unstressed conditions.

	Inhibition Target	**IC$_{50}$ (μM)**	**K_D (nM)**
COL1A1	eIF5B	3	1
	PIC2$_{nc}$	80	1
	TC$_{nc}$	100	1
	RIB5B	0.002	1
β-actin	eIF5B	3	1
	PIC2$_{nc}$	80	1
	TC$_{nc}$	100	1
	RIB5B	0.003	1

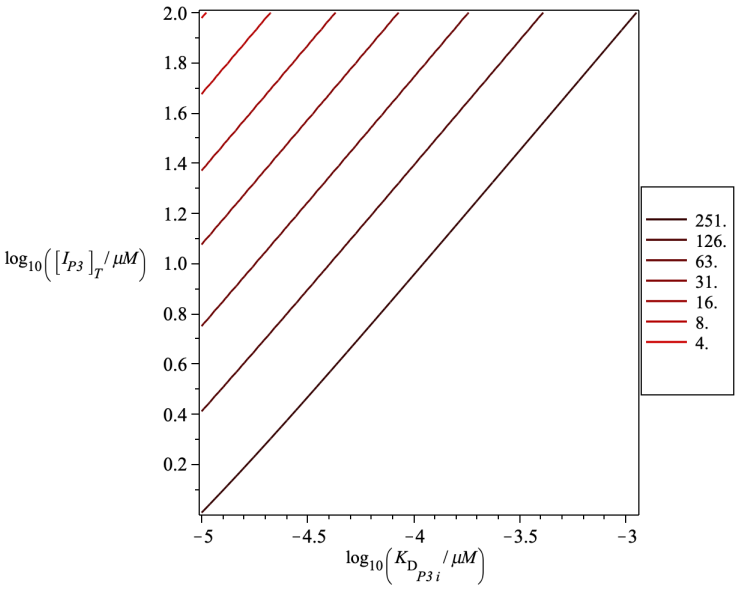

Figure 4.18: A contour plot of the direct inhibition of PIC3 in the *COL1A1* canonical translation initiation model under unstressed conditions. The contour lines represent the number of RIB5B$_{COL1A1}$ complexes. A combination of inhibitor concentration and K_D values that result in a 2-fold reduction of RIB5B$_{COL1A1}$ complexes are provided on the darkest contour line. The red line represents 4 RIB5B$_{COL1A1}$ complexes. The IC$_{50}$ is $\sim 80\,\mu$M when the K_D is 1 nM. The region of inhibition is much smaller than that under hypoxic conditions (see figure 4.5).

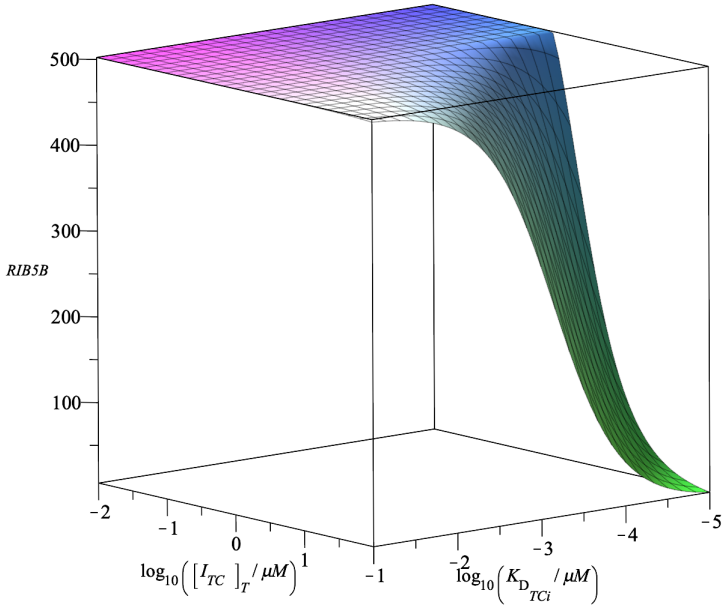

Figure 4.19: A 3D surface plot of TC inhibition in the canonical model for *COL1A1* translation initiation under unstressed conditions. At smaller concentrations of inhibitor (10^0 – $10^{-2}\mu$M), there is no effect on the number of RIB5B$_{COL1A1}$ complexes regardless of the K_D value. The number of RIB5B$_{COL1A1}$ complexes decreases as the concentration of the inhibitor increases, and the K_D decreases. Only at the highest inhibitor concentration ($10^2\mu$M) and lowest K_D value ($10^{-5}\mu$M) considered does the number of RIB5B$_{COL1A1}$ complexes approach a minimum. The region of inhibition is much smaller in this mechanism compared to the eIF5B inhibition mechanism (see figure 4.2).

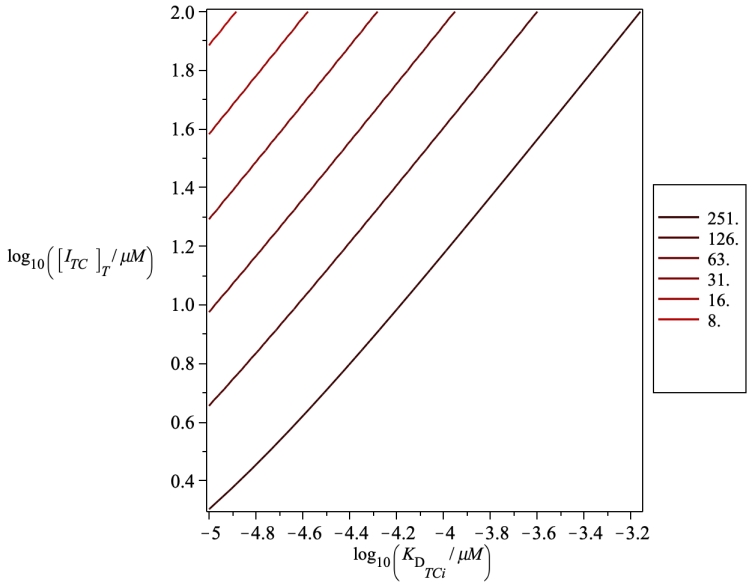

Figure 4.20: A contour plot of the direct inhibition of TC in the *COL1A1* canonical translation initiation model under unstressed conditions. The contour lines represent the number of RIB5B$_{COL1A1}$ complexes. A combination of inhibitor concentration and K_D values that result in a 2-fold reduction of RIB5B$_{COL1A1}$ complexes are provided on the darkest contour line. The red line represents 8 RIB5B$_{COL1A1}$ complexes. The IC$_{50}$ is greater than 100 μM when the K_D is 1 nM. The region of inhibition is much smaller under unstressed conditions compared to hypoxic conditions (see figure 4.7).

4.5 Effects of inhibition mechanisms

In section 4.3, when the eIF5B inhibition surface plots were compared, we observed similar parameter regions in which the number of RIB5B complexes were limited in the non-canonical and canonical models when the canonical mechanism was considered to be under hypoxic conditions. A similar reduction in RIB5B complexes as we approach the effective parameter region to inhibit the number of non-canonical RIB5B complexes is observed under unstressed conditions as well. The parameter region that results in the fewest number of RIB5B complexes in the non-canonical model is similar to the parameter region which limits the number of RIB5B complexes for the canonical *COL1A1* and β-*actin* translation initiation mechanisms. The parameter region for effective eIF5B inhibition in the non-canonical mechanism is similar to that in the canonical mechanism. Therefore, inhibiting eIF5B directly may have a negative effect on canonically translated structural proteins such as COL1A1 and β-actin, which may leave the patient with muscle and bone weakness, among other side effects [95, 96]. However, it should again be acknowledged that there is an alternative canonical translation initiation pathway that does not require eIF5B, so therefore eIF5B remains a promising therapeutic target.

As was discussed in section 4.3, the non-canonical PIC2 inhibitor has the potential to impact the number of canonically assembled RIB5B complexes under hypoxic conditions. The same cannot be said under unstressed conditions. The parameter region required to limit the number of RIB5B complexes in the non-canonical model is larger than that observed in the canonical models. This is further exemplified through the comparison of the non-canonical PIC2 inhibition contour plot provided in figure 3.8 and the canonical PIC3 inhibition contour plots provided in figures 4.18 and B.4. Under unstressed conditions, the IC_{50} is $\sim 80\,\mu$M for both COL1A1 and β-actin, when the K_D is 1 nM (see figures 4.18 and B.4). This means that a 40-fold higher concentration of inhibitor is required to reduce the canonical RIB5B complexes by half than to reduce the non-canonical RIB5B complexes by half. Therefore, it is possible a non-canonical PIC inhibitor may be a promising option to

inhibit the non-canonical mechanism without having a strong impact on canonically translated proteins such as COL1A1 and β-actin under unstressed conditions.

In section 4.3, it was discussed that non-canonical TC inhibition may result in the inhibition of canonical COL1A1 and β-actin RIB5B complexes under hypoxic conditions as well. Interestingly, the parameter region in which the number of RIB5B complexes are fewest in the non-canonical model is larger than that of the canonical models for COL1A1 and β-actin translation initiation under unstressed conditions. This means that many inhibitor concentration and K_D value combinations should not have an effect on the canonical mechanism, or at the very least, should not result in crossing the IC_{50} threshold. This is further confirmed through the comparison of IC_{50} values in table 5.1.

Applying the RIB5B inhibition mechanism to the canonical model resulted in a large parameter area where the number of RIB5B complexes were decreased significantly. Even at low concentrations of inhibitor and relatively large values of K_D, there is still a large decrease in the number of RIB5B complexes. Under unstressed conditions, the IC_{50} values for COL1A1 and β-actin do not change greatly across the two conditions considered in this analysis. Therefore, as the IC_{50} for non-canonical RIB5B inhibition is the similar canonical RIB5B inhibition, inhibiting the RIB5B complex may have a negative effect on canonically translated structural proteins such as COL1A1 and β-actin under unstressed conditions.

Chapter 5

Discussion

5.1 Effects on the XIAP translation initiation mechanism and biological impacts

XIAP is an anti-apoptotic protein involved in glioblastoma cell survival that inhibits caspase-3, which in turn can inhibit apoptosis [14, 16, 17]. Targeting the XIAP non-canonical translation initiation pathway should limit the number of XIAP proteins available to inhibit caspase-3, thereby allowing apoptosis to occur. There are a number of other IAP proteins present in the cell, in addition to other apoptotic pathways, however, XIAP is the best characterized, and the most potent endogenous caspase inhibitor, and therefore a promising target for cancer therapies [14].

Some therapies have already been developed that target eIF5B [31], however the concentrations needed for these therapies to perform efficiently are very high and may be toxic to the patient. Four possible inhibition targets have been proposed in this thesis that either directly or indirectly inhibit eIF5B in the eIF5B-mediated non-canonical pathway. If implemented, these inhibition mechanisms may limit the expression of XIAP, and therefore aid the apoptotic process in cancer cells.

5.2 Inhibition effects on canonical mechanism

5.2.1 Global translation initiation

If we decrease the concentration of eIF5B by targeting it directly, this may have negative effects on canonically translated proteins such as COL1A1 and β-actin. Indeed, this is

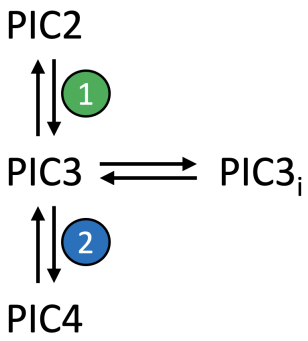

Figure 5.1: The equilibria in which PIC3 participates when the PIC3 inhibition mechanism is applied to the canonical model.

reinforced in the contour plots found in figures 4.3, 4.12, B.1, and B.3, as the IC_{50} curves are similar, and the IC_{50} values given a 1 nM inhibitor are similar. Furthermore, the 3D surface plots for all the direct eIF5B inhibition mechanisms, both canonical and non-canonical, are similar in appearance.

In section 3.3, we discussed four possible inhibition mechanisms. In this prelude, it was mentioned that targeting the $PIC2_{nc}$ and RIB5B complexes may have unfortunate effects in the canonical mechanism. While the RIB5B results were consistent with this hypothesis, the PIC3 results in the canonical model were not. However, upon further evaluation, it is perhaps not as puzzling as it may seem.

The PIC3 complex is in equilibrium with PIC2, $PIC3_i$, and PIC4, as illustrated in figure 5.1. Le Chatelier's principle tells us that if this equilibrium is disturbed, the equilibrium will shift to compensate for that disturbance. For example, when we apply the PIC3 inhibition mechanism to the canonical model, some of the PIC3 complexes will be converted to the inhibited form. If this happens, equilibrium 1, as noted in green on the mechanism in figure 5.1, will shift to produce more PIC3, thus partially compensating for the complexes that were lost during inhibition. Similarly, the PIC3–PIC4 equilibrium, denoted as the blue equilibrium 2 in figure 5.1 will also shift toward generating more PIC3 complexes.

The same reasoning cannot be applied to the RIB5B inhibition mechanism, because neither the step after subunit joining (eIF4E and 4G dissociation), nor the final step of the

mechanism (eIF5B dissociation) are reversible. Therefore, there is no equilibrium available to shift and compensate for any potential disturbances to concentrations in the complexes. Additionally, the majority of the compensation in the PIC3 inhibition step is likely provided by transforming PIC2 complexes into PIC3 complexes. PIC2 is comprised of the 40S subunit, eIF3, and eIF5. All three are in relatively high abundance as well (within the range of $0.8\,\mu$M – $5\,\mu$M). PIC8, which is the complex present before RIB5B, is comprised of the 40S subunit, eIFs 1, 3, 5, and 5B, as well as the initiator tRNA, the mRNA complex, and the 60S subunit. The concentrations of all the components are relatively large, with the exception of the total concentration of eIF5B, and the total concentration of mRNA, which is limiting in all three cases (*XIAP, COL1A1* and β-*actin*). Therefore, at any given time during the pre-initiation complex assembly process, there are many more PIC2 complexes assembled than PIC8 complexes. If there are an abundance of PIC2 complexes, there are many available to transform into PIC3 complexes. The same cannot be said for the number of PIC8 complexes available to compensate for a loss of RIB5B complexes, even if this was an equilibrium step.

It is clear that inhibiting the RIB5B complex will have a negative effect on global translation initiation, and will therefore *not* result in minimal toxicity to the patient. However, it may be possible to develop a less toxic inhibitor that targets eIF5B directly, the eIF5B-ternary complex, or the $PIC2_{nc}$ complex in the non-canonical translation initiation mechanism. A discussion of the best inhibitor classes to analyze moving forward is provided in section 5.4.

5.3 Sensitivity analysis

It is important to once again note that the sensitivities reported in this thesis are local sensitivities, meaning the sensitivities reported are with respect to the parameter values provided in the models. This is the reason we observe the changes in RIB5B sensitivity to $[\text{eIF5B}]_\text{T}$ and $[\text{mRNA}]_\text{T}$ in tables 3.3–3.5. The sensitivities reported in the tables provided

in this thesis are equivalent to the slope on a loglog plot of the variable and the parameter. For example, if something has a relative sensitivity of 1, then if the parameter changes by 10%, so does the variable. If something has a sensitivity of 2, then if the parameter changes 10%, the variable will experience a 20% change.

Throughout this thesis, the effects that different parameters have on RIB5B were examined. RIB5B is the representative variable for available translation competent ribosomes. Therefore, when analyzing the tables of relative sensitivities provided in chapters 3 and 4, it is important to analyze the relative sensitivities of RIB5B with respect to the chosen parameters of interest. With this in mind, when analyzing the tables of sensitivities provided in chapters 3 and 4, we see that RIB5B is only sensitive to parameters k_7, $[\text{mRNA}]_\text{T}$, and $[\text{eIF5B}]_\text{T}$ in the non-canonical model; and is not particularly sensitive to any parameter analyzed in the canonical model.

5.3.1 Canonical model sensitivities

Interestingly, under hypoxic conditions, neither the canonical assembly of the COL1A1 ribosome, nor the β-actin ribosome were sensitive to any parameters analyzed in this study, with the exception of their respective total mRNA concentrations. This is observed in tables 4.3 and 4.4. The unstressed conditions results were similar to that of the hypoxic conditions. These results indicate that, at least locally, the RIB5B complex is not sensitive to any of the parameters analyzed in this study, again, with the exception of the total mRNA concentration. Importantly, this analysis showed that the RIB5B complex is not sensitive to perturbations in the total eIF5B concentration. However, as we observed in the 3D surface and contour plots of eIF5B inhibition and the parameter scans in figures 4.1 and 4.10, if the total concentration of eIF5B in the cell decreases below the IC_{50} point, the expression of COL1A1 and β-actin are limited. This is not to say that the viability of the cell decreases, but rather the potential expression of these two proteins decreases.

5.4 The best inhibitor option(s)

5.4.1 Non-canonical model

If we isolate the non-canonical and canonical inhibition results, the RIB5B inhibitor is the most promising. However, as was noted earlier in this chapter, targeting the RIB5B complex can result in serious effects to canonical translation initiation. Therefore, an inhibitor that targets the RIB5B complex, including an inhibitor that affects the hydrolysis of GTP on eIF5B should be avoided.

If we compare figures 3.6 and A.2, we see that the parameter region in which the number of RIB5B complexes is minimized is greater in the eIF5B inhibition mechanism than in the TC inhibition mechanism. This is further exemplified in their respective contour plots provided in figures 3.7 and 3.9. Interestingly, the conditions at which the number of RIB5B complexes is halved are similar, as was discussed in chapter 3. Discerning which inhibitor of the two is more desirable depends on the level of inhibition needed to promote apoptosis, the cost of developing the inhibitors, and the *in vivo* and *in vitro* effects of the inhibitors.

If we compare figures 3.8 and 3.9, we see that the $PIC2_{nc}$ inhibitor may be less effective than the TC_{nc} inhibitor. When we compare the surface plots in these figures, we see that the region of inhibition is greater for the TC inhibitor than the PIC2 inhibitor. Based on the figures provided in section 3.3, the best inhibitor options are either a direct eIF5B inhibitor or a ternary complex inhibitor. To determine which is the best option of the two, it is important to consider their respective effects on the canonical mechanism as well.

Several IC_{50} values were presented throughout chapters 3 and 4. A summary of these values is provided in table 5.1.

5.4.2 Canonical model

As mentioned previously, targeting the RIB5B complex will likely negatively affect global translation initiation. This effect is clearly observed by comparing the IC_{50} values in table 5.1.

Table 5.1: Summary of approximate IC_{50} values and their respective K_D values for non-canonical and canonical inhibition targets.

Conditions	**mRNA**	**Inhibition Target**	**IC_{50} (μM)**	**K_D (nM)**
Hypoxic	*XIAP*	eIF5B	2	1
		$PIC2_{nc}$	5	1
		TC_{nc}	5	1
		RIB5B	0.003	1
Hypoxic	*COL1A1*	eIF5B	3	1
		$PIC2_{nc}$	2	1
		TC_{nc}	3	1
		RIB5B	0.001	1
	β-*actin*	eIF5B	3	1
		$PIC2_{nc}$	2	1
		TC_{nc}	3	1
		RIB5B	0.003	1
Unstressed	*COL1A1*	eIF5B	3	1
		$PIC2_{nc}$	80	1
		TC_{nc}	100	1
		RIB5B	0.002	1
	β-*actin*	eIF5B	3	1
		$PIC2_{nc}$	80	1
		TC_{nc}	100	1
		RIB5B	0.003	1

Interestingly, targeting eIF5B directly may have a negative effect on the translation initiation of *COL1A1* and β-*actin*. As was noted earlier, the parameter region in which the direct eIF5B inhibitor is effective in the non-canonical model is similar to the region in which the canonical mechanisms are affected. This is an important consideration to take into account when deriving a chemotherapy that targets the non-canonical mechanism. We would expect the IC_{50} value of a 1 nM inhibitor to be slightly greater than that observed here, if we consider a branched mechanism that includes an eIF5B-independent pathway. However, as noted previously, this eIF5B-independent pathway is much less efficient [37]. Therefore, we should not expect a large difference from the values reported in this thesis.

Targeting the PIC2 complex in the non-canonical mechanism correlates to the PIC3 complex in the canonical mechanism. This potential inhibitor may also impact the number of RIB5B complexes available to translate *COL1A1* and β-*actin*. Interestingly, the IC_{50} values are similar under hypoxic conditions, however, a 16-fold higher concentration of inhibitor under unstressed conditions is required to reduce the number of canonical RIB5B complexes by half, compared to the concentration required to decrease the number of non-canonical RIB5B complexes by half. Therefore, it is possible a PIC inhibitor may not have a strong impact on canonically translated proteins, and by extension, global translation initiation. A similar conclusion can be made for the TC_{nc} inhibitor as well.

Interestingly, it seems likely that the safest and most efficient option for inhibiting the eIF5B-mediated non-canonical translation initiation pathway with minimal toxicity to the patient is through targeting the eIF5B-ternary complex. There are a few ways of targeting this complex that will not affect the canonical translation pathway, at least not mechanistically. These include: targeting the eIF5B-ternary complex as a whole (i.e. an inhibitor that makes contacts with both eIF5B and the initiator tRNA when bound to the complex), which is not present in the canonical pathway; and targeting eIF5B after it has bound to the ternary complex. However, this assumes there is a conformational change to either the initiator tRNA or eIF5B after they have bound to create the ternary complex that could be

specifically targeted by a drug. It may be possible to develop an inhibitor to target the active site where GTP is hydrolyzed or exchanged, however this may have disastrous impacts to the canonical model, as was observed in the 3D surface and contour plots of RIB5B inhibition.

5.5 Study analysis

This study incorporated the use of deterministic modeling methods. While these provide useful results, which have been highlighted and described throughout this thesis, stochastic methods are often used in biological models, as they account for the fluctuations observed in small populations, rather than assuming a spatially homogenous system [57, 61]. While it would have been useful to compare the results from the deterministic models presented here and a series of corresponding stochastic models, the timespan of this study did not permit it.

Some aspects of the canonical model were simplified or ignored. For example, the poly-A binding protein (PABP) was not considered in the canonical mechanism. This was due to the fact that this protein facilitates the binding of the 3' poly-A tail to the 5' cap structure and likely remains on the complex throughout all of initiation and elongation, as the mRNA remains circularized during these processes [102]. Additionally, the eIF dissociation steps in the canonical model were simplified to show groups of them dissociating from the ribosome together rather than one at a time. The reason for this was that, to the best of my knowledge, there is no data available with respect to the order in which the eIFs in their aforementioned groups dissociate from the pre-initiation complex. Although this information was not known, the results would not be affected by a change in order as this is a step-wise mechanism, and no intervention via inhibition mechanisms targeted any complex that relies upon this series of steps.

Finally, the canonical mechanism derived and used in this thesis is not the only mode of canonical translation initiation. As noted previously, eIF5B is not necessary for healthy

cell survival [18]. Therefore, proteins must be able to be translated without the presence of eIF5B. The mechanism of canonical translation presented in this thesis did not consider other modes of translation initiation in the absence of eIF5B, primarily because the most efficient assembly of the ribosome complex utilizes eIF5B.

5.5.1 Study limitations

Some data was not available at the time of this study. For example, some rate constants and species concentrations were either not available, or not measured in human cells. Therefore, these parameters were either calculated or assumed. This is, unfortunately, a limitation to mathematical modeling, however it is also an opportunity to work in tandem with experimentalists to provide the most up-to-date and accurate information possible. It is important to note however, that the risk of over-interpretation of the results was mitigated by carrying out sensitivity analyses that showed very low sensitivity to any of the unknown parameters.

Additionally, this was a preliminary analysis to determine the most promising therapeutic targets, and therefore the concentrations and K_D values for the inhibitors discussed in this thesis are approximate values and may differ in practice for a number of reasons. Firstly, the non-canonical model explored here focused on the synthesis of a single protein: XIAP. The concentration of XIAP and ratio of XIAP to pro-apoptotic proteins required to promote cell survival or cell death are unknown to the best of my knowledge. Therefore, it was assumed in this study that the number of ribosomes available to synthesize XIAP must be reduced by at least 50%. However, the models derived and analyzed in this study are able to be returned to at a later date after future information regarding this cell fate switch limit has been obtained to establish other IC_{50} and K_D values necessary to inhibit the non-canonical pathway.

Moreover, eIF5B was the initiation factor of interest in this study, with respect to XIAP synthesis and glioblastoma cell survival. Previous research has indicated that eIF4E is

also an important initiation factor involved in cancer cell survival [79]. Therefore, the results presented in this thesis are just one piece of the larger puzzle in designing novel chemotherapeutics.

Finally, the inhibition mechanisms proposed in this thesis were only applied to two essential proteins: type-1 collagen, and β-actin. However, there are numerous other important proteins in the cell. The synthesis of these proteins may be affected by the inhibition mechanisms proposed here, depending on their respective mRNA abundance in the cell. This is further discussed in the next section.

5.6 Future directions

5.6.1 Considering effects of inhibition mechanisms on other essential proteins

It is important to consider the effect of these inhibition mechanisms on other essential proteins in the cell. In this thesis, we analyzed COL1A1 and β-actin. The number of transcripts in the cell that codes these two proteins differ by an order of magnitude, as we saw in chapter 4. It may be beneficial to analyze the proposed inhibition mechanisms on a protein with less-abundant mRNA such as citrate synthase[4] (Uniprot ID: P53396), which is an enzyme involved in the Krebs cycle that converts acetyl-coenzyme A and oxaloacetate into coenzyme A and citrate [103]. Additionally, many of the proteins that comprise the 40S and 60S ribosomal subunits have less than 100 transcript copies/cell [68]. As these two subunits are required for translation of proteins, we should ensure the inhibition classes proposed in this thesis do not affect the synthesis of the proteins that comprise the 40S and 60S subunits.

5.6.2 Stochastic simulations

As noted above, a series of stochastic simulations in parallel to the deterministic models provided in this thesis should be performed. One important aspect of this study was

[4]There are, on average, approximately 81 transcript copies/cell of citrate synthase [68].

to determine the properties of possible inhibitors to limit the number of RIB5B complexes in the non-canonical model. Consequently, the concentrations of eIF5B, RIB5B, and/or the targeted complexes will become very small. It may be of interest to perform stochastic simulations to figure out the distribution of RIB5B numbers across a cell population. This would allow us to elucidate how many cells would likely maintain high XIAP populations despite the treatment, due to the fact that some cells will randomly have more RIB5B complexes. Therefore, it is important to conduct stochastic simulations on this system to confirm and add to the results presented in this thesis.

5.6.3 Future experiments

As mentioned previously, no modeling or experimental data has been provided on the concentration of XIAP required for the cell to switch fates to the best of my knowledge. Therefore, it will be beneficial to conduct a study which examines the effects of different concentrations of XIAP in the cell. It is likely this would be a stochastic study, as this may require analyzing a distribution of XIAP concentrations across a cell population. However, it may also be possible to take a microscopic deterministic approach to this problem through the modeling of the intrinsic and extrinsic apoptotic pathways. This approach could result in a concentration of XIAP necessary to avoid apoptosis. This concentration could be used in future studies, and be applied to the non-canonical model discussed in this thesis. Once the switch limit has been elucidated, the level of inhibition can be established, and with the knowledge of the K_D of a potential inhibitor, we will be able to numerically calculate the concentration of the inhibitor required to obtain this level of inhibition.

Throughout this thesis, the most promising classes of non-canonical inhibitors were analyzed and discussed. One of the potential options is the non-canonical ternary complex inhibitor. As was mentioned previously, there are multiple ways we could think about inhibiting this complex. If the entire complex is targeted, it is important to understand the structural similarities between the eIF5B-TC and the eIF2-TC, as inadvertently inhibiting

the eIF2-TC will impact global canonical translation initiation. Some questions to consider in these experiments include: how does eIF5B's binding to $tRNA_i$ differ from that of eIF2? When eIF5B binds to the initiator tRNA, does it undergo a conformational change? Is this conformational change similar to that observed with eIF2? Is the canonical TC significantly structurally different from the non-canonical TC? Targeting the eIF5B-TC appears to be the most biologically safe option since it has the least chance of affecting the canonical translation initiation pathways, provided sufficient inhibitor specificity. However, before implementing this into a therapy, it is important to consider the structural similarities and differences between the two ternary complexes.

If possible, it would be advantageous to characterize the two ternary complexes and the $PIC2_{nc}$ complex. Cryo-EM images of the RIB5B complex are provided in the literature [104, 105]. Obtaining crystal structures of these complexes will provide useful data in the *in silico* component in the synthesis of the inhibitors. Specifically, it is important to compare the active sites on eIF5B. It would be detrimental to the canonical translation initiation pathway to derive or establish an inhibitor that compromises the RIB5B complex's ability to move into the elongation phase of translation. Furthermore, as the non-canonical ternary complex is the most promising chemotherapeutic target, obtaining a crystal structure of this complex will greatly aid in the derivation or establishment of a suitable inhibitor. Part of this process may include characterising the $PIC2_{nc}$ complex as well to understand the non-canonical ternary complex's connections to the pre-intiation complex. It may also be beneficial to characterize the $PIC3_{nc}$ complex to confirm these connections and identify any conformational changes within the complexes upon binding.

The results provided in this thesis should be confirmed using other methods such as stochastic simulations as mentioned earlier and, most importantly, *in vitro* experiments. As mentioned previously, some rate constants were not available in the literature. One important value that was assumed in this study was the K_D of the non-canonical ternary complex binding to the pre-initiation complex. Fluorescent labelling of eIF5B has been performed

previously [37], and has not affected its function. Therefore, it would be beneficial to perform a series of *in vitro* fluorescence stopped flow experiments that combine labeled eIF5B-ternary complexes with a previously assembled solution of $PIC2_{nc}$ complexes in the absence of the 60S ribosomal subunit. This will ensure that translation initiation will be truncated at the $PIC3_{nc}$ complex, and the K_D for this critical binding step should be able to be measured.

Once the inhibitor(s) and the concentration of XIAP required to switch cell fates have been established, *in vitro* and *in cellulo* experiments may be performed to confirm the results presented in this thesis. Several contour lines that represent the same level of inhibition were provided throughout this thesis. Therefore, these will provide future researchers with approximate concentrations with respect to the K_D of the inhibitor required to obtain a specific level of inhibition.

Once the inhibitor has been proven to be effective *in vitro*, it should be tested in a live specimen. Typically, orthotopic xenograft mouse model experiments are performed using immunocompromised mice for glioblastoma studies [106]. In this process, brain tumour initiating cells (BTICs) are implanted in mice brains and a survival analysis is performed. Treating these mice with the proposed chemotherapy will provide insight into the inhibitor's effectiveness and toxicity. Should the specimen die, whole BTIC-implanted brains can be extracted and immunohistochemistry (IHC) can be performed, which can identify key cellular features such as hormone or human epidermal growth factor receptor 2 (HER2) receptors on the cell surface [107]. IHC is often performed on biopsy samples to aid in treatment planning, and can also be used in mice models to determine tumour size and intratumoral immune cell populations [108]. The survival and IHC analysis will help us understand the effectiveness of the potential chemotherapy before moving onto human trials.

Finally, as was mentioned previously, it is important for experimentalists and theoreticians to work together to share the most up-to-date and accurate information. The models provided in this thesis are able to be returned to easily as more data becomes available, and

as the field continues to advance.

Chapter 6

Conclusion

Currently, glioblastoma is essentially incurable. It is possible, through the knowledge provided by this study, that a new therapy could be proposed, which could provide patients with a new hope of survival.

Several inhibition targets were proposed in chapter 3. The feasibility of targeting eIF5B for treatment in glioblastoma patients was discussed throughout chapters 3 and 4. An understanding of the biological implications of establishing eIF5B as a therapeutic target was obtained by comparing the canonical and non-canonical models. Throughout this thesis, it became clear that a ternary complex inhibitor will be the most effective at limiting the number of non-canonical RIB5B complexes without a large impact on the canonical translation initiation mechanism. The data presented in this thesis suggests a direct-eIF5B inhibitor will likely affect the translation initiation of canonically translated proteins such as COL1A1 and β-actin. However, it should still be noted that a direct eIF5B inhibitor may still be promising due to previous and ongoing studies.

Targeting eIF5B directly is likely an easier, and less biologically expensive option. Targeting eIF5B *before* it creates the ternary complex likely only requires the consideration of its contacts with the initiator tRNA. Targeting the ternary complex as a whole requires considerations of eIF5B's contacts with the initiator tRNA, *and* the ternary complex's contacts with the pre-initiation complex. Furthermore, targeting a downstream complex is more biologically expensive, as the cell would use a lot of energy to create them before the pathway is inhibited. Additionally, a direct eIF5B inhibitor (LWW31) is already in development.

The TC_{nc} is a promising therapeutic target assuming there is a region of TC_{nc} that provides some specificity of binding while interfering with its role in the non-canonical pathway. Molecular modeling experiments would be useful in determining the region, or regions, of specificity such that the TC_{nc} inhibitor will not impact the canonical ternary complex. The $PIC2_{nc}$ inhibitor did not appear to have a large effect on the canonical translation initiation mechanism, however calculations show that it would require high inhibitor concentrations and a low K_D. According to the results provided in this study, RIB5B is the worst therapeutic target, as this may have negative effects on the canonical mechanism and global translation initiation.

According to the sensitivity analyses presented in this thesis, the non-canonical model is sensitive to the total free concentration of eIF5B when the eIF5B and TC_{nc} inhibitors are applied. Therefore, mutations that increase the expression of eIF5B will result in a greater number of RIB5B complexes by a factor of 1.04 under eIF5B inhibition conditions (table 3.6) and 0.43 under TC_{nc} inhibition conditions (table 3.8). Moreover, the canonical model was not sensitive to the total free concentration of eIF5B, which confirms previous experimental results [81].

The contour plots in this thesis provided useful insight into the necessary concentrations for non-canonical and canonical inhibition. Several IC_{50} values were established considering an inhibitor with a K_D of 1 nM. A summary of these values is provided in table 5.1. Based on these results, an eIF5B inhibitor may impact the canonical translation of *COL1A1* and β-*actin*. However, as noted previously, eIF5B is not essential for cell viability, and therefore eIF5B remains a promising therapeutic target. Finally, a TC_{nc} inhibitor with poor specificity has the potential to impact the canonical translation initiation mechanism and may affect *COL1A1* and β-*actin* translation initiation under hypoxic conditions. However, a TC_{nc} inhibitor will likely have only a small effect (if any) under unstressed conditions. Although a TC_{nc} inhibitor may be more biologically expensive, there are several ways it will not affect the canonical mechanism, save the obvious decrease in the cellular pool of

eIF5B due to this inhibition. Further *in silico*, *in vitro* and *in vivo* experiments will help elucidate which is the better inhibitor option. Before these experiments are performed, however, compounds need to be elucidated and tested to ensure proper binding specificities and efficacies. Therefore, the eIF5B contacts with the 40S and 60S ribosomal subunits, and the initiator tRNA in both the non-canonical pathway (ternary complex) and the canonical pathway (stabilizing agent) must be confirmed. Once the locations have been identified, a small molecule inhibitor can be either synthetically derived or found.

Several groups from varying chemistry and biochemistry disciplines have partnered into a cooperative study on glioblastoma, supported by a New Frontiers in Research Fund grant. This thesis is one step of many involved in this initiative. The critical information obtained here will be utilized to guide further experiments including: *in silico* drug development, the synthesis of potential targeting compounds, and both *in vitro* and *in vivo* experimental testing of these compounds. *In silico* experiments should consider the classes of inhibitors presented in this study and examine eIF5B and the complexes to determine suitable areas of these targets for inhibitor binding. Furthermore, *in vitro* labelling assays such as eIF5B fluorescent labelling assays may assist and supplement the *in silico* drug development. This project is a contribution to developing a new innovative approach to such a devastating disease, and will provide valuable insight regarding new treatment and therapy options for those suffering from glioblastoma.

The data presented in this thesis has shown that targeting pre-initiation complexes may not only be less effective than other inhibition options, but may also impact canonical translation initiation. The most promising therapeutic targets listed in this thesis are eIF5B and TC_{nc}, both of which are independent from the pre-initiation complexes before binding. Therefore, the inhibition targets that have the most impact on the *XIAP* non-canonical translation mechanism, and by extension, other non-canonical translation initiation mechanisms, are the ones that can be targeted before they have bound to the pre-initiation complex. Cap-independent non-canonical translation initiation is not specific to cancer. Several viruses

initiate translation using non-canonical pathways including HCV [47], and CrPV [109]. Therefore, the methods and approaches discussed in this study may be useful in future studies of novel viral therapies regarding the inhibition of translation initiation machinery.

Bibliography

[1] Brain Tumour Foundation of Canada; *Glioblastoma (GB)*; 2020. https://www.braintumour.ca/brain_tumour_types/glioblastoma-gb/#:~:text=The%20incidence%20of%20glioblastoma%20(GB,%2D60%25%20of%20astrocytic%20tumours.

[2] Koshy, M.; Villano, J. L.; Dolecek, T. A.; Howard, A.; Mahmood, U.; Chmura, S. J.; Weichselbaum, R. R.; McCarthy, B. J. *J. Neurooncol.* **2012**, *107*, 207–212.

[3] Tamimi, A. F.; Juweid, M. In *Glioblastoma*; DeVleeschouwer, S, Ed.; Codon Publications, 2017; pp 143–153.

[4] Ostrom, Q. T.; Gittleman, H.; Farah, P.; Ondracek, A.; Chen, Y.; Wolinsky, Y.; Stroup, N. E.; Kruchko, C.; Barnholtz-Sloan, J. S. *Neuro-Oncol* **2013**, *15*, 1–56.

[5] Bar, E. E.; Lin, A.; Mahairaki, V.; Matsui, W.; Eberhart, C. G. *Am. J. Pathol.* **2010**, *177*, 1491–1502.

[6] Terenin, I. M.; Dmitiev, S. E.; Andreev, D. E.; Shatsky, I. N. *Nat. Struct. Mol. Biol.* **2008**, *15*, 836–841.

[7] Hernandez-Martinez, R.; Covarrubias, L. *Develop. Growth Differ.* **2011**, *53*, 245–258.

[8] Kerr, J.; Wyllie, A.; Currie, A. *Br. J. Cancer* **1972**, *26*, 239–257.

[9] Elmore, S. *Toxicol. Pathol.* **2007**, *35*, 495–516.

[10] Wong, R. S. *J. Exp. Clin. Cancer Res.* **2011**, *30*, 87.

[11] Tower, J. *Ageing Res. Rev.* **2015**, *23(Pt A)*, 90–100.

[12] Brentnall, M.; Rodriguez-Menocal, L.; Guevara, R. L. D.; Cepero, E.; Boise, L. H. *BMC Cell Biol.* **2013**, *14*, 32.

[13] Tenev, T.; Zachariou, A.; Wilson, R.; Ditzel, M.; Meier, P. *Nat. Cell Biol.* **2005**, *7*, 70–77.

[14] Wei, Y.; Fan, T.; Yu, M. *ABBS* **2008**, *40*, 278–288.

[15] Deveraux, Q.; Reed, T. *Genes Dev.* **1999**, *13*, 239–252.

[16] Scott, F. L.; Denault, J.-B.; Riedl, S. J.; Shin, H.; Renatus, M.; Salvesen, G. S. *EMBO J.* **2005**, *24*, 645–655.

[17] Suzuki, Y.; Nakabayashi, Y.; Takahashi, R. *PNAS* **2001**, *98*, 8662–8667.

[18] Thakor, N.; Holcik, M. *Nucleic Acids Res.* **2012**, *40*, 541–552.

[19] Tirapelli, D.; Lustosa, I.; Menezes, S.; Franco, I.; Rodrigues, A.; Peria, F.; Marinho, A.; Serafini, L.; Carlotti, C. J.; Tirapelli, L. *Arq. Neuropsiquiatr.* **2017**, *75*, 875–880.

[20] Ho, J. J. D.; Balukoff, N. C.; Cervantes, G.; Malcolm, P. D.; Krieger, J. R.; Lee, S. *Cell Rep.* **2018**, *22*, 17–26.

[21] Pestova, T. V.; de Breyne, S.; Pisarev, A. V.; Abaeva, I. S.; Hellen, C. U. T. *EMBO J.* **2008**, *27*, 1060–1072.

[22] Li, Q.; Xiao, M.; Shi, Y.; Hu, J.; Bi, T.; Wang, C.; Yan, L.; Li, X. *BMC Cancer* **2021**, *21*, 1022.

[23] guang Wang, Z.; Zheng, H.; Gao, W.; Han, J.; zhu Cao, J.; Yang, Y.; Li, S.; Gao, R.; Liu, H.; ya Pan, Z.; yuan Fu, S.; ming Gu, F.; Xing, H.; sheng Ni, J.; li Yan, H.; Ren, H.; ping Zhou, W. *Oncotarget* **2016**, *7*, 62327–62339.

[24] Ross, J. A.; Bressler, K. R.; Thakor, N. *Int. J. Mol. Sci.* **2018**, *19*, 4032.

[25] Alonso, M. M.; Gomez-Manzano, C.; Bekele, B. N.; Yung, W. A.; Fueyo, J. *Cancer Res.* **2007**, *67*, 11499–11504.

[26] Singh, N.; Miner, A.; Hennis, L.; Mittal, S. *Cancer Drug Resist.* **2021**, *4*, 17–43.

[27] Yu, W.; Zhang, L.; Wei, Q.; Shao, A. *Front. Oncol.* **2020**, *9*, 1547.

[28] Clement, P. M.; Dirven, L.; Eoli, M.; Sepulveda-Sanchez, J. M.; Walenkamp, A. M.; Frenel, J. S.; Franceschi, E.; Weller, M.; Chinot, O.; Vos, F. Y. D.; Whenham, N.; Sanghera, P.; Looman, J.; Kundu, M. G.; de Geus, J. P.; Nuyens, S.; Spruyt, M.; Gorlia, T.; Coens, C.; Golfinopoulos, V.; Reijneveld, J. C.; van den Bent, M. J. *Eur. J. Cancer* **2021**, *147*, 1–12.

[29] Liau, L. M.; Ashkan, K.; Tran, D. D.; Campian, J. L.; Trusheim, J. E.; Cobbs, C. S.; Heth, J. A.; Salacz, M.; Taylor, S.; D'andre, S. D.; Iwamoto, F. M.; Dropcho, E. J.; Moshel, Y. A.; Walter, K. A.; Pillainayagam, C. P.; Aiken, R.; Chaudhary, R.; Goldlust, S. A.; Bota, D. A.; Duic, P.; Grewal, J.; Elinzano, H.; Toms, S. A.; Lillehei, K. O.; Mikkelsen, T.; Walpert, T.; Abram, S. R.; Brenner, A. J.; Brem, S.; Ewend, M. G.; Khagi, S.; Portnow, J.; Kim, L. J.; Loudon, W. G.; Thompson, R. C.; Avigan, D. E.; Fink, K. L.; Geofroy, F. J.; Lindhorst, S.; Lutzky, J.; Sloan, A. E.; Schackert, G.; Krex, D.; Meisel, H.-J.; Wu, J.; Davis, R. P.; Duma, C.; Etame, A. B.; Mathieu, D.; Kesari, S.; Piccioni, D.; Westphal, M.; Baskin, D. S.; New, P. Z.; Lacroix, M.; May, S.-A.; Pluard, T. J.; Tse, V.; Green, R. M.; Villano, J. L.; Pearlman, M.; Petrecca, K.; Schulder, M.; Taylor, L. P.; Maida, A. E.; Prins, R. M.; Cloughesy, T. F.; Mulholland, P.; Bosch, M. L. *J. Transl. Med.* **2018**, *16*, 142.

[30] Geribaldi-Doldan, N.; Hervas-Corpion, I.; Gomez-Oliva, R.; Dominguez-Garcia, S.; Ruiz, F. A.; Iglesias-Lozano, I.; Carrascal, L.; Pardillo-Diaz, R.; Gil-Salu, J. L.; Nunez-Abades, P.; Valor, L. M.; Castro, C. *Biomedicines* **2021**, *9*, 381.

[31] Wu, C.-Y.; Wang, D.-H.; Wang, X.; Dixon, S. M.; Meng, L.; Ahadi, S.; Enter, D. H.; Chen, C.-Y.; Kato, J.; Leon, L. J.; Ramirez, L. M.; Maeda, Y.; Reis, C. F.; Ribeiro, B.; Weems, B.; Kung, H.-J.; Lam, K. S. *ACS Comb. Sci.* **2016**, *18*, 320–329.

[32] Wick, W.; Steinbach, J. P.; Platten, M.; Hartmann, C.; Wenz, F.; von Deimling, A.; Shei, P.; Moreau-Donnet, V.; Stoffregen, C.; Combs, S. E. *Neuro-Oncol.* **2013**, *15*, 1405–1412.

[33] Kearse, M. G.; Wilusz, J. E. *Genes Dev.* **2017**, *31*, 1717–1731.

[34] Sonenberg, N.; Hinnebusch, A. G. *Cell* **2009**, *136*, 731–745.

[35] Jackson, R. J.; Hellen, C. U. T.; Pestova, T. V. *Mol. Cell. Biol.* **2010**, *11*, 113–127.

[36] Wagner, S.; Herrmannova, A.; Hronova, V.; Gunisova, S.; Sen, N. D.; Hannan, R. D.; Hinnebusch, A. G.; Shirokikh, N. E.; Preiss, T.; Valasek, L. S. *Mol. Cell* **2020**, *79*, 546–560.

[37] Wang, J.; Johnson, A. G.; Lapointe, C. P.; Choi, J.; Prabhakar, A.; Dong-Hua Chen, A. N. P.; Puglisi, J. D. *Nature* **2019**, *573*, 605–608.

[38] Simonetti, A.; Guca, E.; Bochler, A.; Kuhn, L.; Hashem, Y. *Cell Rep.* **2020**, *31*, 107497.

[39] Wang, J.; Wang, J.; Shin, B.-S.; Kim, J.-R.; Dever, T. E.; Puglisi, J. D.; Fernández, I. S. *Nat. Commun.* **2020**, *11*, 5003.

[40] Huang, B. Y.; Fernández, I. S. *PNAS* **2020**, *117*, 1429–1437.

[41] Unbehaun, A.; Borukhov, S. I.; Hellen, C. U.; Pestova, T. V. *Genes Dev.* **2004**, *18*, 3078–1093.

[42] Chukka, P. A. R.; Wetmore, S. D.; Thakor, N. *Front. Genet.* **2021**, *12*, 737433.

[43] Yi, S.-H.; Petrychenko, V.; Schliep, J. E.; Goyal, A.; Linden, A.; Chari, A.; Urlaub, H.; Stark, H.; Rodnina, M. V.; Adio, S.; Fischer, N. *Nucleic Acids Res.* **2022**, *50*, 5282–5298.

[44] Pisareva, V. P.; Hellen, C. U. T.; Pestova, T. V. *Biochem.* **2007**, *46*, 2622–2629.

[45] Holčík, M.; Gordon, B. W.; Korneluk, R. G. *Mol. Cell. Biol.* **2003**, *23*, 280–288.

[46] Jang, S. K.; Kräusslich, H. G.; Nicklin, M. J.; Duke, G. M.; Palmenberg, A. C.; Wimmer, E. *J. Virol.* **1988**, *62*, 2636–2643.

[47] Perard, J.; Rasia, R.; Medenbach, J.; Ayala, I.; Boisbouvier, J.; Drouet, E.; Baudin, F. *FEBS Lett.* **2009**, *583*, 70–74.

[48] Yang, Y.; Wang, Z. *J. Mol. Cell. Biol.* **2019**, *11*, 911–919.

[49] Meng, Z.; Jackson, N. L.; Shcherbakov, O. D.; Choi, H.; Blume, S. W. *J. Cell. Biochem.* **2010**, *110*, 531–544.

[50] Weingarten-Gabbay, S.; Elias-Kirma, S.; Nir, R.; Gritsenko, A. A.; Stern-Ginossar, N.; Yakhini, Z.; Weinberger, A.; Segal, E. *Science* **2016**, *351*, aad4939.

[51] Shatsky, I. N.; Terenin, I. M.; Smirnova, V. V.; Andreev, D. E. *Trends Biochem. Sci.* **2018**, *43*, 882–895.

[52] Vaupel, P.; Harrison, L. *Oncologist* **2004**, *9*, 4–9.

[53] Jiao, D.; Cai, Z.; Choksi, S.; Ma, D.; Choe, M.; Kwon, H.-J.; Baik, J. Y.; Rowan, B. G.; Liu, C.; ; gang Liu, Z. *Cell. Res.* **2018**, *28*, 868–870.

[54] Gadiyar, V.; Lahey, K. C.; Calianese, D.; Devoe, C.; Mehta, D.; Bono, K.; Desind, S.; Davra, V.; Birge, R. B. *Cells* **2020**, *9*, 2207.

[55] Amirbeigiarab, S.; Kiani, P.; Sanchez, A. V.; andAndriy Kazantsev, C. K.; Fester, L.; Schlüter, H.; Ignatova, Z. *PNAS* **2019**, *116*, 24907.

[56] Firczuk, H.; Kannambath, S.; Pahle, J.; Claydon, A.; Beynon, R.; Duncan, J.; Westerhoff, H.; Mendes, P.; McCarthy, J. E. G. *Mol. Sys. Biol.* **2013**, *9*, 635.

[57] Hahl, S. K.; Kremling, A. *Front. Genet.* **2016**, *7*, 157.

[58] Trofimenkoff, E. A. M.; Roussel, M. R. *Math. Biosci.* **2020**, *325*, 108376.

[59] Engleman, V. S. *J. Phys. Chem* **1977**, *81*, 2320–2322.

[60] Ingalls, B. *Essays Biochem.* **2008**, *45*, 177–193.

[61] Wilkinson, D. J. *Nat. Rev. Genet.* **2009**, *10*, 122–133.

[62] Hellen, C. U. T. *Biochim. Biophys. Acta. Gene Regul. Mech.* **2009**, *1789*, 558–570.

[63] The UniProt Consortium *Nucleic Acids Res.* **2021**, *49*, D480–D489.

[64] Fraser, C. S.; Berry, K. E.; Hershey, J. W. B.; Doudna, J. A. *Mol. Cell.* **2007**, *26*, 811–819.

[65] Guillon, L.; Schmitt, E.; Blanquet, S.; Mechulam, Y. *Biochemistry* **2005**, *44*, 15594–15601.

[66] Walters, B.; Axhemi, A.; Jankowsky, E.; Thompson, S. R. *Nucleic Acids Res.* **2020**, *48*, 8063–8073.

[67] Yuliya Gordiyenko, J. L. L.; Ramakrishnan, V. *Nat. Commun.* **2019**, *10*, 2640.

[68] Schwanhäusser, B.; Busse, D.; Li, N.; Dittmar, G.; Schuchhardt, J.; Wolf, J.; Chen, W.; Selbach, M. *Nature* **2011**, *473*, 337–342.

[69] Milo, R.; Phillips, R. *Cell Biology by the Numbers*, 1st ed.; Garland Science, 2015.

[70] Tzur, A.; Kafri, R.; LeBleu, V. S.; Lahav, G.; Kirschner, M. W. *Science* **2009**, *325*, 167–171.

[71] Kieft, J. S.; Zhou, K.; Jubin, R.; Doudna, J. A. *RNA* **2001**, *7*, 194–206.

[72] Goss, D.; Rounds, D.; Harrigan, T.; Woodley, C.; Wahba, A. *Biochemsitry* **1988**, *27*, 1489–1494.

[73] Blobel, G.; Potter, V. *J. Mol. Biol.* **1967**, *26*, 279–292.

[74] Roussel, M. R. *J. Phys. Chem.* **1996**, *100*, 8323–8330.

[75] Roussel, M. R. *Nonlinear Dynamics: A hands-on introductory survey*; Morgan & Claypool, 2019.

[76] Chen, S. S.; Sperling, E.; Silverman, J. M.; Davis, J. H.; Williamson, J. R. *Mol. Biosyst.* **2012**, *8*, 3325–3334.

[77] Zhang, R.; Lahens, N. F.; Ballance, H. I.; Hughes, M. E.; Hogenesch, J. B. *PNAS* **2014**, *111*, 16219–16224.

[78] Golub, G. H.; Loan, C. F. V. *Matrix Computations*; Baltimore : The Johns Hopkins University Press, 1996.

[79] Chukka, P. A. R.; Master's thesis; University of Lethbridge; 2021. `https://hdl.handle.net/10133/6213`.

[80] Liston, D. R.; Davis, M. *Clin. Cancer Res.* **2017**, *23*, 3489–3498.

[81] Ross, J. A.; Dungen, K. V.; Bressler, K. R.; Fredriksen, M.; Sharma, D. K.; Balasingam, N.; Thakor, N. *Cell Death Dis.* **2019**, *10*, 57.

[82] King, P.; Perry, M. *Oncologist* **2001**, *6*, 162–176.

[83] Mudd, T. W.; Guddati, A. K. *AJCR* **2021**, *11*, 3461–3474.

[84] Pabla, N.; Dong, Z. *Kidney Int.* **2008**, *73*, 994–1007.

[85] Santos, M. L. C.; de Brito, B. B.; da Silva, F. A. F.; Botelho, A. C. d. S.; de Melo, F. F. *World J. Clin. Oncol.* **2020**, *11*, 4.

[86] Pfeilschifter, J.; Diel, I. *Am. J. Clin. Oncol.* **2000**, *18*, 1570–1593.

[87] Shin, B.-S.; Kim, J.-R.; Walker, S. E.; Dong, K.; Lorsch, J. R.; Dever, T. E. *Nat. Struct. Mol. Biol.* **2011**, *18*, 1227–1234.

[88] Algire, M. A.; Maag, D.; Lorsch, J. R. *Mol. Cell* **2005**, *20*, 251–262.

[89] Wolin, S.; Walter, P. *EMBO J.* **1988**, *7*, 3559–3569.

[90] Olofsson, S. O.; Boström, K.; Carlsson, P.; Borén, J.; Wettesten, M.; Bjursell, G.; Wiklund, O.; Bondjers, G. *Am. H. J.* **1987**, *113*, 446–452.

[91] Petrova, V.; Annicchiarico-Petruzzelli, M.; Melino, G.; Amelio, I. *Oncogenesis* **2018**, *7*, 10.

[92] West, N. *Front. Immunol.* **2019**, *10*, 1093.

[93] Somasundaram, R.; Schuppan, D. *J. Biol. Chem.* **1996**, *271*, 26884 –26891.

[94] Malfait, F.; Symoens, S.; Backer, J. D.; Hermanns-Lê, T.; Sakalihasan, N.; Lapière, C. M.; Coucke, P.; Paepe, A. D. *Hum. Mutat.* **2007**, *28*, 387–395.

[95] König, D.; Oesser, S.; Scharla, S.; Zdzieblik, D.; Gollhofer, A. *Nutrients* **2018**, *10*, 97.

[96] Zdzieblik, D.; Oesser, S.; Baumstark, M. W.; Gollhofer, A.; ; König, D. *Br. J. Nutr.* **2015**, *114*, 1237–1245.

[97] Duc, K. D.; Song, Y. S. *PLoS Genet.* **2018**, *14*, e1007620.

[98] Ji, Y.; Ferracci, G.; Warley, A.; Ward, M.; Leung, K.-Y.; Samsuddin, S.; Lévêque, C.; Queen, L.; Reebye, V.; Pal, P.; Gkaliagkousi, E.; Seager, M.; Ferro, A. *Proc. Natl. Acad. Sci. USA* **2007**, *104*, 8839–8844.

[99] Kaczmarski, W.; Barua, M.; Mazur-Kolecka, B.; Frackowiak, J.; Dowjat, W.; Mehta, P.; Bolton, D.; Hwang, Y.-W.; Rabe, A.; Albertini, G.; Wegiel, J. *J. Neurosci. Res.* **2014**, *92*, 162–173.

[100] Jacquet, K.; Fradet-Turcotte, A.; Avvakumov, N.; Lambert, J.-P.; Roques, C.; Pandita, R. K.; Paquet, E.; Herst, P.; Gingras, A.-C.; Pandita, T. K.; Legube, G.; Doyon, Y.; Durocher, D.; Côté, J. *Mol. Cell.* **2016**, *62*, 409–421.

[101] Sweeney, M. D.; Zhao, Z.; Montagne, A.; Nelson, A. R.; Zlokovic, B. V. *Physiol. Rev.* **2019**, *99*, 21–78.

[102] A K Christensen, C. M. B., L E Kahn *Am. J. Anat.* **1987**, *178*, 1–10.

[103] Ma, Z.; Chu, C.-H.; Cheng, D. *J. Lipid Res.* **2009**, *50*, 2131–2135.

[104] Fernandez, I. S.; Bai, X.-C.; Hussain, T.; Kelley, A. C.; Lorsch, J. R.; Ramakrishnan, V.; Scheres, S. H. W. *Science* **2013**, *342*, 1240585.

[105] Yamamoto, H.; Unbehaun, A.; Loerkel, J.; Behrmannl, E.; Collier, M.; Buerger, J.; Mielke, T.; Spahn, C. M. T. *Nat. Struct. Mol. Biol.* **2014**, *21*, 721–727.

[106] Miyai, M.; Tomita, H.; Soeda, A.; Yano, H.; Iwama, T.; Hara, A. *J. Neuro-Oncol.* **2017**, *135*, 423–432.

[107] Ahmed, N.; Salsman, V. S.; Kew, Y.; Shaffer, D.; Powell, S.; Zhang, Y. J.; Grossman, R. G.; Heslop, H. E.; Gottschalk, S. *Clin. Cancer Res.* **2010**, *16*, 474–485.

[108] Enriquez Perez, J.; Kopecky, J.; Visse, E.; Darabi, A.; Siesjo, P. *BMC Cancer* **2020**, *20*, 7.

[109] Wilson, J. E.; Pestova, T. V.; Hellen, C. U.; Sarnow, P. *Cell* **2000**, *102*, 511–520.

Appendix A

Surface Plots

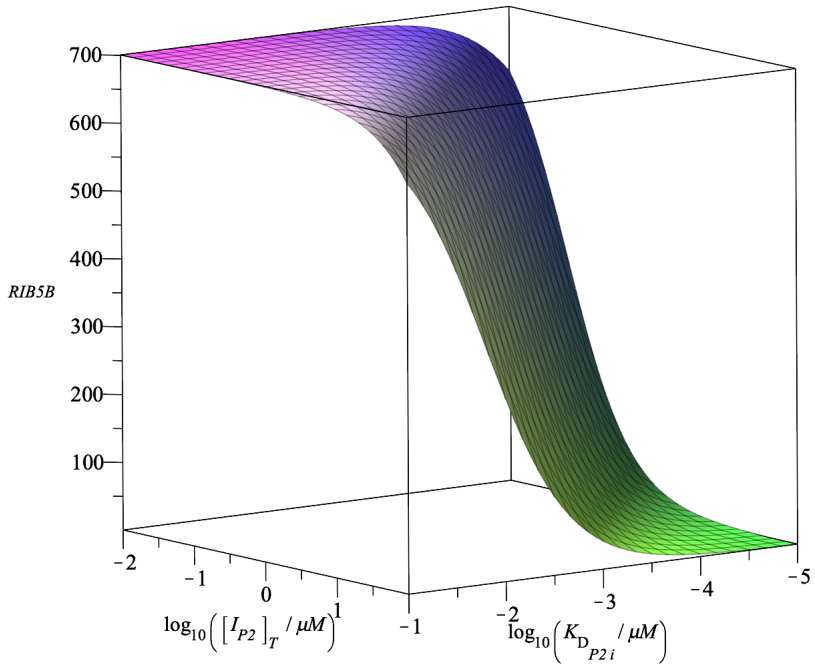

Figure A.1: A 3-D surface plot of the number of RIB5B complexes in the cell as the total concentration of the inhibitor ($[I_{P2}]_T$) and the dissociation constant of the inhibitor ($K_{D_{PIC2i}}$) are varied in the non-canonical model. The region of minimal RIB5B complexes is much smaller than that in figure 3.6

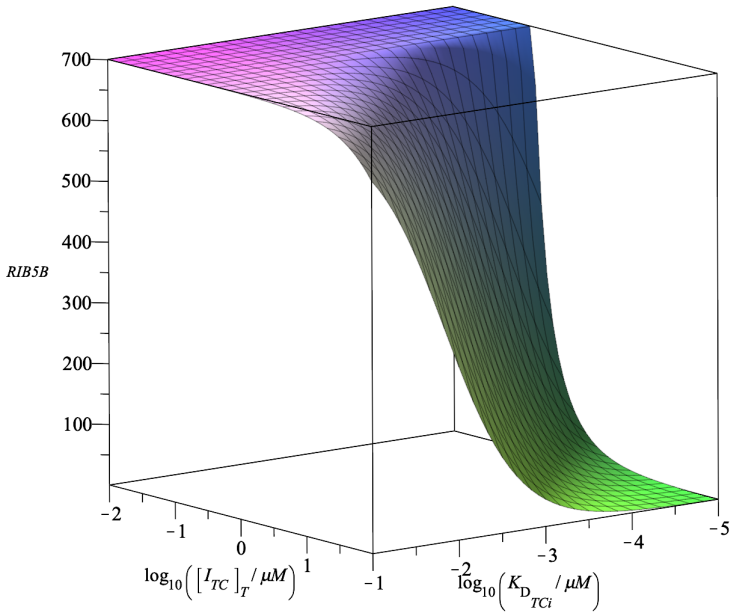

Figure A.2: A 3-D surface plot of the number of RIB5B complexes in the cell as the total concentration of the inhibitor ($[I_{TC}]_T$) and the dissociation constant of the inhibitor ($K_{D_{TCi}}$) are varied in the non-canonical model. The region of minimal RIB5B complexes is larger than that in figure A.1, but smaller than that in figure 3.6

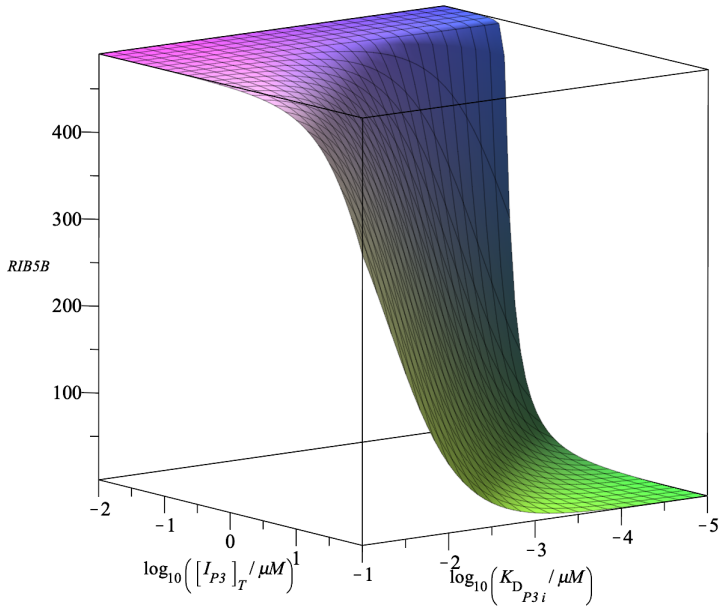

Figure A.3: A 3D surface plot of PIC3 inhibition in the canonical model for COL1A1 translation initiation under hypoxic conditions. There is no effect on the number of RIB5B$_{COL1A1}$ complexes regardless of the K_D value at smaller concentrations of inhibitor ($\sim 10^{-1.5}$ – $10^{-2}\mu$M). The region of minimal RIB5B$_{COL1A1}$ complexes is smaller than that in figure A.3.

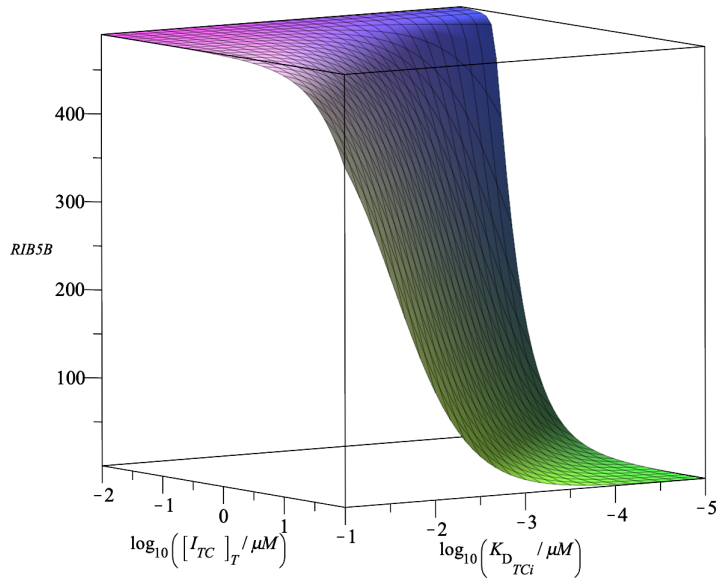

Figure A.4: A 3D surface plot of TC inhibition in the canonical model for COL1A1 translation initiation under hypoxic conditions. The region of minimal RIB5B$_{COL1A1}$ complexes is smaller than that in figure A.3, and similar to that in figure 4.2.

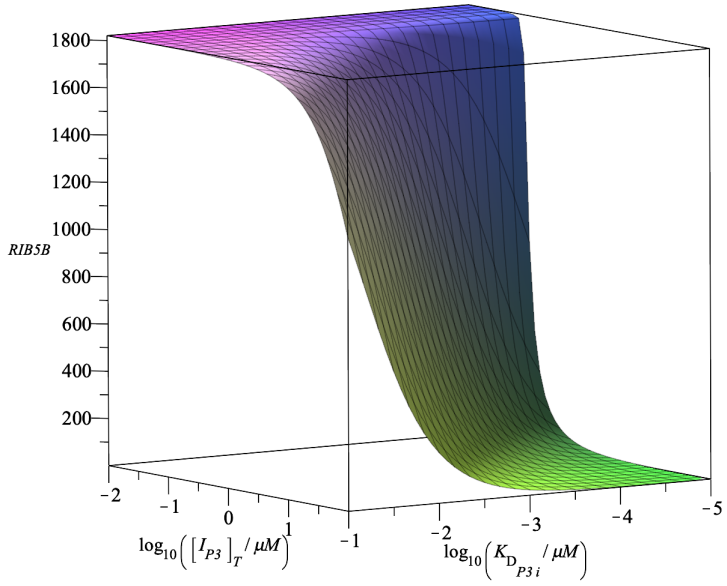

Figure A.5: A 3D surface plot of PIC3 inhibition in the canonical model for β-actin translation initiation under hypoxic conditions. The region of minimal $\text{RIB5B}_{\beta-actin}$ complexes is larger than that in figure 4.11 smaller than that of the COL1A1 model under the same conditions observed in figure A.3.

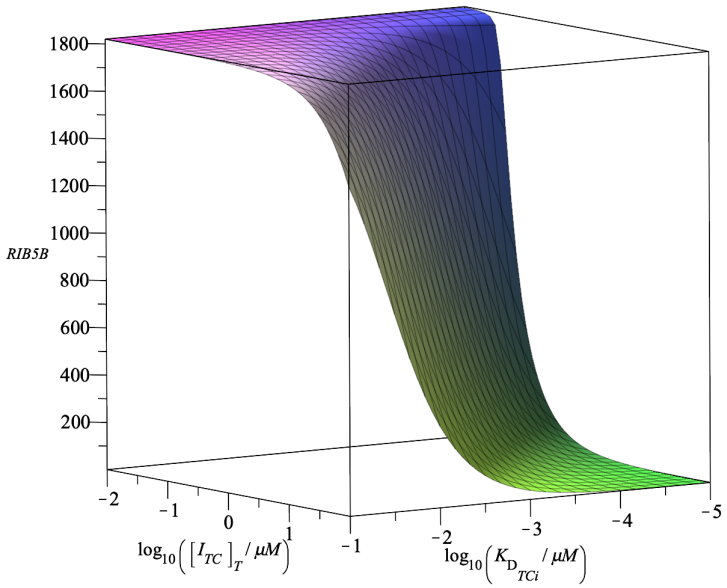

Figure A.6: A 3D surface plot of TC inhibition in the canonical model for β-actin translation initiation under hypoxic conditions. The region of minimal $\text{RIB5B}_{\beta-actin}$ complexes is larger than that in figure 4.11, smaller than that in figure A.5, and smaller than that in the COL1A1 model under the same conditions in figure A.4.

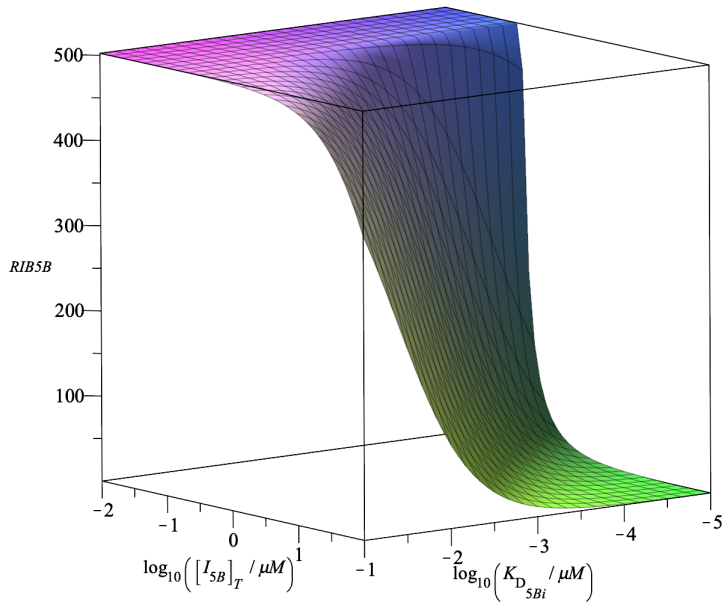

Figure A.7: A 3D surface plot of direct eIF5B inhibition in the canonical model for COL1A1 translation initiation under unstressed conditions. The region of minimal RIB5B$_{COL1A1}$ complexes is similar to that under hypoxic conditions in figure 4.2.

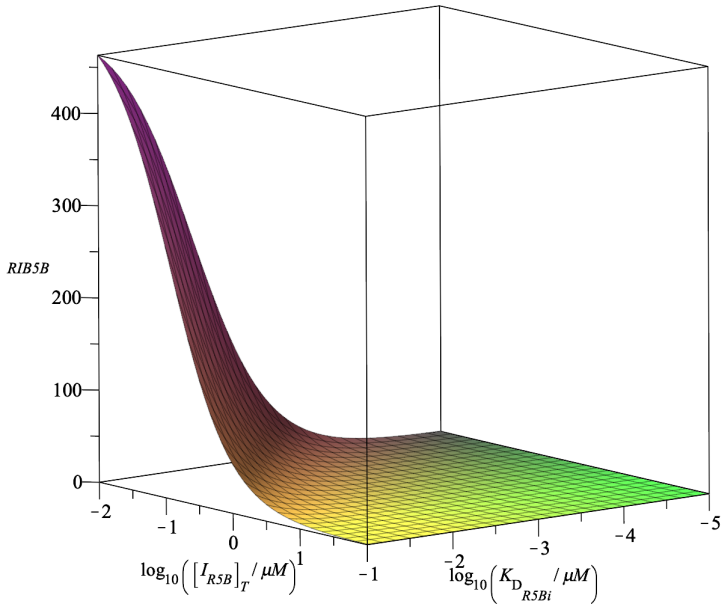

Figure A.8: A 3D surface plot of RIB5B inhibition in the canonical model for COL1A1 translation initiation under unstressed conditions. Only at the smallest concentration of inhibitor ($10^{-2}\mu$M) and highest value of K_D considered ($10^2\mu$M) does the number of RIB5B$_{COL1A1}$ complexes approach the maximum (503 ribosomes).

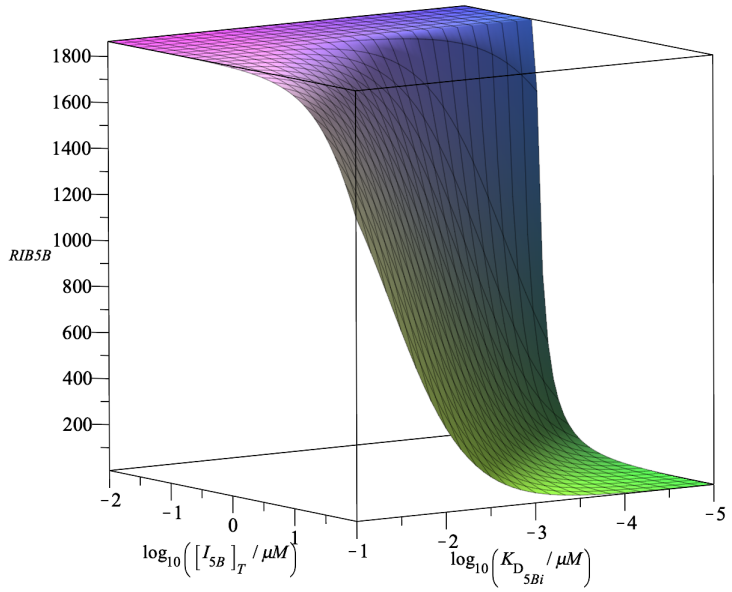

Figure A.9: A 3D surface plot of direct eIF5B inhibition in the canonical model for β-actin translation initiation under unstressed conditions. At smaller concentrations of inhibitor ($\sim 10^{-1}$ – $10^{-2}\mu$M), there is no effect on the number of RIB5B$_{\beta-actin}$ complexes regardless of the K_D value. The region of minimal RIB5B$_{\beta-actin}$ complexes is smaller than that of the same mechanism under hypoxic conditions in figure 4.11, and smaller than that of COL1A1 under the same conditions in figure A.7.

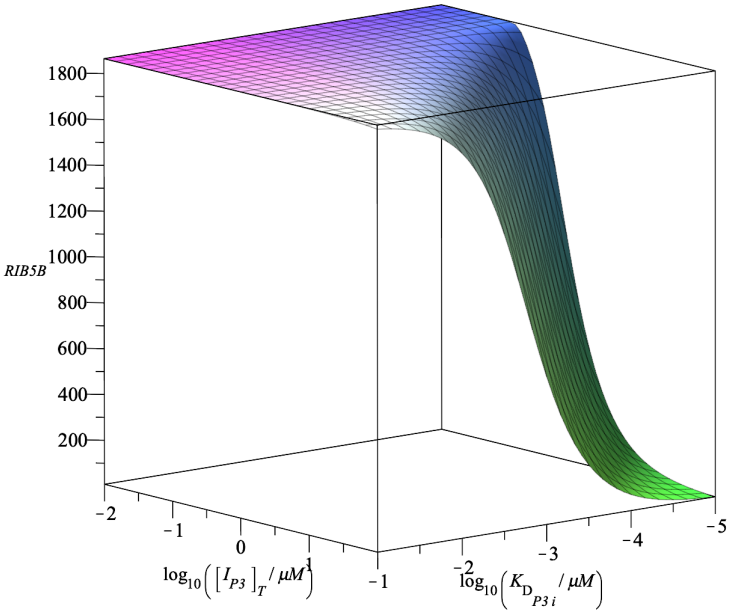

Figure A.10: A 3D surface plot of PIC3 inhibition in the canonical model for β-actin translation initiation under unstressed conditions. At smaller concentrations of inhibitor ($\sim 10^{-0.5}$ – $10^{-2}\mu$M), there is no effect on the number of RIB5B$_{\beta-actin}$ complexes regardless of the K_D value. Only at large inhibitor concentrations and low values of K_D does the number of RIB5B$_{\beta-actin}$ complexes approach a minimum.

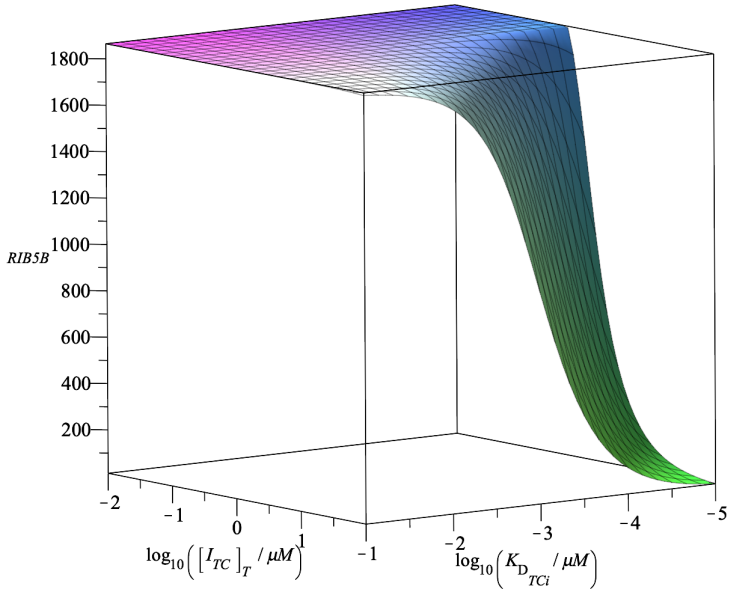

Figure A.11: A 3D surface plot of TC inhibition in the canonical model for β-actin translation initiation under unstressed conditions. At smaller concentrations of inhibitor (10 – $10^{-2}\mu$M), there is no effect on the number of RIB5B$_{\beta-actin}$ complexes regardless of the K_D value. Only at large concentrations of inhibitor and small values of K_D does the number of RIB5B$_{\beta-actin}$ complexes approach a minimum.

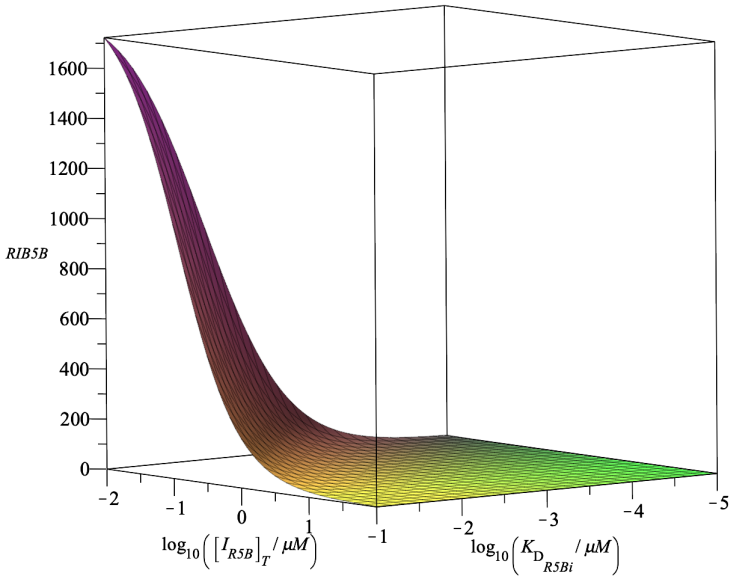

Figure A.12: A 3D surface plot of RIB5B inhibition in the canonical model for β-actin translation initiation under unstressed conditions. Only at the smallest concentration of inhibitor ($10^{-2}\mu$M) and highest value of K_D considered ($10^{2}\mu$M) does the number of RIB5B$_{\beta-actin}$ complexes approach the maximum (1860 ribosomes).

Appendix B

Contour Plots

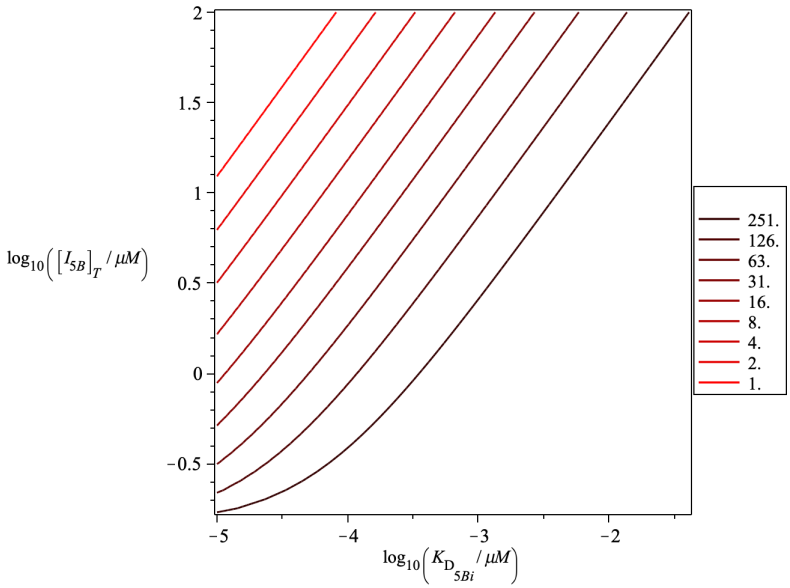

Figure B.1: A contour plot of the direct inhibition of eIF5B in the COL1A1 canonical translation initiation model under unstressed conditions. The contour lines represent the number of RIB5B$_{COL1A1}$ complexes. A combination of inhibitor concentration and K_D values that result in a 2-fold reduction of RIB5B$_{COL1A1}$ complexes are provided on the darkest contour line. The IC$_{50}$ is $\sim 3\,\mu$M when the K_D is 1 nM.

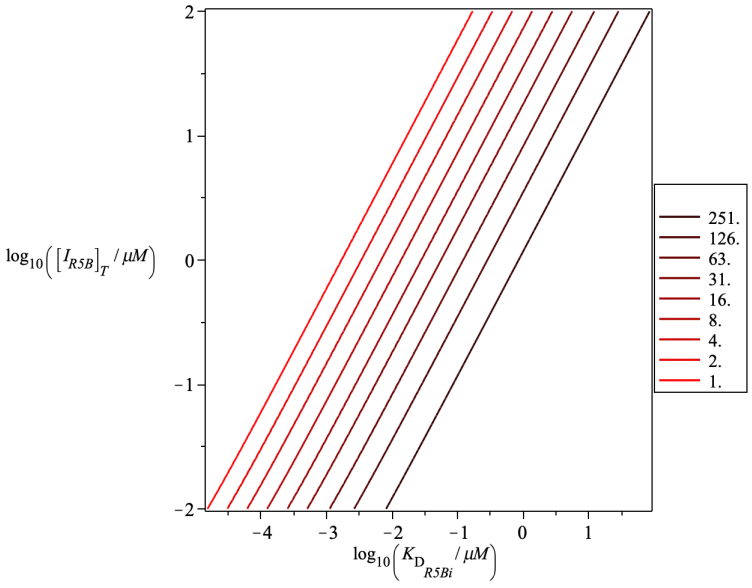

Figure B.2: A contour plot of the direct inhibition of RIB5B in the COL1A1 canonical translation initiation model under unstressed conditions. The contour lines represent the number of RIB5B$_{COL1A1}$ complexes. A combination of inhibitor concentration and K_D values that result in a 2-fold reduction of RIB5B$_{COL1A1}$ complexes are provided on the darkest contour line. By extrapolation, the IC$_{50}$ is $\sim 2\times10^{-3}\,\mu$M when the K_D is 1 nM.

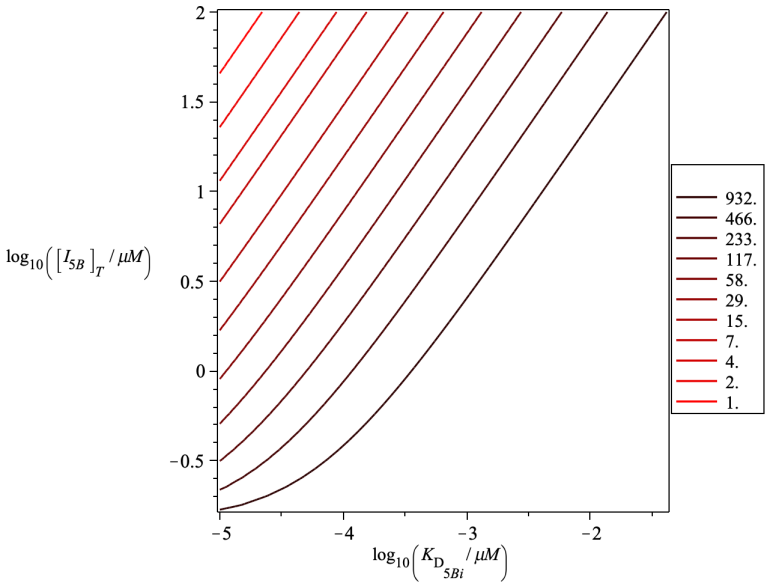

Figure B.3: A contour plot of the direct inhibition of eIF5B in the β-actin canonical translation initiation model under unstressed conditions. The contour lines represent the number of RIB5B$_{\beta-actin}$ complexes. A combination of inhibitor concentration and K_D values that result in a 2-fold reduction of RIB5B$_{\beta-actin}$ complexes are provided on the darkest contour line. The IC$_{50}$ is $\sim 3\,\mu$M when the K_D is 1 nM.

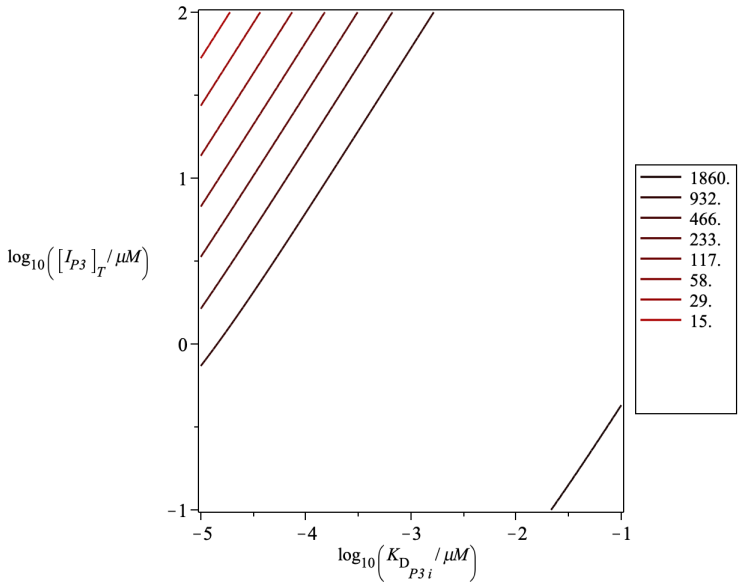

Figure B.4: A contour plot of the direct inhibition of PIC3 in the β-actin canonical translation initiation model under unstressed conditions. The contour lines represent the number of RIB5B$_{\beta-actin}$ complexes, where the black line represents the largest whole number of ribosomes (1860), and the red the fewest (15). The IC$_{50}$ is $\sim 80\,\mu$M when the K_D is 1 nM. A combination of inhibitor concentration and K_D values that result in a 2-fold reduction of RIB5B$_{\beta-actin}$ complexes are provided on the second darkest contour line.

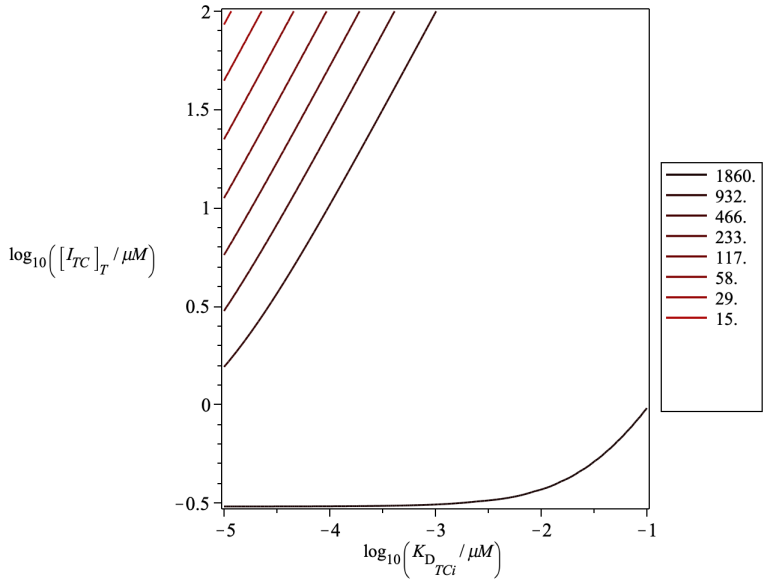

Figure B.5: A contour plot of the direct inhibition of TC in the β-actin canonical translation initiation model under unstressed conditions. The contour lines represent the number of $\text{RIB5B}_{\beta-actin}$ complexes, where the black line represents the largest whole number of ribosomes (1860), and the red the fewest (15). The IC_{50} is $\sim 100\,\mu\text{M}$ when the K_D is 1 nM. A combination of inhibitor concentration and K_D values that result in a 2-fold reduction of $\text{RIB5B}_{\beta-actin}$ complexes are provided on the second darkest contour line.

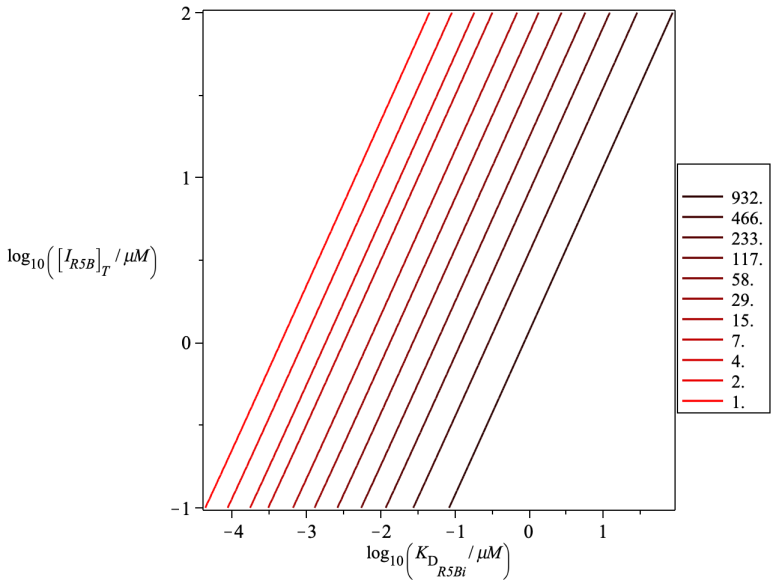

Figure B.6: A contour plot of the direct inhibition of RIB5B in the β-actin canonical translation initiation model under unstressed conditions. The contour lines represent the number of $\text{RIB5B}_{\beta-actin}$ complexes. A combination of inhibitor concentration and K_D values that result in a 2-fold reduction of $\text{RIB5B}_{\beta-actin}$ complexes are provided on the darkest contour line. By extrapolation, the IC_{50} is $\sim 3 \times 10^{-3}\,\mu\text{M}$ when the K_D is 1 nM.

Appendix C

Sensitivity Tables

Table C.1: Complete table of sensitivities for non-canonical direct eIF5B inhibition. The total concentration of mRNA used in this analysis was assumed to be $2.0 \times 10^{-3}\mu$M, the total inhibitor concentration used was 2μM, and the K_D of the inhibitor was 1nM.

	k_1	k_{-1}	k_2	k_{-2}	k_3	k_{-3}	k_4	k_{-4}	k_5
eIF3	-0.999	0.999	0.000	0.000	0.005	0.000	0.000	0.000	0.000
eIF5B	0.000	0.000	0.000	0.000	-0.005	0.000	0.000	0.000	0.000
PIC1	0.001	-0.001	0.000	0.000	0.005	0.000	0.000	0.000	0.000
PIC2	0.000	0.000	0.009	-0.009	-1.228	0.044	-0.044	0.007	-0.002
PIC3	0.000	0.000	0.000	0.000	0.951	-0.034	0.034	-0.005	-0.994
PIC4	0.000	0.000	0.000	0.000	0.951	-0.034	0.034	-0.005	0.006
TC	0.000	0.000	-0.009	0.009	2.179	-0.078	-0.921	0.146	-0.151
mRNA	-0.001	0.001	-0.991	0.978	-1.204	0.043	-0.044	0.007	-0.002
I_{5B}	0.000	0.000	0.000	0.000	0.000	0.000	0.000	0.000	0.000
$eIF5B_i$	0.000	0.000	0.000	0.000	-0.004	0.000	0.000	0.000	0.000
RIB5B	0.000	0.000	0.000	0.000	0.951	-0.034	0.034	-0.005	0.006

	k_{-5}	k_6	k_7	$[\text{mRNA}]_T$	τ	$[\text{eIF5B}]_T$	$[I_{5B}]_T$	$K_{D_{5Bi}}$
eIF3	0.000	0.000	-0.003	-0.009	0.000	0.006	-0.006	0.005
eIF5B	0.000	0.000	0.004	0.000	0.000	1.091	-1.086	0.995
PIC1	0.000	0.000	-0.003	-0.009	0.000	0.006	-0.006	0.005
PIC2	0.000	0.004	0.715	2.189	-0.001	-1.346	1.340	-1.227
PIC3	0.142	-0.142	0.030	0.079	0.000	1.043	-1.038	0.951
PIC4	-0.001	-0.999	0.030	0.079	0.000	1.043	-1.038	0.951
TC	0.022	-0.026	-0.685	-2.110	0.001	2.389	-2.378	2.178
mRNA	0.000	0.004	0.709	2.171	-0.001	-1.320	1.314	-1.204
I_{5B}	0.000	0.000	0.000	0.000	0.000	-0.092	1.091	0.000
$eIF5B_i$	0.000	0.000	0.004	0.000	0.000	1.000	0.005	-0.005
RIB5B	-0.001	0.001	-0.970	0.079	0.000	1.043	-1.038	0.951

Table C.2: Complete table of sensitivities for non-canonical PIC2 inhibition. The total concentration of mRNA used in this analysis was assumed to be $2.0 \times 10^{-3}\mu$M, the total inhibitor concentration used was $5\,\mu$M, and the K_D of the inhibitor was 1nM.

	k_1	k_{-1}	k_2	k_{-2}	k_3	k_{-3}	k_4	k_{-4}	k_5
eIF3	-0.999	0.999	0.000	0.000	0.000	0.000	0.002	0.000	0.000
eIF5B	0.000	0.000	0.000	0.000	-0.906	0.901	0.000	0.000	0.000
PIC1	0.001	-0.001	0.000	0.000	0.000	0.000	0.002	0.000	0.000
PIC2	0.000	0.000	0.000	0.000	-0.053	0.052	-0.554	0.088	-0.086
PIC3	0.000	0.000	0.000	0.000	0.042	-0.042	0.444	-0.071	-0.927
PIC4	0.000	0.000	0.000	0.000	0.042	-0.042	0.444	-0.071	0.073
TC	0.000	0.000	0.000	0.000	0.095	-0.094	-0.002	0.000	0.000
mRNA	-0.001	0.001	-1.000	0.015	0.040	-0.040	0.426	-0.068	0.070
I_{P2}	0.000	0.000	0.000	0.000	0.000	0.000	0.000	0.000	0.000
$PIC2_i$	0.000	0.000	0.000	0.000	-0.053	0.052	-0.554	0.088	-0.086
RIB5B	0.000	0.000	0.000	0.000	0.042	-0.042	0.444	-0.071	0.073

	k_{-5}	k_6	k_7	$[\text{mRNA}]_T$	τ	$[\text{eIF5B}]_T$	$[I_{P2}]_T$	$K_{D_{P2i}}$
eIF3	0.000	0.000	-0.001	-0.004	0.000	0.002	-0.002	0.002
eIF5B	0.000	0.000	0.004	0.001	0.000	0.999	0.000	0.000
PIC1	0.000	0.000	-0.001	-0.004	0.000	0.002	-0.002	0.002
PIC2	0.012	-0.010	0.323	1.003	0.000	-0.557	-0.446	0.446
PIC3	0.132	-0.131	0.325	0.998	0.000	0.446	-0.444	0.444
PIC4	-0.010	-0.988	0.325	0.998	0.000	0.446	-0.444	0.444
TC	0.000	0.000	0.002	-0.004	0.000	1.002	0.002	-0.002
mRNA	-0.010	0.012	0.327	1.003	0.000	0.428	-0.442	0.442
I_{P2}	0.000	0.000	0.000	0.000	0.000	0.000	1.000	0.000
$PIC2_i$	0.012	-0.010	0.323	1.002	0.000	-0.556	0.554	-0.554
RIB5B	-0.010	0.012	-0.675	0.998	0.000	0.446	-0.444	0.444

Table C.3: Complete table of sensitivities for non-canonical TC inhibition. The total concentration of mRNA used in this analysis was assumed to be $2.0 \times 10^{-3}\mu$M, the total inhibitor concentration used was $5\,\mu$M, and the K_D of the inhibitor was 1nM.

	k_1	k_{-1}	k_2	k_{-2}	k_3	k_{-3}	k_4	k_{-4}	k_5
eIF3	-0.999	0.999	0.000	0.000	0.000	0.000	0.002	0.000	0.000
eIF5B	0.000	0.000	0.004	-0.004	-1.000	0.038	0.398	-0.063	0.065
PIC1	0.001	-0.001	0.000	0.000	0.000	0.000	0.002	0.000	0.000
PIC2	0.000	0.000	0.004	-0.004	0.000	0.000	-0.585	0.093	-0.091
PIC3	0.000	0.000	0.004	-0.004	0.000	0.000	0.413	-0.066	-0.932
PIC4	0.000	0.000	0.004	-0.004	0.000	0.000	0.413	-0.066	0.068
TC	0.000	0.000	0.000	0.000	0.001	0.000	-0.002	0.000	0.000
mRNA	-0.001	0.001	-0.996	0.982	0.000	0.000	-0.573	0.091	-0.089
I_{TC}	0.000	0.000	0.000	0.000	0.000	0.000	0.000	0.000	0.000
TC_i	0.000	0.000	0.000	0.000	0.001	0.000	-0.002	0.000	0.000
RIB5B	0.000	0.000	0.004	-0.004	0.000	0.000	0.413	-0.066	0.068

	k_{-5}	k_6	k_7	$[\text{mRNA}]_T$	τ	$[\text{eIF5B}]_T$	$[I_{TC}]_T$	$K_{D_{TCi}}$
eIF3	0.000	0.000	-0.001	-0.004	0.000	0.002	-0.002	0.002
eIF5B	-0.009	0.011	0.330	0.960	0.000	0.453	-0.450	0.435
PIC1	0.000	0.000	-0.001	-0.004	0.000	0.002	-0.002	0.002
PIC2	0.013	-0.011	0.341	1.003	0.000	-0.608	0.605	-0.584
PIC3	0.133	-0.131	0.343	0.998	0.000	0.430	-0.428	0.413
PIC4	-0.010	-0.988	0.343	0.998	0.000	0.430	-0.428	0.413
TC	0.000	0.000	0.003	-0.005	0.000	1.037	-1.032	0.998
mRNA	0.013	-0.011	0.342	1.007	0.000	-0.595	0.592	-0.572
I_{TC}	0.000	0.000	0.000	0.000	0.000	-0.035	1.035	0.000
TC_i	0.000	0.000	0.002	-0.005	0.000	1.003	0.002	-0.002
RIB5B	-0.010	0.012	-0.657	0.998	0.000	0.430	-0.428	0.413

Table C.4: Complete table of sensitivities for non-canonical RIB5B inhibition. The total concentration of mRNA used in this analysis was assumed to be $2.0 \times 10^{-3}\mu$M, the total inhibitor concentration used was $3 \times 10^{-3}\,\mu$M, and the K_D of the inhibitor was 1nM.

	k_1	k_{-1}	k_2	k_{-2}	k_3	k_{-3}	k_4	k_{-4}	k_5
eIF3	-0.999	0.999	0.000	0.000	0.000	0.000	0.000	0.000	0.000
eIF5B	0.000	0.000	0.000	0.000	-0.906	0.901	0.000	0.000	0.000
PIC1	0.001	-0.001	0.000	0.000	0.000	0.000	0.000	0.000	0.000
PIC2	0.000	0.000	0.000	0.000	-0.095	0.094	-1.000	0.159	-0.157
PIC3	0.000	0.000	0.000	0.000	0.000	0.000	0.000	0.000	-0.998
PIC4	0.000	0.000	0.000	0.000	0.000	0.000	0.000	0.000	0.002
TC	0.000	0.000	0.000	0.000	0.095	-0.094	0.000	0.000	0.000
mRNA	-0.001	0.001	-1.000	0.015	-0.001	0.001	-0.015	0.002	0.000
IR5B	0.000	0.000	0.000	0.000	0.000	0.000	0.000	0.000	-0.001
RIB5Bi	0.000	0.000	0.000	0.000	0.000	0.000	0.000	0.000	0.002
RIB5B	0.000	0.000	0.000	0.000	0.000	0.000	0.000	0.000	0.002

	k_{-5}	k_6	k_7	$[\text{mRNA}]_T$	τ	$[\text{eIF5B}]_T$	$[\text{I}_{\text{R5B}}]_T$	$K_{D_{R5Bi}}$
eIF3	0.000	0.000	0.000	0.000	0.000	0.000	0.000	0.000
eIF5B	0.000	0.000	0.005	-0.004	0.000	1.005	-0.006	0.004
PIC1	0.000	0.000	0.000	0.000	0.000	0.000	0.000	0.000
PIC2	0.022	-0.021	0.769	1.185	0.000	-1.010	-0.963	0.623
PIC3	0.143	-0.141	0.771	1.175	0.000	0.000	-0.965	0.624
PIC4	0.000	-0.998	0.771	1.175	0.000	0.000	-0.965	0.624
TC	0.000	0.000	0.001	-0.010	0.000	1.010	-0.002	0.001
mRNA	0.000	0.002	0.771	1.176	0.000	-0.016	-0.965	0.624
IR5B	0.000	-0.001	0.064	-0.330	0.000	0.000	1.816	-0.175
RIB5Bi	0.000	0.002	-0.165	0.845	0.000	0.000	0.851	-0.551
RIB5B	0.000	0.002	-0.229	1.175	0.000	0.000	-0.965	0.624

Table C.5: Relative sensitivity table for COL1A1 under hypoxic conditions.

	k_{-3}	k_8	k_{-8}	k_{10}	k_{-10}	
eIF3	0.017	0.000	0.000	0.000	0.000	
eIF5	0.538	0.000	0.000	0.000	0.000	
eIF1	0.010	0.000	0.000	0.000	0.000	
eIF2	0.323	0.000	0.000	0.000	0.000	
eIF4E	0.000	0.000	0.000	0.000	0.000	
eIF4G	0.000	0.000	0.000	0.000	0.000	
eIF5B	0.000	0.000	0.000	0.000	0.000	
PIC1	0.017	0.000	0.000	0.000	0.000	
PIC2	0.556	0.000	0.000	0.000	0.000	
PIC3	-0.433	0.000	0.000	0.000	0.000	
PIC4	-0.110	0.000	0.000	0.000	0.000	
PIC5	-0.001	0.005	0.000	0.000	0.000	
PIC6	-0.001	0.005	0.000	-1.000	0.500	
PIC7	-0.001	0.005	0.000	0.000	0.000	
PIC8	-0.001	0.005	0.000	0.000	0.000	
PIC9	-0.001	0.005	0.000	0.000	0.000	
TC	0.323	0.000	0.000	0.000	0.000	
$mRNA_i$	0.010	-0.095	0.007	0.000	0.000	
$mRNA_c$	0.110	-0.995	0.071	0.000	0.000	
$eIF4_c$	0.000	0.000	0.000	0.000	0.000	
RIB5B	-0.001	0.005	0.000	0.000	0.000	
	k_{11}	k_{-12}	k_{13}	$[eIF5B]_T$	τ	$[mRNA_T]$
eIF3	0.000	0.000	0.000	0.000	0.000	0.000
eIF5	0.001	0.000	0.000	0.000	0.000	0.003
eIF1	0.000	0.000	0.000	0.000	0.000	0.000
eIF2	0.000	0.000	0.000	0.000	0.000	0.003
eIF4E	0.000	0.000	0.000	0.000	0.000	0.000
eIF4G	0.000	0.000	0.000	0.000	0.000	0.000
eIF5B	0.000	0.000	0.000	1.000	0.000	-0.005
PIC1	0.000	0.000	0.000	0.000	0.000	0.000
PIC2	0.000	0.000	0.000	0.000	0.000	0.000
PIC3	0.000	0.000	0.000	0.000	0.000	0.000
PIC4	0.000	0.000	0.000	0.000	0.000	0.000
PIC5	0.029	0.012	0.034	0.000	-0.058	1.000
PIC6	-0.471	0.012	0.034	-1.000	-0.059	1.005
PIC7	-0.971	0.012	0.034	0.000	-0.058	1.000
PIC8	0.029	-1.223	-0.466	0.000	-0.058	1.000
PIC9	0.029	0.012	-0.966	0.000	-0.058	1.000

	k_{11}	k_{-12}	k_{13}	$[eIF5B]_T$	τ	$[mRNA_T]$
TC	0.000	0.000	0.000	0.000	0.000	0.001
$mRNA_i$	0.029	0.012	0.034	0.000	-0.058	1.000
$mRNA_c$	0.029	0.012	0.034	0.000	-0.058	1.001
$eIF4_c$	0.000	0.000	0.000	0.000	0.000	0.000
RIB5B	0.029	0.012	0.034	0.000	-0.058	1.000

Table C.6: Relative sensitivity table for β-actin under hypoxic conditions.

	k_{-3}	k_8	k_{-8}	k_{10}	k_{-10}	
eIF3	0.017	0.000	0.000	0.000	0.000	
eIF5	0.532	0.000	0.000	0.000	0.000	
eIF1	0.010	0.000	0.000	0.000	0.000	
eIF2	0.321	0.000	0.000	0.000	0.000	
eIF4E	0.000	0.000	0.000	0.000	0.000	
eIF4G	0.000	0.000	0.000	0.000	0.000	
eIF5B	0.000	0.000	0.000	0.000	0.000	
PIC1	0.017	0.000	0.000	0.000	0.000	
PIC2	0.555	0.000	0.000	0.000	0.000	
PIC3	-0.433	0.000	0.000	0.000	0.000	
PIC4	-0.111	0.000	0.000	0.000	0.000	
PIC5	-0.001	0.005	0.000	0.000	0.000	
PIC6	-0.001	0.005	0.000	-1.000	0.500	
PIC7	-0.001	0.005	0.000	0.000	0.000	
PIC8	-0.001	0.005	0.000	0.000	0.000	
PIC9	-0.001	0.005	0.000	0.000	0.000	
TC	0.323	0.000	0.000	0.000	0.000	
$mRNA_i$	0.011	-0.095	0.007	0.000	0.000	
$mRNA_c$	0.110	-0.995	0.071	0.000	0.000	
$eIF4_c$	0.000	0.000	0.000	0.000	0.000	
RIB5B	-0.001	0.005	0.000	0.000	0.000	
	k_{11}	k_{-12}	k_{13}	$[eIF5B]_T$	τ	$[mRNA_T]$
eIF3	0.000	0.000	0.000	0.000	0.000	0.000
eIF5	0.002	0.000	0.000	0.000	-0.001	0.011
eIF1	0.000	0.000	0.000	0.000	0.000	0.000
eIF2	-0.001	0.000	0.000	0.000	-0.001	0.010
eIF4E	0.000	0.000	0.000	0.000	0.000	0.000
eIF4G	0.000	0.000	0.000	0.000	0.000	0.001
eIF5B	0.000	0.000	0.000	1.000	0.001	-0.020

	k_{11}	k_{-12}	k_{13}	$[\text{eIF5B}]_T$	τ	$[\text{mRNA}_T]$
PIC1	0.000	0.000	0.000	0.000	0.000	0.000
PIC2	0.002	0.000	0.000	0.000	0.000	0.001
PIC3	0.002	0.000	0.000	0.000	0.000	-0.003
PIC4	0.000	0.000	0.000	0.000	0.000	-0.003
PIC5	0.029	0.012	0.034	0.000	-0.058	1.000
PIC6	-0.471	0.012	0.034	-1.000	-0.059	1.020
PIC7	-0.971	0.012	0.034	0.000	-0.058	1.000
PIC8	0.029	-1.223	-0.466	0.000	-0.058	1.000
PIC9	0.029	0.012	-0.966	0.000	-0.058	1.000
TC	-0.001	0.000	0.000	0.000	0.000	0.004
mRNA_i	0.029	0.012	0.033	0.000	-0.058	1.001
mRNA_c	0.029	0.012	0.034	0.000	-0.058	1.003
eIF4_c	0.000	0.000	0.000	0.000	0.000	-0.001
RIB5B	0.029	0.012	0.034	0.000	-0.058	1.000

Table C.7: Relative sensitivity table for COL1A1 under unstressed conditions.

	k_{-3}	k_8	k_{-8}	k_{10}	k_{-10}
eIF3	0.003	0.000	0.000	0.000	0.000
eIF5	0.929	0.000	0.000	0.000	0.000
eIF1	0.002	0.000	0.000	0.000	0.000
eIF2	0.006	0.000	0.000	0.000	0.000
eIF4E	0.000	0.000	0.000	0.000	0.000
eIF4G	0.000	0.000	0.000	0.000	0.000
eIF5B	0.000	0.000	0.000	0.000	0.000
PIC1	0.003	0.000	0.000	0.000	0.000
PIC2	0.958	0.000	0.000	0.000	0.000
PIC3	-0.029	0.000	0.000	0.000	0.000
PIC4	-0.023	0.000	0.000	0.000	0.000
PIC5	0.000	0.001	0.000	0.000	0.000
PIC6	0.000	0.001	0.000	-1.000	0.500
PIC7	0.000	0.001	0.000	0.000	0.000
PIC8	0.000	0.001	0.000	0.000	0.000
PIC9	0.000	0.001	0.000	0.000	0.000
TC	0.006	0.000	0.000	0.000	0.000
mRNA_i	0.001	-0.022	0.002	0.000	0.000
mRNA_c	0.023	-0.999	0.071	0.000	0.000
eIF4_c	0.000	0.000	0.000	0.000	0.000

	k_{-3}	k_8	k_{-8}	k_{10}	k_{-10}	
RIB5B	0.000	0.001	0.000	0.000	0.000	
	k_{11}	k_{-12}	k_{13}	$[\text{eIF5B}]_\text{T}$	τ	$[\text{mRNA}_\text{T}]$
eIF3	0.000	0.000	0.000	0.000	0.000	0.000
eIF5	0.001	0.000	0.001	0.000	-0.002	0.036
eIF1	0.000	0.000	0.000	0.000	0.000	0.000
eIF2	0.000	0.000	0.000	0.000	0.000	0.000
eIF4E	0.000	0.000	0.000	0.000	0.000	0.000
eIF4G	0.000	0.000	0.000	0.000	0.000	0.000
eIF5B	0.000	0.000	0.000	1.000	0.000	-0.006
PIC1	0.000	0.000	0.000	0.000	0.000	0.000
PIC2	0.001	0.000	0.000	0.000	-0.001	0.010
PIC3	0.000	0.000	0.000	0.000	0.000	0.000
PIC4	0.000	0.000	0.000	0.000	0.000	0.000
PIC5	0.030	0.014	0.035	0.000	-0.060	1.000
PIC6	-0.470	0.013	0.035	-1.000	-0.060	1.006
PIC7	-0.970	0.014	0.035	0.000	-0.060	1.000
PIC8	0.030	-1.221	-0.465	0.000	-0.060	1.000
PIC9	0.030	0.014	-0.965	0.000	-0.060	1.000
TC	0.000	0.000	0.000	0.000	0.000	0.000
mRNA_i	0.030	0.013	0.035	0.000	-0.060	1.000
mRNA_c	0.030	0.014	0.035	0.000	-0.060	1.000
eIF4_c	0.000	0.000	0.000	0.000	0.000	0.000
RIB5B	0.030	0.014	0.035	0.000	-0.060	1.000

Table C.8: Relative sensitivity table for β-actin under unstressed conditions.

	k_{-3}	k_8	k_{-8}	k_{10}	k_{-10}
eIF3	0.003	0.000	0.000	0.000	0.000
eIF5	0.844	0.000	0.000	0.000	0.000
eIF1	0.002	0.000	0.000	0.000	0.000
eIF2	0.006	0.000	0.000	0.000	0.000
eIF4E	0.000	0.000	0.000	0.000	0.000
eIF4G	0.000	0.000	0.000	0.000	0.000
eIF5B	0.000	0.000	0.000	0.000	0.000
PIC1	0.003	0.000	0.000	0.000	0.000
PIC2	0.931	0.000	0.000	0.000	0.000
PIC3	-0.029	0.000	0.000	0.000	0.000
PIC4	-0.023	0.000	0.000	0.000	0.000

	k_{-3}	k_8	k_{-8}	k_{10}	k_{-10}	
PIC5	0.000	0.001	0.000	0.000	0.000	
PIC6	0.000	0.001	0.000	-1.000	0.500	
PIC7	0.000	0.001	0.000	0.000	0.000	
PIC8	0.000	0.001	0.000	0.000	0.000	
PIC9	0.000	0.001	0.000	0.000	0.000	
TC	0.006	0.000	0.000	0.000	0.000	
$mRNA_i$	0.001	-0.022	0.002	0.000	0.000	
$mRNA_c$	0.023	-0.999	0.071	0.000	0.000	
$eIF4_c$	0.000	0.000	0.000	0.000	0.000	
RIB5B	0.000	0.001	0.000	0.000	0.000	
	k_{11}	k_{-12}	k_{13}	$[eIF5B]_T$	τ	$[mRNA_T]$
eIF3	0.000	0.000	0.000	0.000	0.000	0.001
eIF5	0.005	0.002	0.004	0.000	-0.007	0.123
eIF1	0.000	0.000	0.000	0.000	0.000	0.000
eIF2	0.000	0.000	0.000	0.000	0.000	0.001
eIF4E	0.000	0.000	0.000	0.000	0.000	0.000
eIF4G	0.000	0.000	0.000	0.000	0.000	0.000
eIF5B	0.000	0.000	0.000	1.000	0.001	-0.024
PIC1	0.000	0.000	0.000	0.000	0.000	0.000
PIC2	0.002	0.000	0.001	0.000	-0.002	0.037
PIC3	0.001	0.000	0.000	0.000	0.000	-0.002
PIC4	0.001	0.000	0.000	0.000	0.000	-0.002
PIC5	0.030	0.014	0.035	0.000	-0.060	1.000
PIC6	-0.470	0.013	0.035	-1.000	-0.061	1.024
PIC7	-0.970	0.014	0.035	0.000	-0.060	1.000
PIC8	0.030	-1.221	-0.465	0.000	-0.060	1.000
PIC9	0.030	0.014	-0.965	0.000	-0.060	1.000
TC	0.000	0.000	0.000	0.000	0.000	0.000
$mRNA_i$	0.030	0.013	0.035	0.000	-0.060	1.000
$mRNA_c$	0.029	0.014	0.035	0.000	-0.060	1.002
$eIF4_c$	0.000	0.000	0.000	0.000	0.000	-0.001
RIB5B	0.030	0.014	0.035	0.000	-0.060	1.000

Appendix D

Parameter Scans

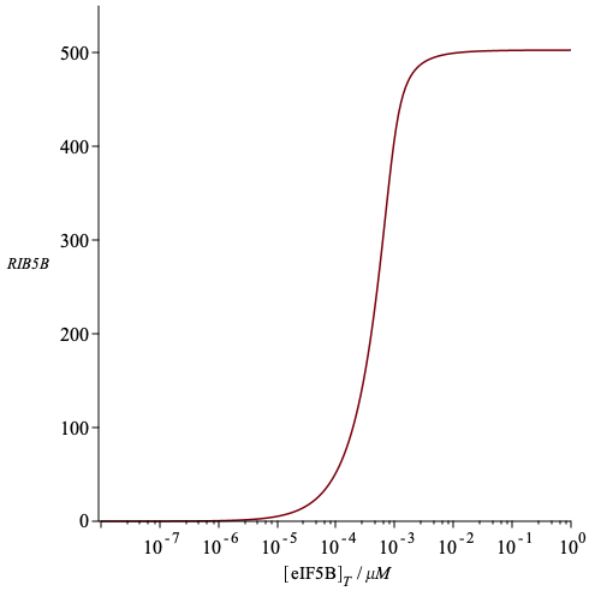

Figure D.1: A parameter scan of RIB5B vs the total eIF5B concentration in canonical COL1A1 translation initiation under unstressed conditions. The system reaches a saturation point of 503 RIB5B_{COL1A1} complexes. The number of possible RIB5B_{COL1A1} complexes is halved when the total concentration of eIF5B is $5.1 \times 10^{-4} \mu$M.

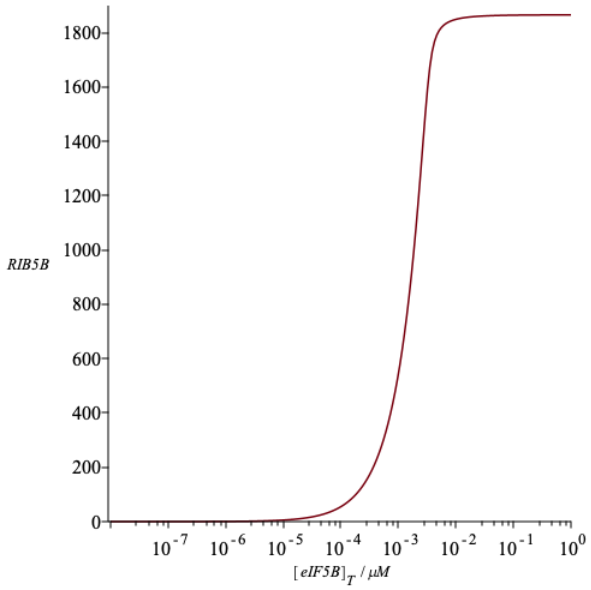

Figure D.2: A parameter scan of RIB5B vs the total eIF5B concentration in canonical β-actin translation initiation under unstressed conditions. The system reaches a saturation point of 1860 $\text{RIB5B}_{\beta-actin}$ complexes. The number of possible $\text{RIB5B}_{\beta-actin}$ complexes is halved when the total concentration of eIF5B is $1.8 \times 10^{-3} \mu$M.